8. SITE 904[1]

Shipboard Scientific Party[2]

HOLE 904A

Date occupied: 1 July 1993

Date departed: 4 July 1993

Time on hole: 1 day, 7 hr, 45 min

Position: 38°51.806′N, 72°46.084′W

Bottom felt (rig floor; m, drill-pipe measurement): 1134.0

Distance between rig floor and sea level (m): 11.2

Water depth (drill-pipe measurement from sea level, m): 1122.8

Total depth (rig floor; m): 1710.7

Penetration (m): 576.7

Number of cores (including cores with no recovery): 62

Total length of cored section (m): 576.7

Total core recovered (m): 557.55

Core recovery (%): 96.7

Oldest sediment cored:
Depth (mbsf): 576.70
Nature: nannofossil clayey chalk
Age: middle Eocene
Measured velocity (km/s): 1.96

Principal results: Site 904 (proposed Site MAT12A) was drilled in 1123 m of water on the upper continental slope offshore New Jersey, 7.8 km south and slightly downslope from Site 902. This is the deepest of four sites (Sites 902 through 904 and 906) on a slope transect designed to sample post-lower Eocene sequence boundaries traced from the adjacent continental shelf. Information from these sites will be used to evaluate the effect of glacio-eustatic changes on the stratigraphic record of siliciclastic passive margins.

Although Sites 902 and 903 met their objectives, they sampled intervals of poorly fossiliferous Miocene strata. Slightly acidic pore waters are thought to have caused postdepositional dissolution of the calcareous microfossils, whereas laminae and concretions associated with alkali maxima were the locus of reprecipitated carbonate. The primary objective of Site 904 was to sample a Miocene succession where its down-dip location relative to the other Leg 150 sites suggests that it is more fossiliferous because of the less destructive pore-water dissolution. An additional objective was to drill through and sample a relatively thick upper and middle Eocene section, and continue down across a diagenetic front near the middle/lower Eocene boundary.

Site 904 was spudded on 1 July 1993, and coring with the advanced hydraulic piston corer (APC) proceeded with 99.8% recovery to 222 m below seafloor (mbsf). Excessive overpull dictated refusal at this depth. Coring resumed with the extended core barrel (XCB), and we had complete recovery until chalk with porcellanite was encountered at ~520 mbsf. The rate of penetration slowed considerably, and recovery fell off with increasing depth into this lithologic unit. Scientific objectives had been met, and with a total of 94.7% recovery for the entire hole, coring ended at 576.7 mbsf on 2 July. Three logging runs comprising the sonic-induction, porosity, and Formation MicroScanner (FMS) tools were completed with the side-entry sub (SES) from total depth to 96 mbsf. The hole was plugged and abandoned on 4 July.

Sites 902, 903, 904, and 906 comprise a transect of post-lower Eocene continental slope sediments. The lithologies at these sites are very similar, and we maintained the same lithologic unit designations among them. Those at Site 904 are the same as at Sites 902 and 903 except that erosion between the upper Miocene and middle Pleistocene removed lithologic Units II and III. As in the other sites, the deepest unit is predominantly carbonate; the overlying units are all predominantly siliciclastic.

Unit I (0–106.2 mbsf): Holocene to middle Pleistocene silty clay; very uniform and fine grained in the upper 64 m; laminae and beds of normally graded fine sand are common from 64 to 92 mbsf; slump deposits of poorly sorted sand and lithic clasts comprise the base of this unit, ending with a sharp contact.

Unit IV (106.2–223.9 mbsf): upper to middle Miocene diatomaceous silty clay to clayey silts with carbonate and pyrite nodules and a 4-m interval of poorly sorted medium to very coarse sand near the middle of the unit; fine sand, partly slumped, comprises ~5 m at the base of the unit.

Unit V (223.9–296.5 mbsf): lower to middle Miocene glauconitic, diatomaceous silty clay with abundant diatoms.

Unit VI (296.5–341.2 mbsf): lower Miocene to upper Oligocene silty clay with minor glauconite, common nannofossils, and rare diatoms; the bottom 4 m of this unit contains very abundant sand- and silt-sized glauconite ending in a sharp, burrowed contact.

Unit VII (341.2–576.7 mbsf): upper to middle Eocene clayey nannofossil chalk with diatoms, radiolarians, and foraminifers. A microtektite layer occurs 8 m above the upper/middle Eocene boundary, as determined by nannofossils; this layer is part of a 15-cm laminated interval containing well-sorted silt- to sand-sized particles. Intervals of porcellanitic nannofossil chalk are common below 525 m.

Density, magnetic susceptibility, and biostratigraphic data provide good correlations of the Pleistocene section to the SPECMAP time scale; this site contains a record of part of the middle Pleistocene back to stage 12. The middle Pleistocene is underlain by lower upper Miocene strata. Considerable uncertainties surround placement of the upper/middle Miocene boundary, with planktonic foraminifers and nannofossils indicating a disconformable contact roughly 20 m below that indicated by diatoms and dinocysts. The upper middle Miocene section contains a spotty record of calcareous plankton, and shipboard biostratigraphy of this section is uncertain. The lower middle Miocene to upper Oligocene section has reasonable calcareous biostratigraphic control, and at least two possible hiatuses were detected (NN5/NN7 and NN2–NN3/NN4). As at Sites 902 and 903, most or all of the early Oligocene is not represented, with possible hiatuses near the Oligocene/Miocene boundary and in the late Oligocene. Eocene biostratigraphic control is good. Preliminary biostratigraphic studies of a microtektite layer show that it is lower upper Eocene.

As at Sites 902, 903, and 906, magnetization intensities in sediments at Site 904 are generally below the detection limit of 1 mA/m for shipboard analyses. Values are strongest in the Pleistocene section above 106 mbsf, and pass-through measurements of both split cores and discrete samples indicate a normal, presumably Brunhes, polarity. Intensities remain measurable through a reversed interval from 106 to 133 mbsf that may correlate

[1] Mountain, G.S., Miller, K.G., Blum, P., et al., 1994. *Proc. ODP, Init. Repts.*, 150: College Station, TX (Ocean Drilling Program).

[2] Shipboard Scientific Party is as given in the list of participants preceding the Table of Contents.

to Chron C4Ar. Intensities are sufficient in five additional intervals between 200 and 400 mbsf to enable tentative assignments to one reversed and four normally polarized magnetochrons. These samples will be reexamined in more detailed shore-based studies.

Methane at Site 904 reaches a maximum of 4% (39,787 ppm) at 446 mbsf as measured in headspace gas. Ethane is the only other hydrocarbon gas detected. Its profile mimics methane and reaches a maximum of 14 ppm at 559 mbsf; it is thought to be biogenically derived. Like Site 903, the values of organic carbon are below 0.5% in Pleistocene sediment and in the Eocene chalk; values in Miocene sediment, by contrast, are as high as 2.1%, and sulfur concentrations reach nearly 3%. This pattern is probably caused by high primary productivity that induced suboxia/anoxia in the water column and/or sediments. Low C/N ratios (<10) suggest that the organic matter preserved in these sediments is primarily marine.

Pore-water studies reveal patterns similar to Sites 902, 903, and (in the pre-Pleistocene section) 906. Salinity increases abruptly at the Pleistocene/Miocene boundary and continues to increase with depth, suggesting evaporite deposits at depth. A corresponding downward decrease in pH to slightly acidic values explains the disappearance of calcareous microfossils. Local ammonium maxima associated with organic-rich intervals are sites of reprecipitated carbonate minerals.

Five physical properties units are recognized at Site 904 based on trends in wet-bulk density. Values generally increase steadily and rapidly in the Pleistocene sediments of Unit I, reaching the highest values of the site (2.19 g/cm^3) at 106 mbsf. Except for locally high densities in sand-prone intervals (several of which correspond to seismic reflectors), density values remain below 1.7 g/cm^3 until Unit V, which corresponds to the siliceous-cemented chalk at the base of lithologic Unit VII. Compressional-wave velocities increase from 1517 m/s at the top of the section to 1700 m/s at the base of Unit IV; velocities increase abruptly to as high as 2000 m/s and more in the siliceous-cemented chalks of Unit VII. Downhole shifts in porosity, thermal conductivity, and penetrometer values generally occur at the same depth as changes in wet-bulk density. Natural gamma-ray emissions were measured routinely on the multisensor track and show close parallels to values measured in the downhole log.

Borehole conditions were particularly good below 230 m, and as a result we obtained an excellent suite of logs below this depth. Abrupt changes in both density and velocity match seismic reflectors and lithologic changes at the top of and within the Eocene nannofossil chalks of lithologic Unit VII. Details provided by the sonic-induction, porosity, and Formation MicroScanner tool strings within this thick interval (341–576 mbsf) will be especially useful in shore-based analysis of this important stratigraphic section. A complete set of shipboard natural gamma-ray measurements were performed for the first time on cores from Site 904, and they show close correspondence to trends of the downhole natural gamma-ray measurements.

The principal result from Site 904 is that we recovered a lower Miocene section with calcareous microfossils that will provide improved integration between biostratigraphic, Sr-isotopic, and magnetostratigraphic chronologies crucial to the objectives of Leg 150. In addition, Site 904 recovered the thickest upper Eocene section yet found in this region. Definitive age estimates of seismic reflectors require further study; the interpretations completed thus far are consistent with the ages of reflectors traced from the continental shelf and dated at Sites 902, 903, and 906. For example, (1) reflector m1 (Tuscan) appears to correlate to a possible disconformity spanning the middle/upper Miocene boundary; (2) reflector m2 (Yellow-2) correlates with a reversed magnetozone that may be Chron C5Ar (~12.5 Ma) as it does at Site 903; (3) reflector m5 (Green) is associated with the middle/lower Miocene boundary; (4) reflector o1 (green-2) correlates with an unconformity separating upper Oligocene siliciclastic from upper Eocene carbonate sediment; and (5) reflector e2 (= A^c) correlates to the top of porcellanitic nannofossil chalk, which has an age approximately the same as at nearby Site 612 (middle-lower part of Zone NP15).

BACKGROUND AND OBJECTIVES

Site 904 was drilled on the New Jersey continental slope, 7.8 km (4.2 nmi) downslope of Site 902 and 4.9 km (2.6 nmi) upslope of DSDP Site 612 (Figs. 1–2). It is located on *Maurice Ewing* Cruise 9009 (Ew9009) MCS Line 1027 and *JOIDES Resolution* Line 2 (Fig. 2). This site is 141 km (77 nmi) east-southeast of Barnegat Inlet, New Jersey. Bathymetric controls for this region are provided by SeaMARC (Farre and Ryan, 1987), SeaBeam (W. Ryan and D. Twitchell, unpubl. data, 1989; Fig. 1), and Hydrosweep data. Site 904 is in 1082 corrected m water depth on *JOIDES Resolution* PDR profiles (Fig. 2; see also Chapter 4, this volume); it is located 0.55 km (0.3 nmi) east-northeast of the thalweg of the north branch of Carteret Canyon on the northeast interfluve (Fig. 1).

The geological background, hydrographic setting, and scientific justification for slope drilling are given in Chapter 2 (this volume). The primary scientific objectives addressed at Site 904 and other slope sites are (1) to date Oligocene–Holocene "Icehouse" seismic sequences traced from the continental shelf, and (2) to evaluate correlation of these sequence boundaries with glacioeustatic age estimates obtained from the $\delta^{18}O$ record. Secondary goals are to determine ages of major Eocene "Doubthouse" unconformities and to test the link between sea-level change and slope failure. The complexity of slope stratigraphy (e.g., Poag, Watts, et al., 1987) requires drilling in several locations to assemble a composite section as free of hiatuses as possible.

The lower Miocene was the prime target for Site 904. Site 903 (approximately 9.6 km [5.2 nmi] upslope) provided the thickest lower Miocene record of the Leg 150 sites (~129 m); however, calcareous fossil abundances were low. Deep submergence vehicle *Alvin* samples obtained from outcrops in Carteret Canyon adjacent to Site 904 show that the lower Miocene contains good calcareous fossils (K.G. Miller, unpubl. data, 1993). Therefore, although the lower Miocene at Site 904 was predicted to be thinner than at Site 903, we hoped that it would recover Miocene strata with good fossil control.

The upper Eocene section at Site 904 should provide the most complete record of any site drilled in this region. A thick middle and moderately thick upper Eocene section was penetrated at nearby Site 612 (Poag, Watts, et al., 1987). The middle Eocene section thins from Site 612 toward Site 904, but the upper Eocene section thickens. This provides not only a chance to date the age of an unconformity straddling the middle/upper Eocene boundary at Site 612, but also a chance to obtain better stratigraphic control on a microtektite layer that immediately overlies this disconformity (Poag, Watts, et al., 1987).

Based on results from Sites 902 and 903 and the Ew9009 seismic grid, we developed a revised time-depth relationship for predicting sub-bottom depths of seismic reflections at Site 904. Seismic profiles connecting Sites 904 and 902 (Cruise Ew9009 MCS Line 1027) predicted that Site 904 would recover 72 m of Pleistocene (seafloor to reflector p4), 93 m of upper–upper middle Miocene (reflectors p4–m1 [Tuscan of Greenlee et al., 1992]), 103 m of middle Miocene (reflector m1 to reflector m5 [Green of Greenlee et al., 1992]), 74 m of lower Miocene (reflectors m4–m6), 22 m of Oligocene, (reflectors m5–o1), and 76 m of upper Eocene (reflectors o1–e1).

OPERATIONS

The seismic gear was streamed as soon as the ship was under way from Site 902. A track was run connecting Site 902, Site 903, and the COST B-3 well with the new Site 904. Speed was reduced as the Site MAT12A global positioning system (GPS) coordinates were approached, and a positioning beacon was dropped on the first crossing.

Hole 904A

As the vessel returned to the beacon position and hydrophones and thrusters were lowered, the beacon was behaving strangely. The signal was received intermittently and appeared to be changing location; shortly thereafter the beacon was floating on the surface. Though the beacon was grappled and recovered easily over the side of the ship, it was necessary to relocate the original drop position by maneuvering

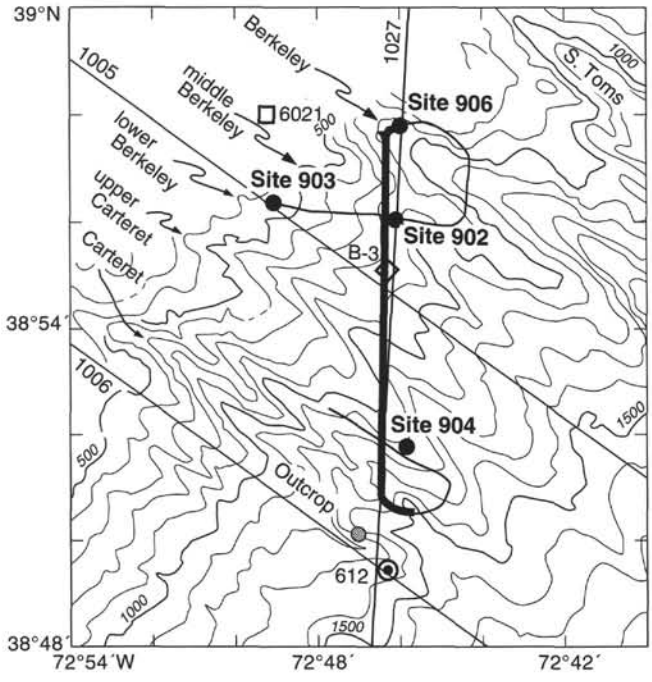

Figure 1. SeaBeam bathymetry with survey tracks near Sites 902 through 906. Heavy line indicates the ship track for *JOIDES Resolution* SCS Line 2; very heavy line indicates the portion of the track shown in Figure 2. Canyons are indicated by arrows. The outcrop indicated near Site 612 was sampled using the *Alvin* in 1989.

in dynamic positioning (DP) mode. A second positioning beacon was launched at 0345 hr (Universal Time Coordinated [UTC]) on 1 July and the pipe trip began at 0430, 3 hr after the original beacon launch.

Because of sloping bathymetry, the water depth was poorly determined by the precision depth recorder (PDR). Four "water cores" were attempted for an additional 2-hr delay before the APC found the seafloor at 1134 m below driller's datum—34 m deeper than the PDR reading (see Chapter 4, this volume).

Despite the slow start, coring proceeded rapidly in silty clays. Some incomplete APC strokes occurred below about 100 mbsf and two APC cores were advanced by recovery (Table 1) at 222 mbsf, overpull refusal was reached. When the core barrel from Core 150-904A-24H could not be withdrawn with 120,000 lb overpull, it was necessary to "drill over" the barrel for 5 m before the suction was broken. The recent APC modifications functioned properly to prevent over-torquing of the rods, but both sections of the core barrel were gouged severely by the polycrystalline diamond compact (PDC) core bit.

Coring with the XCB proceeded with excellent recovery and rate of penetration (ROP) through more silty clay and mudstones to chalk at 340 mbsf. The benign conditions persisted until porcellanitic chalk was encountered at about 524 mbsf. Lower ROP and some core jamming prevailed below that depth (Table 1), but scientific objectives were declared fulfilled at 576.7 mbsf and coring operations were discontinued.

In contrast to the previous hole, logging operations went quite smoothly. The standard wiper trip was made, with no resistance encountered in the hole, and a mud sweep was circulated. With the pipe at 96 mbsf, the SES was rigged and logging began. Successful sonic induction–gamma ray, lithoporosity, and FMS logs were recorded from within about 30 m of total depth over the accessible open-hole interval. Though fill at the bottom of the hole increased by several meters after each run, the hole was found to be in excellent condition for logging below about 235 mbsf and fair to good shape above that. Favorable conditions were attributed to a "young" hole produced by rapid penetration and low circulation rates.

Table 1. Coring summary, Site 904.

Core no.	Date (July 1993)	Time (UTC)	Depth (mbsf)	Length cored (m)	Length recovered (m)	Recovery (%)
150-904A-						
1H	1	0950	0.0–9.0	9.0	8.62	95.8
2H	1	1020	9.0–18.5	9.5	9.31	98.0
3H	1	1035	18.5–28.0	9.5	9.47	99.7
4H	1	1050	28.0–37.5	9.5	9.08	95.6
5H	1	1130	37.5–47.0	9.5	9.64	101.0
6H	1	1200	47.0–56.5	9.5	9.93	104.0
7H	1	1230	56.5–66.0	9.5	9.93	104.0
8H	1	1255	66.0–75.5	9.5	9.81	103.0
9H	1	1340	75.5–85.0	9.5	9.92	104.0
10H	1	1410	85.0–94.5	9.5	10.07	106.0
11H	1	1440	94.5–104.0	9.5	9.96	105.0
12H	1	1520	104.0–111.0	7.0	7.23	103.0
13H	1	1600	111.0–120.5	9.5	9.94	104.0
14H	1	1645	120.5–130.0	9.5	9.89	104.0
15H	1	1710	130.0–139.5	9.5	9.17	96.5
16H	1	1740	139.5–149.0	9.5	9.11	95.9
17H	1	1810	149.0–158.5	9.5	10.01	105.3
18H	1	1840	158.5–168.0	9.5	9.27	97.6
19H	1	1910	168.0–177.5	9.5	9.73	102.0
20H	1	1945	177.5–187.0	9.5	7.71	81.1
21H	1	2020	187.0–196.5	9.5	8.74	92.0
22H	1	2145	196.5–203.0	6.5	6.52	100.0
23H	1	2215	203.0–212.5	9.5	9.12	96.0
24H	1	2315	212.5–222.0	9.5	9.36	98.5
25X	2	0000	222.0–231.3	9.3	9.23	99.2
26X	2	0045	231.3–240.9	9.6	9.90	103.0
27X	2	0115	240.9–250.3	9.4	9.80	104.0
28X	2	0215	250.3–260.1	9.8	7.84	80.0
29X	2	0255	260.1–269.8	9.7	9.78	101.0
30X	2	0325	269.8–279.5	9.7	9.86	101.0
31X	2	0355	279.5–289.1	9.6	9.80	102.0
32X	2	0415	289.1–298.8	9.7	9.78	101.0
33X	2	0440	298.8–308.4	9.6	9.80	102.0
34X	2	0500	308.4–317.8	9.4	9.91	105.0
35X	2	0525	317.8–327.2	9.4	9.75	104.0
36X	2	0555	327.2–336.5	9.3	9.77	105.0
37X	2	0625	336.5–345.8	9.3	9.23	99.2
38X	2	0655	345.8–355.5	9.7	9.50	97.9
39X	2	0730	355.5–365.1	9.6	9.81	102.0
40X	2	0755	365.1–374.8	9.7	9.80	101.0
41X	2	0820	374.8–384.4	9.6	9.93	103.0
42X	2	0850	384.4–394.1	9.7	9.81	101.0
43X	2	0925	394.1–403.8	9.7	9.75	100.0
44X	2	0950	403.8–413.4	9.6	9.80	102.0
45X	2	1020	413.4–423.0	9.6	9.90	103.0
46X	2	1050	423.0–432.5	9.5	9.78	103.0
47X	2	1135	432.5–442.0	9.5	9.85	103.0
48X	2	1205	442.0–451.5	9.5	9.82	103.0
49X	2	1235	451.5–461.2	9.7	9.88	102.0
50X	2	1305	461.2–470.9	9.7	9.54	98.3
51X	2	1350	470.9–480.5	9.6	9.83	102.0
52X	2	1415	480.5–490.2	9.7	9.70	100.0
53X	2	1455	490.2–499.8	9.6	9.90	103.0
54X	2	1530	499.8–509.5	9.7	9.84	101.0
55X	2	1630	509.5–518.8	9.3	9.52	102.0
56X	2	1730	518.8–528.4	9.6	8.93	93.0
57X	2	1820	528.4–529.4	1.0	0.24	24.0
58X	2	2015	529.4–538.0	8.6	8.44	98.1
59X	2	2200	538.0–547.7	9.7	9.05	93.3
60X	3	0000	547.7–557.3	9.6	0.77	8.0
61X	3	0130	557.3–567.0	9.7	7.98	82.2
62X	3	0300	567.0–576.7	9.7	0.69	7.1
Coring totals				576.7	557.55	96.7

Upon completion of logging operations and rig-down of the SES and logging equipment, the drill string was run back into the hole for plugging. Tight hole or fill was encountered at 541 mbsf, so the bit was raised a few meters and 150 bbl of 10 lb/gal mud were displaced into the hole. Plugging was completed by spotting a 15-bbl batch of 15 lb/gal cement slurry at 216 mbsf.

Site 904 was abandoned at 1130 hr, 4 July 1993, when the core bit arrived on deck and the vessel departed for Site 905.

LITHOSTRATIGRAPHY

The stratigraphic section recovered at Site 904 represents a partial record of the continental slope stratigraphy preserved at Sites 902 and 903. With the exception of lithologic Units II and III of Site 903, all lithostratigraphic subdivisions recognized at the two previous slope

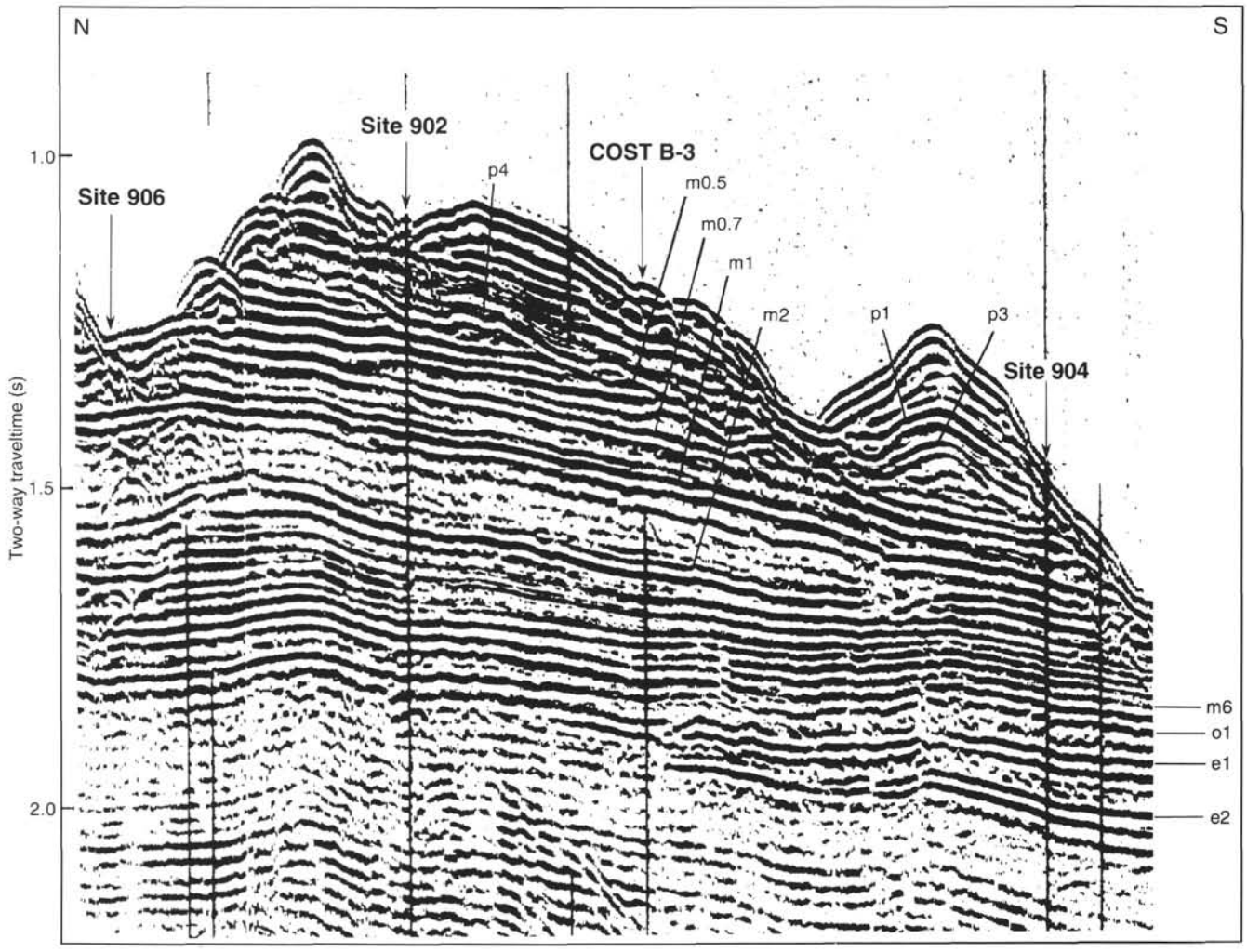

Figure 2. Part of *JOIDES Resolution* SCS Line 2 across Sites 902, 904, and 906 and stratigraphic test well COST B-3. Ship track is shown as heavy line in Figure 1. Each of the reflectors identified on this profile were penetrated and correlated to cores recovered at Site 904. C/C = change course.

sites can also be recognized at Site 904 (Table 2 and Figs. 3–4). The Pleistocene to Oligocene section at Site 904 is only 340 m thick, compared with 1064 m at Site 903 and 681 m at Site 902. This reduced thickness is the result of erosion of Units II and III and, probably, a combination of erosion and lower accumulation rates in Units I, IV, V, and VI. We recognize that the unit boundaries used for correlating Site 904 with Sites 902 and 903 are not time lines and may represent diachronous facies or diagenetic boundaries. Core recovery at Site 904 was very good and represents a very complete record of sedimentation on the present-day middle slope. Apart from zones of flow-in at the base of many APC cores, the only significant core losses were in Core 150-904A-28X, in Unit V and at the base of the hole (Fig. 4).

Unit I

Intervals: Sections 150-904A-1H-1, 0 cm, to -12H-2, 65 cm
Depth: 0–106.2 mbsf
Age: Holocene to middle Pleistocene

This unit grades broadly from gray and pinkish gray, homogeneous and slightly bioturbated silty clays at the top, through an interval of thinly interbedded, graded, fine sands and color-banded silty clays to coarse, poorly sorted mass-flow deposits at the base. The thick interval of thinly bedded, normally graded sands and color banding was not observed at the base of Unit I at previous sites. The Holocene/upper Pleistocene boundary occurs at 4.27 mbsf (Section 150-904A-1H-3, 127 cm), associated with a color change (greenish gray to pinkish gray) and an increase in the lithification of the sediment from soupy to moderately firm.

Homogeneous to heavily bioturbated silty clays characterize the upper 64 m of Unit I. These silty clays display thick, pinkish gray and gray color bands (typically 50–100 cm), with both gradational and sharp boundaries and no distinct pattern to coloration above or below sharp boundaries. Pinkish gray silty clay also commonly fills burrows, resulting in a distinctly mottled appearance. Iron monosulfides are abundant between 4.5 and 43 mbsf, concentrated largely in small burrows (<1 cm) filled with silty clay and very fine to fine quartz sand. Iron monosulfides also occur as streaks across the freshly cut core. At 17.7, 19.3, and 27.3 mbsf, small (<1 cm) pyrite nodules occur. The common intervals of very fine- to fine-sand-filled burrows together with the rare occurrence of undisturbed, thin laminae of normally graded very fine to fine quartz and mica sand suggests that a portion of this interval was deposited as laminated silty clay and thin sand laminae, then intermixed by bioturbation. Rare, complete shells and fragments are scattered throughout the sequence. The X-ray diffraction (XRD) analyses indicate that Unit I is characterized by low calcite and the occurrence of dolomite (possibly reworked), opal-A, and pyrite (Fig. 5).

Between 42 and 64 mbsf, greenish gray silty clay is interbedded with gray silty clays. The green color correlates with increased diatom

Table 2. Lithostratigraphy, Site 904.

Units or subunits	Series	Depth (mbsf)	Lithology	Process
I	upper to middle Pleistocene	0–106.2 mbsf (150-904A-1H-1, 0 cm, through -12H-2, 65 cm)	Greenish gray silty clay, thin interbeds of graded fine sand, glauconite sands at base.	Hemipelagic, low-density turbidity currents, slumps, and mass flows at the base.
		Major disconformity		
IVA	upper to ?middle Miocene	106.2–167.8 mbsf (150-904A-12H-2, 65 cm, through -18H-CC, 18 cm)	Greenish gray silty clay siderite/calcite nodules and bands; sand interval near the base.	Hemipelagic, low-density turbidity currents, and mass-flow.
IVB	?upper to middle Miocene	168.0–223.9 mbsf (150-904A-19H-1, 0 cm, through -25X-2, 35 cm)	Greenish gray silty clay siderite/calcite nodules and bands; sand interval near the base.	Hemipelagic, low-density turbidity currents, and mass-flow.
V	lower to middle Miocene	223.9–296.5 mbsf (150-904A-25X-2, 35 cm, through -32X-5, 140 cm)	Dark greenish brown interbedded glauconitic silty clays with abundant diatoms.	Hemipelagic and gravity- controlled flows.
VI	lower Miocene to upper Oligocene	296.5–341.2 mbsf (150-904A-32X-5, 140 cm, through -37X-4, 20 cm)	Olive gray clayey silts and silty clays with silt-sized glauconite and abundant nannofossils.	Hemipelagic and gravity- controlled flows.
		Major disconformity		
VIIA	upper to middle Eocene	341.2–418.9 mbsf (150-904A-37X-4, 20 cm, through -45X-4, 100 cm)	Greenish gray clayey nannofossil chalk with diatoms, radiolarians, and foraminifers.	Pelagic with minor hemipelagic input.
VIIB	middle Eocene	418.9–567.7 mbsf (150-904A-45X-4, 100 cm, through -62X-CC, 43 cm)	Light greenish gray clayey nannofossil chalk with diatoms, radiolarians, and foraminifers.	Pelagic with minor hemipelagic input.

abundance (generally 10%, with a high of 30% at 44 mbsf according to smear-slide data; the maximum opal-A peak defined by XRD also occurs at 44 mbsf). The abundance of glauconite is less than 4%. Smear slides also show that nannofossils are relatively abundant in this interval (10%–15%). The boundaries between the diatom-rich and -poor silty clays are gradational to sharp and show no sign of burrowing. Thus, the intervals of greenish gray silty clay apparently represent periods of higher surface-water productivity, whereas the gray silty clays are periods of dominantly terrigenous sediment with lower biogenic productivity.

The lithologic character of Unit I is distinctly different between 64.0 and 106.1 mbsf. Well-defined color laminations and undisturbed, normally graded sand laminae occur from 63 to 95 m (Cores 150-904A-7H to -12H). These sediments are not bioturbated, suggesting that some factor suppressed the activity of the benthic organisms. Low TOC and sulfur values suggest that dysaerobic-anaerobic bottom-water conditions were not developed (see "Organic Geochemistry" section, this chapter); therefore, it is unlikely that these sediments were deposited in a well-developed oxygen minimum zone. Four cycles of thinly laminated silty clays and fine sands (63.3–68.2, 68.2–74.4, 74.4–80.8, and 80.8–94.8 mbsf) can be distinguished (Fig. 6). Each cycle can be divided into four different facies. These are, from top to bottom, (1) an upper zone of slightly bioturbated silty clays; (2) a zone of color-banded silts and silty clays, which display very fine, normal grading; (3) color-banded silts and silty clays (2–5 cm thick) with common, normally graded, very fine to fine quartz sand laminae; and (4) a basal zone of graded, fine quartz sand layers (2–5 cm thick) with sharp erosional bases interbedded with silty clays.

Smear slides show a slight decrease in quartz and sand abundance from the base to the top of each cycle. This pattern suggests an upward waning of sediment input. Taken as a whole, the four cycles suggest four pulses of rapid sedimentation, followed by a period of gradually decreasing sediment supply.

A 4-m-thick interval of convoluted strata composed of color-banded silt and silty clay occurs between 96 and 99 mbsf (Core 150-904A-11H). It appears to represent a slump deposit and displays isoclinal and recumbent folds with possible fluid-escape structures at 97.6 and 98.3 mbsf. This interval grades up into bioturbated silty clay. The lower contact of the slump with underlying coarse sand mass flows is uncertain because 4.5 m of flow-in occurs at the base of Core 150-904A-11H.

The basal sediments of Unit I consist of three beds of poorly sorted sand with lithic clasts (Sections 150-904A-12H-1 to -2, 66 cm). The upper bed grades upward from a coarse sand with abundant granules at the base through sandy silts with rare lithic pebbles into gray silty clay, similar in composition and color to the overlying slumped silty clays. The two basal sand intervals are similar and consist of poorly sorted glauconite, quartz, and lithic grains with no evidence of grading. These beds have sharp, possibly erosional bases. The poor sorting of these sand units suggest they represent sandy mass-flow deposits.

The nature of the lower boundary of the basal mass-flow sand (106.2 mbsf; Fig. 7) is uncertain. The contact has an irregular surface, suggesting either erosional scouring (e.g., flute casts) or burrowing. Burrows are concentrated in a 20-cm interval below the Unit I/IV boundary. These contain pale buff-colored, fine sand of apparently different provenance than the mass-flow sands above the boundary. The occurrence of these burrows and the absence of glauconitic material in their fills indicates that bioturbation occurred at this boundary; however, it predated the glauconitic mass-flow sands and postdated an extensive erosional event. This erosional event is indicated by a large hiatus (middle Pleistocene to late Miocene; see "Biostratigraphy" section, this chapter) and the absence of Units II and III of Site 903. This boundary may correlate to reflector m 0.7 (blue) (see "Seismic Stratigraphy" section, this chapter).

Unit IV

Interval: Sections 150-904A-12H-2, 65 cm, to -25X-2, 35 cm
Depth: 106.2–223.9 mbsf
Age: upper to middle Miocene

Subunit IVA

Interval: Sections 150-904A-12H-2, 65 cm, to -18H-CC, 18 cm
Depth: 106.2–167.8 mbsf

Subunit IVB

Interval: Sections 150-904A-19H-1, 0 cm, to -25X-2, 35 cm
Depth: 168.0–223.9 mbsf

Unit IV is lithologically very similar to the upper middle to upper Miocene sediments of Unit IV at Sites 902, 903, and 906, and is like-

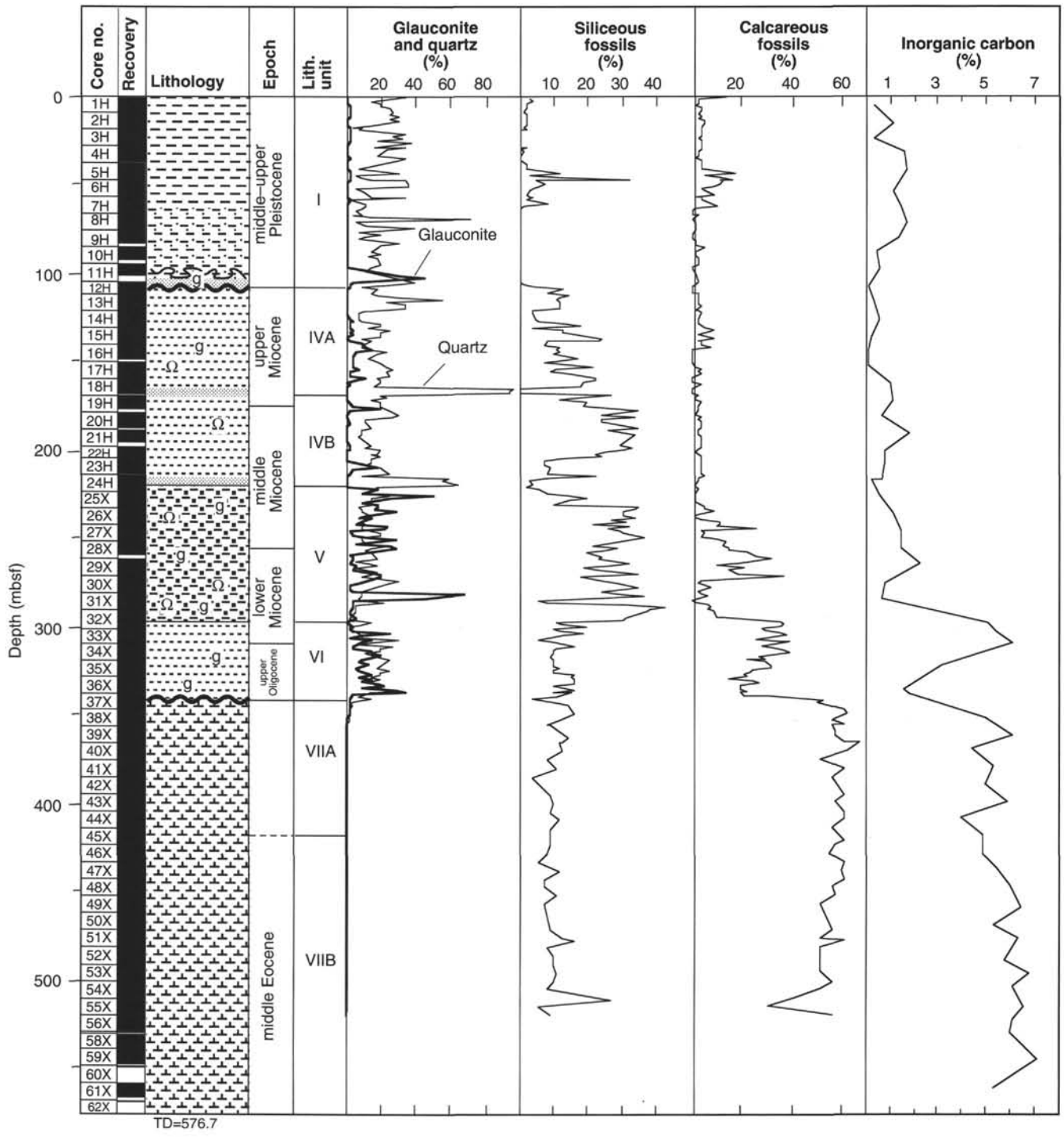

Figure 3. Generalized lithologic column for Hole 904A showing abundances of glauconite and quartz, siliceous and calcareous fossil content (determined from smear slides), and total inorganic carbon.

wise divided into Subunits IVA and IVB. Unit IV is characterized by gray to dark gray, bioturbated silty clay with sporadic buff-colored carbonate and black pyrite nodules. Distinctive, sandy intervals occur in the middle and just above the base of the unit. The recovery gap at the base of the middle sandy interval marks the boundary between Subunits IVA and IVB (Sections 150-904A-18H-CC, 18 cm, to -19H-1, 0 cm; 167.8–168.0 mbsf). The XRD analyses indicate that calcite is almost absent in Unit IV. This agrees with the inorganic carbon analyses (see "Organic Geochemistry" section, this chapter), although smear slides indicate a few percent of calcareous fossils (Fig. 3). The abundance of feldspar and quartz decreases in abundance downhole (Fig. 5).

The gray, moderately to heavily bioturbated, silty clays that dominate Unit IV also contain interbeds of diatom-rich silty clays with variable quantities of glauconite. Although the boundaries of these diatom/glauconite-rich units are typically gradational, sharp, highly burrowed contacts are also observed (e.g., 137.9 and 180.3 mbsf). The diatom-poor silty clays are gray to dark gray (10Y 5/1 to 10Y 4/1)

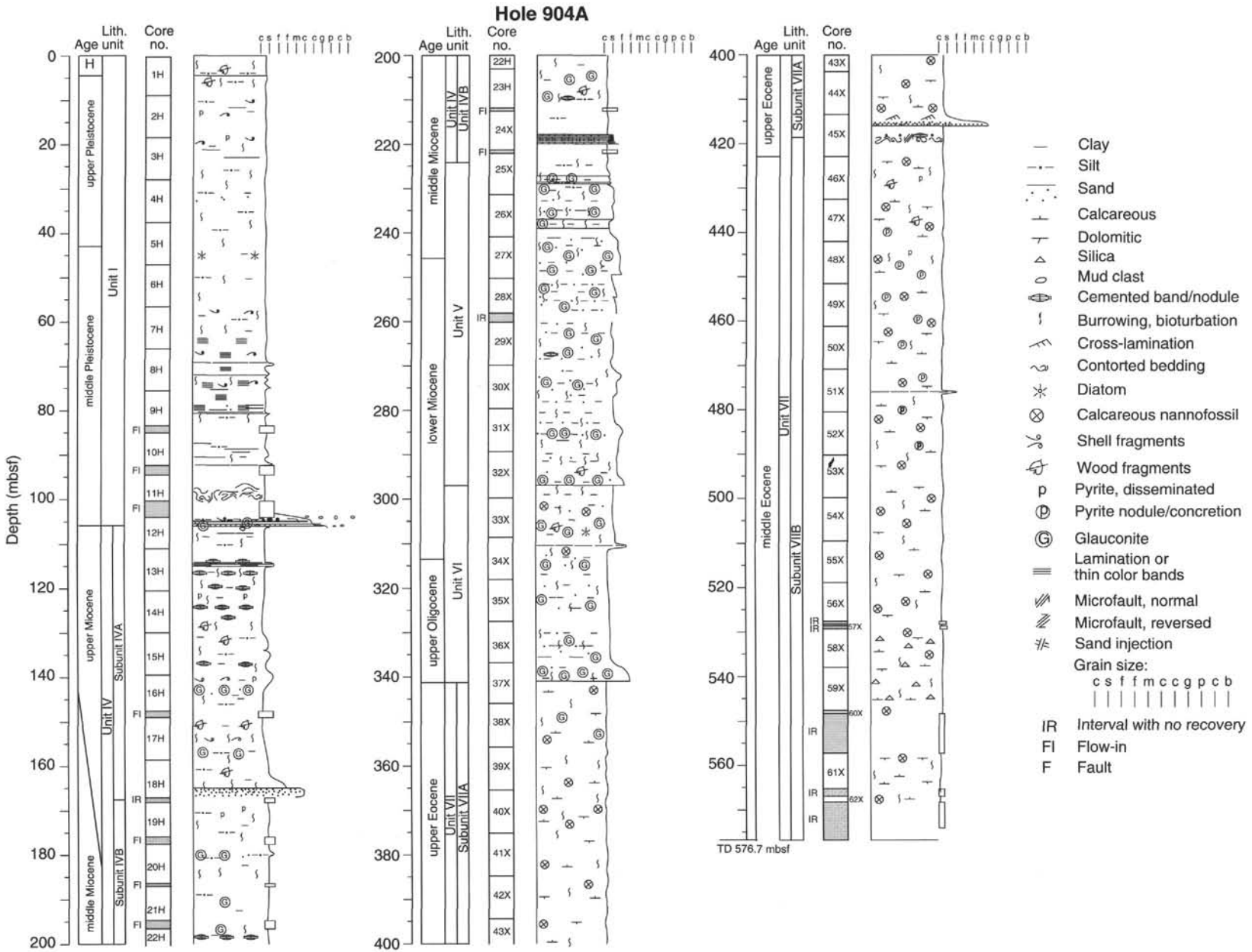

Figure 4. Detailed summary lithologic columns, Hole 904A. See also Plate 2 (in back-pocket foldout). H = Holocene. TD = total depth.

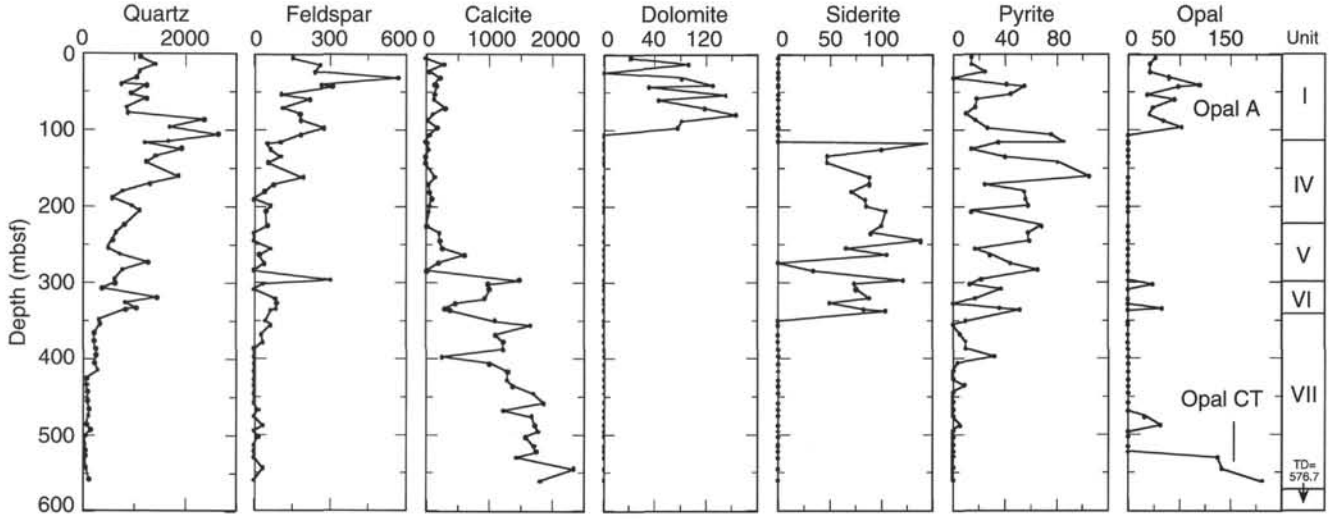

Figure 5. X-ray diffraction analyses for Hole 904A plotted according to the intensity of the mineral's main diffraction peak: quartz (3.33Å), feldspar (3.25Å), calcite (2.89Å), dolomite (2.89Å), siderite (2.8Å), pyrite (2.71Å), opal-A (very broad peak at 4Å), and opal-CT (near 4.1Å).

and moderately to heavily bioturbated; they contain quartz and mica silt. Cream- to buff-colored nodules and bands occur exclusively in this lithology (114.4–128.0, 168.8–175.5, and 193–212.5 mbsf). The nodules are poorly lithified (in contrast to the well-lithified nodules of Unit IV in Sites 903 and 902), typically have diffuse margins, and are composed of microcrystalline siderite and calcite. Small pyrite nodules, rarely larger than 1 cm, occur throughout the same interval as the carbonate nodules and bands (e.g., 120.5–124.5 and 168–171 mbsf). Smear slides indicate that these gray, silty clays contain little biogenic material.

Thin beds and laminae of graded, very fine to fine quartz sand with sharp bases are interbedded sporadically with the gray, silty clay (e.g., 114.3 mbsf, Section 150-904A-13H-3). Abundant small burrows filled with very fine to fine quartz and mica sand occur in the heavily bioturbated zones, commonly concentrated over short intervals (e.g., 5–10 cm). This suggests either the redistribution of sandy laminae by burrowing or the concentration of disseminated sand by bioturbating organisms.

The diatom-rich silty clays are dark greenish gray and moderately to heavily bioturbated; they contain abundant silt- to fine sand-sized glauconite, minor amounts of quartz silt and fine sand, and up to 30% diatoms. These greenish silty clay intervals are 5–7 m thick and grade down into gray silty clays. At 137.8 mbsf (Section 150-904A-15H-6), the contact between the gray silty clay and the overlying green-gray diatom-rich silty clay is sharp. Large, very irregular burrows, filled with glauconitic sand, extend 40 cm below this contact. The reverse relationship occurs at 141.3 mbsf (Section 150-904A-16H-2), where burrows filled with gray, silty clay occur in diatom-rich silty clay below.

The sand interval at the base of Subunit IVA (164–168 mbsf, Core 150-904A-18H), is a poorly consolidated, poorly sorted medium to very coarse sand. Subangular to well-rounded quartz is the dominant constituent with minor glauconite, fragmental pyrite, and shell fragments. The interval is normally graded from granules and very coarse sand at the base, fining upward to medium sand. The top contact of the bed is highly bioturbated and is a 25-cm-thick zone of intermixed sand and silty clay.

A 5.1-m-thick interval of thinly laminated, internally graded, very fine to fine quartz sand occurs 1.9 m above the base of Unit IV (215.6–220.7 mbsf, Core 150-904A-24H). This interval displays a basal upward-coarsening zone, a middle zone of laminated sand and silts, and an upper upward-fining zone that grades into the gray silty clays above. The basal zone consists of interbedded clayey silt and sandy silt laminae, in which the clay-rich laminae are replaced by siderite. The occurrence of truncation surfaces and soft-sediment deformation features, including small reverse faults, suggest that this zone is slumped (Fig. 8). The middle zone is a 3.5-m-thick interval of thinly laminated silty sand and silt. The laminae have sharp bases, with basal zones of very fine to fine quartz sand that grade upward to quartz silt. Laminae (1–2 mm thick) of comminuted plant fragments commonly occur at the contact between the sand and the silt. Silt-filled *Skolithos* commonly cross-cut the laminae. The thickness of each sand lamina decreases upward from 3–4 cm at the base to <1 cm at the top. Although bioturbation is typically limited, some intervals have been moderately bioturbated; consequently, much of the primary texture is lost. Siderite replacement of the silty zones occurs commonly. The upper portion is less well laminated because of moderate to heavy bioturbation. Sand abundance and grain size decreases upward to a gradational contact with the overlying gray silty clay. The top of these sands appears to correlate with reflector m2 (Yellow-2).

The sediments in the top 1.9 m of Core 150-904A-25X are very similar to the gray silty clays of Unit IV. Subvertical, tabular bodies of pyrite and siderite + calcite occur in this interval. The boundary with Unit V is gradational and coincides with a strongly bioturbated interval with well-preserved *Chondrites, Thalassinoides,* and *Terebellina* (Section 150-904A-25X-2, 35 cm).

Unit V

Interval: Sections 150-904A-25X-2, 35 cm, to -32X-5, 140 cm
Depth: 223.9–296.5 mbsf
Age: middle to lower Miocene

Highly bioturbated, dark green-brown, interbedded glauconitic sandy silts, silts, and silty clays are the dominant lithologies of Unit V. A major factor differentiating this unit from Unit IV is a higher calcium carbonate (calcite) content (Fig. 5; see also "Organic Geochemistry" section, this chapter), which is attributable to a gradational downward increase in calcareous nannofossil abundance to a maximum in the middle of the unit.

The alternation between glauconitic silty sands, silts, and silty clays is fairly rhythmic with glauconitic silty clays passing downward to glauconitic silty sands. Most bed boundaries are gradational; however, the lower contacts of beds of glauconitic sandy silts with underlying silty clays mark abrupt changes in the abundance of glauconite sand concentration. The surfaces between the two lithologies has been obscured by burrowing (e.g., at 231.3, 248.2, and 254.3 mbsf). The contacts between beds of glauconitic silty clay and the underlying glauconitic silty sand are less commonly sharp and highly bur-

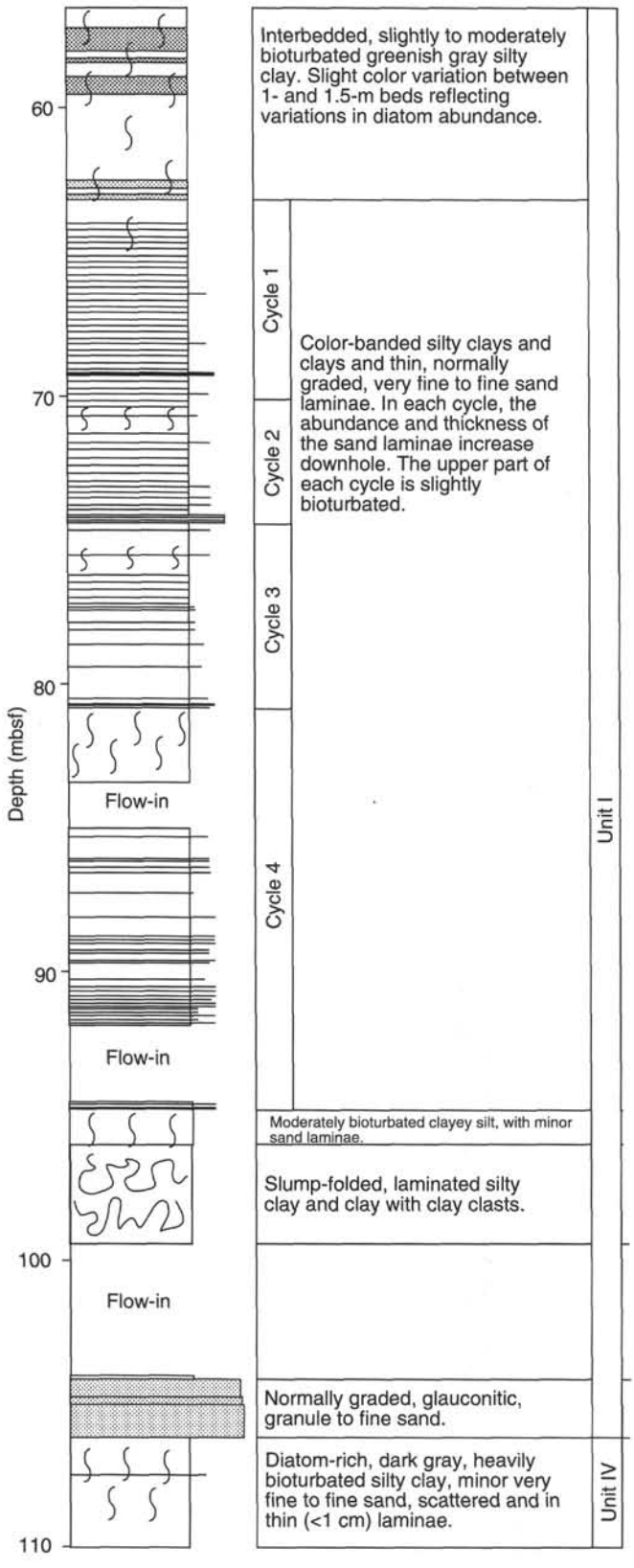

Figure 6. Detailed lithologic column of the lower part of Unit I and the uppermost part of Unit IV, Hole 904A (56.5–110 mbsf), showing the four upward-fining cycles near the base of Unit I.

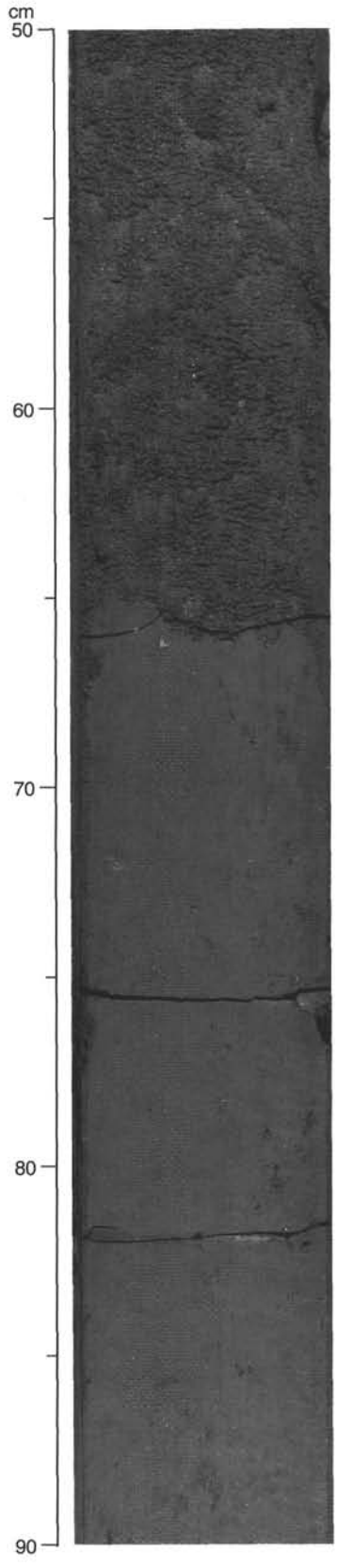

Figure 7. Detail of the unconformity between the basal, coarse, silty, glauconitic sand (middle Pleistocene) of Unit I and the bioturbated, gray silty clay (upper Miocene) of Unit IV (Interval 150-904A-12H-2, 50–90 cm).

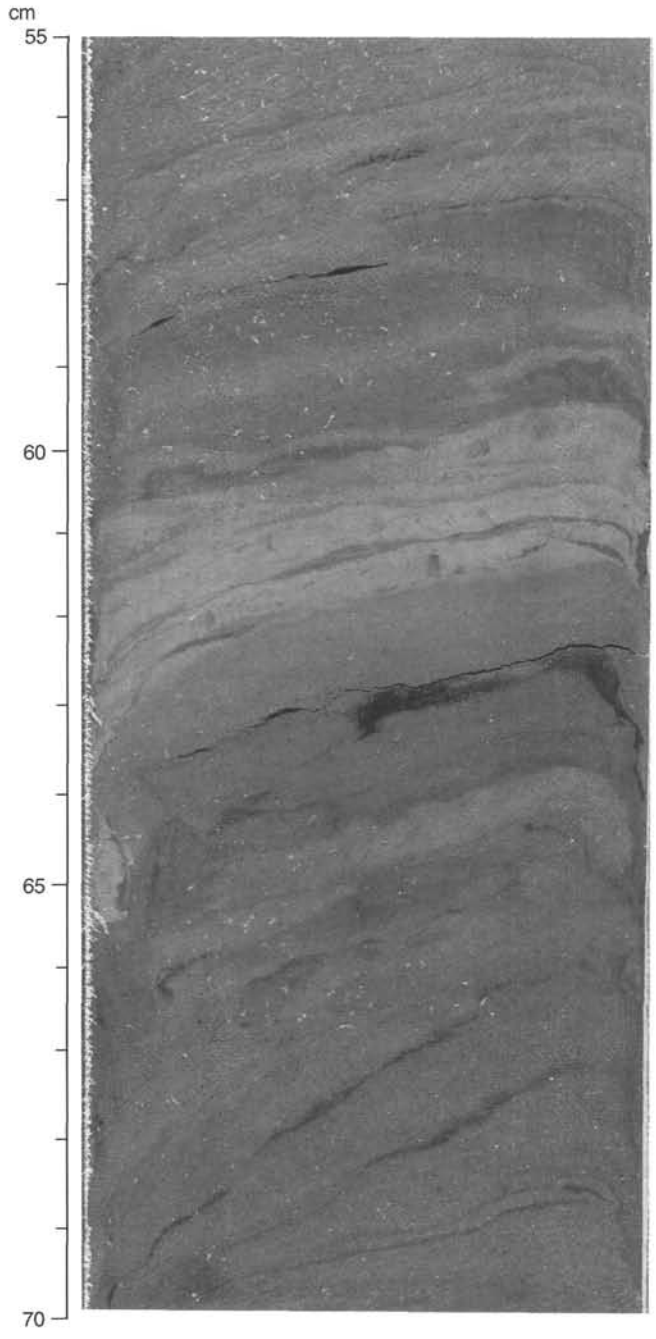

Figure 8. Thinly laminated silts and silty clays at 220.6 mbsf (Interval 150-904A-24H-6, 55–70 cm), displaying soft-sediment deformation structures.

rowed. An example of such a sharp contact occurs at 252.1 mbsf (Section 150-904A-28X-2, 30 cm). Bioturbation throughout the unit is heavy, with trace fossils including *Zoophycos, Chondrites, Planolites,* and *Thalassinoides.* An excellently displayed *Zoophycos* showing the axial shaft and the associated subhorizontal back-filled zones occurs at 252.2 mbsf (Fig. 9A).

Smear slides show a clear association between quartz and sand abundances and the occurrence of glauconite silty sands. No evidence is available to determine whether the sand-sized glauconite formed in situ or was derived from the continental shelf. The abundant sandy terrigenous material may reflect either increased terrigenous input or concentration of small amounts of material in a condensed, glauconite-forming environment. The glauconitic silty clays typically contain 30% diatoms and, in the middle of the unit between 260.5 and 272 mbsf, up to 30% calcareous nannofossils and minor quartz silt. The concentration of microfossils and the occurrence of disseminated silt-sized glauconite suggests that these intervals represent low sedimentation rates. Therefore, it would appear that the glauconitic silty sands were deposited during periods of relatively high sediment input from the shelf and the biogenic-rich silty clays were deposited during lulls in terrigenous input.

The lower boundary of Unit V is at the base of a 65-cm-thick, heavily bioturbated, glauconite sand bed (Section 150-904A-32X-5, 140 cm). The boundary between this bed and the underlying, olive gray clayey silts of Unit VI is sharp and highly burrowed. This boundary marks a significant downward increase in the abundance of calcareous nannofossils and a decrease in the diatom concentration.

Unit VI

Interval: Sections 150-904A-32X-5, 140 cm, to -37X-4, 20 cm
Depth: 296.5–341.2 mbsf
Age: lower Miocene to upper Oligocene

Unit VI consists primarily of bioturbated, olive gray clayey silts and silty clays with variable abundances of silt-sized glauconite and abundant calcareous nannofossils and common foraminifers. Rare plant fragments occur in the upper 15 m of the unit. Variations in concentrations of silt-sized glauconite result in thick color banding between olive gray and very dark gray. The glauconite-rich zones also contain more abundant quartz silt and fine sand. The contacts between glauconite-rich and -poor zones typically appear gradational; however, closer inspection shows that they are commonly sharp, but highly burrowed contacts. Unit VI contains a well-preserved ichnofauna that includes *Planolites, Zoophycos,* and rare *Skolithos.*

Smear slides indicate that calcareous nannofossils comprise 25%–30% of the sediment volume at the top of Unit VI. Abundances steadily decrease to 15% at the base of the unit. Diatoms are relatively abundant (10%) at the top and base of the unit, but they decrease to <5% in the middle (306–326 mbsf).

The basal 3.8 m of Unit VI is heavily bioturbated, olive gray, silty clay with very abundant sand- and silt-sized glauconite (Core 150-904A-37X). Glauconite concentrations increase downward to 340.3 mbsf and then decrease between 340.7 and 341.2 mbsf. The upper boundary of this interval with the overlying glauconite sands is heavily burrowed. The lower boundary with Unit VII is sharp, with no evidence of burrowing activity penetrating down into the underlying chalks (Fig. 10). The lighter color of this interval may be caused by calcareous material reworked from Unit VII.

Unit VII

Interval: Sections 150-904A-37X-4, 20 cm, to -62X-CC, 40 cm
Depth: 341.2–576.7 mbsf
Age: upper to middle Eocene

Subunit VIIA

Interval: Sections 150-904A-37X-4, 20 cm, to -45X-4, 100 cm
Depth: 341.2–418.9 mbsf

Subunit VIIB

Interval: Sections 150-904A-45X-4, 100 cm, to -62X-CC, 40 cm
Depth: 418.9–576.7 mbsf

Unit VII consists of bioturbated, nannofossil chalk with minor clay and common foraminifers. Unit VII can be divided into two subunits (VIIA and VIIB). The boundary between the subunits occurs at 417.9 mbsf and corresponds to an abrupt, downhole decrease in clay content and an associated color change from greenish gray (5GY 6/1) above to light greenish gray (5GY 7/1) below the contact. This boundary is clearly seen in the gamma-ray logs (see "Downhole Logging"

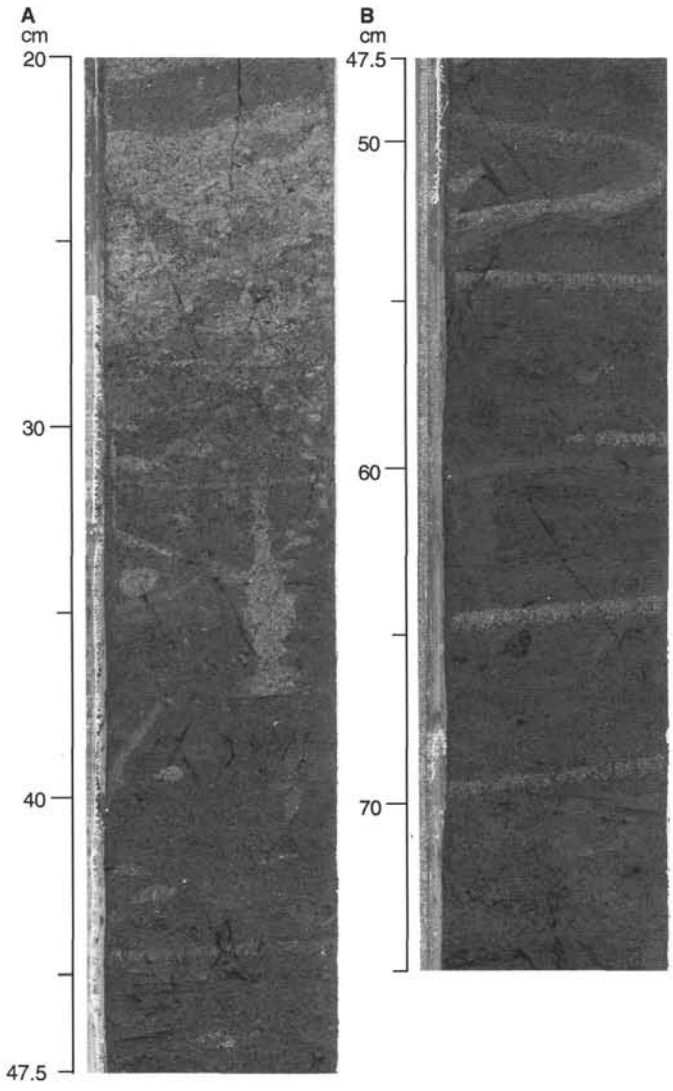

Figure 9. Well-preserved *Zoophycos* below a sharp contact at 252.1 mbsf. The axial shaft and associated subhorizontal back-filled zones can be seen clearly. **A.** Interval 150-904A-28X-2, 20–47.5 cm. **B.** Interval 150-904A-28X-2, 47.5–75 cm. Note differences in scale.

section, this chapter). The upper/middle Eocene boundary occurs just below this lithologic boundary, between 417.9 and 423.3 mbsf (in the lower half of Core 150-904A-45X; see "Biostratigraphy" section, this chapter). A thin, but distinctive zone, between 415.6 and 418.9 mbsf (Core 150-904A-45X), contains diverse lithologies, including chalk slumps, early diagenetic nodules, and thin graded laminae containing abundant microtektites. The base of this zone coincides with the base of Subunit VIIA. Near the bottom of Hole 904A, below about 525 mbsf, the chalks become more lithified because of an abrupt increase in the concentration of opal-CT (Fig. 5).

The original depositional fabric is largely masked by intense bioturbation. Faint 10- to 15-cm color banding is rarely observed (Section 150-904A-44X-7; 412.8 mbsf). The ichnofauna is well expressed because of the color contrast between the burrow fills (olive gray) and the chalk forming the background (light greenish gray). The ichnofauna in this unit is more diverse than it is in the units above. Trace fossils include *Chondrites, ?Diplocraterion, Planolites, Skolithos, Teichichnus, Thalassinoides, Zoophycos,* and other, unnamed, forms.

The microtektite-bearing interval contains three medium to very coarse sand laminae overlain by cross-laminated silts (Fig. 11). Close

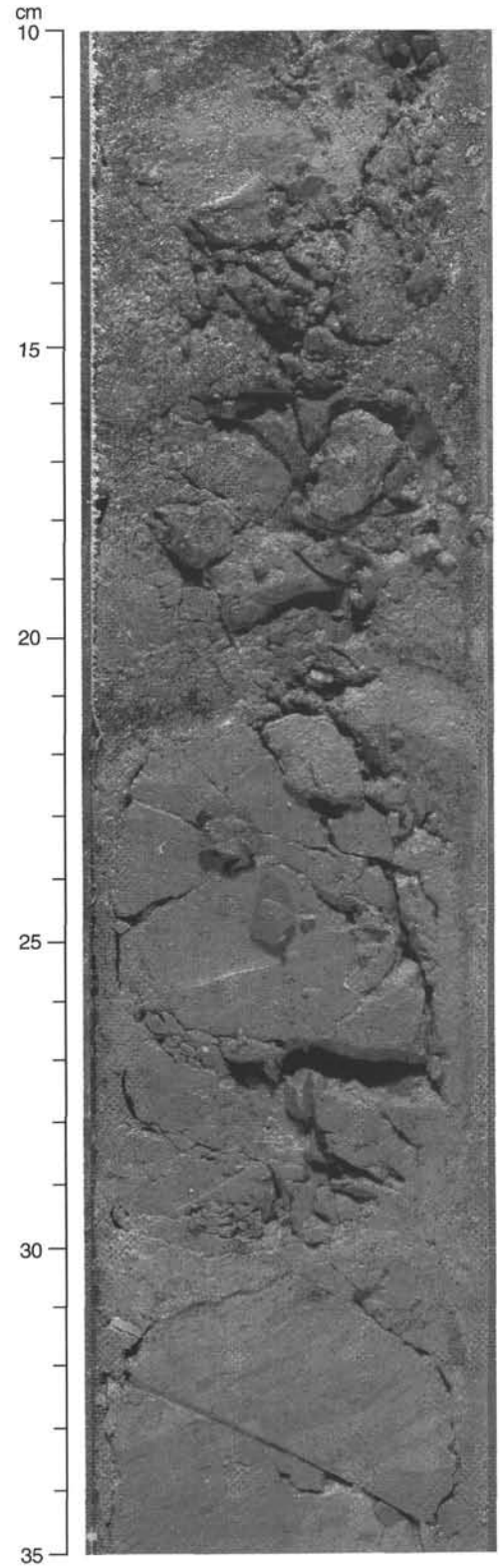

Figure 10. Sharp erosional contact between the glauconitic sandy silt of Unit VI (upper Oligocene) and clayey nannofossil chalk of Unit VII (upper Eocene) at 341.2 mbsf (Interval 150-904A-37X-4, 10–35 cm). There is no evidence of burrows piping glauconite sand below this contact.

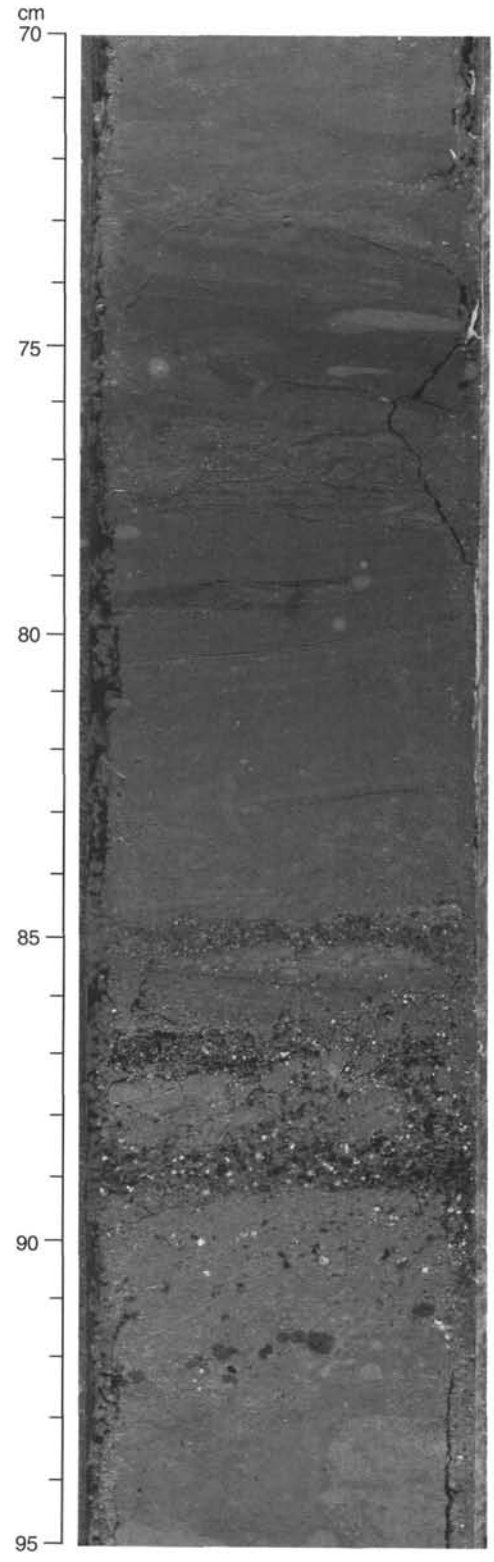

Figure 11. The tektite layer between 415.5 and 415.9 mbsf (Interval 150-904A-45X-2, 70–95 cm) in Unit VII (see Fig. 12).

inspection shows an intricate stratigraphy (Fig. 12). The lowermost lamina, which contains abundant microtektites, occurs at 415.8 mbsf and is 5 to 10 mm thick. This lamina is sharp-based and contains very coarse sand with 80% microtektites, 4% glauconite, and 5% opaques. This fines upward to clayey silt with calcareous nannofossils, diatoms, radiolarians, and minor foraminifers. Scattered microtektites occur in the chalk down to 2 cm below this sand lamina. The second lamina is 2 cm thick and contains coarse sand at the base, which fines up to planar, microlaminated, medium sand. This layer contains up to 80% microtektites with 3% glauconite at the base and 10% quartz and 5% opaques at the top. The overlying 5-mm-thick silt contains calcareous nannofossils, minor radiolarians, diatoms, and foraminifers. The upper of the three sand laminae contains very fine- to fine-sized sand with minor coarse sand grains. Microtektite abundance is only 30% and quartz is 30%. The top of this sand lamina marks a change in the depositional style from thin, normally graded sands to a 9-cm-thick interval of bioturbated laminated silt. A basal zone with *Chondrites* is overlain by cross-laminated silt. The top of this interval is convoluted. The silt grades up to clayey nannofossil chalk at 415.6 mbsf. The quartz abundance in the silt interval increases from 5% at the base to 50% at the top. Calcareous nannofossils decrease in abundance upward and diatoms and radiolarians increase slightly.

Close examination of the coarse fraction from this interval (see Fig. 12 for sample intervals) indicates that the microtektites are fine- to coarse-grained, sand-sized glass particles (100–1000 μm) (Fig. 13). The glass fragments are spherical, teardrop, cylindrical, and irregular in shape. Grains with conchoidal fractures are common. Most microtektites are pale yellowish to brownish in color with a vitreous luster and are transparent under plane polarized light. Some grains are translucent and have buff-colored frosted surfaces. All microtektites have dark birefringence between cross nicols. Glass fragments with gas inclusions and/or vesicular surfaces are common. The surfaces of some grains are smooth whereas others show evidence of corrosion, such as pitting and etching.

Microtektites occur in association with pyrite (up to 10%), and some glass fragments are coated with a metallic and/or dark film, possibly a sulfide. Quartz grains are common (up to 30%) and show evidence of strain such as irregular and undulatory extinction. Glauconite grains are a minor component (5%).

Clay mineral associations from 14 samples across the microtektite layer (Interval 150-904A-45X-2, 50–130 cm) are predominantly smectite with minor illite and kaolinite (Fig. 14). Clay mineral variations are slight, but the microtektite layer is significantly enriched with smectite, which is also more abundant above this layer than below. Eocene clay sedimentation in the North Atlantic is dominated by smectite, partly reworked from continental areas (Chamley, 1989). The smectite enrichment in the microtektite layer and the sediment above may have resulted from submarine alteration of glass spherules. A similar trend is observed at the Cretaceous/Tertiary boundary at Stevns Klint, Denmark (Kastner et al., 1984).

Examination of benthic foraminifers from nine samples encompassing the microtektite layer (Sections 150-904A-45X-2, 79 through 96 cm; Fig. 12) show that the faunas are almost exclusively middle to lower bathyal (600–2000 m). These faunas are similar to those from the rest of the upper Eocene section at Site 904, consistent with in situ deposition (see "Biostratigraphy" section, this chapter, for a description of the faunas). Only two shallow-water specimens were noted: *Elphidium* spp. (generally <100 m) was found in Sample 150-904A-45X-2, 87–88 cm; and one abraded specimen of *Cibicidoides* sp. cf. *dutemplei* (100–600 m) was found in Sample 150-904A-45X-2, 95–96 cm. Thus, we conclude that little benthic foraminifer faunal evidence exists for downslope transport of sediments during deposition of the microtektite layer.

The clayey nannofossil chalk below the microtektite interval contains evidence that the diagenetic conditions in this interval were different from those that affected the remainder of Unit VII at Site 904. A calcite nodule occurs at 416.3 mbsf. Within the nodule are burrows

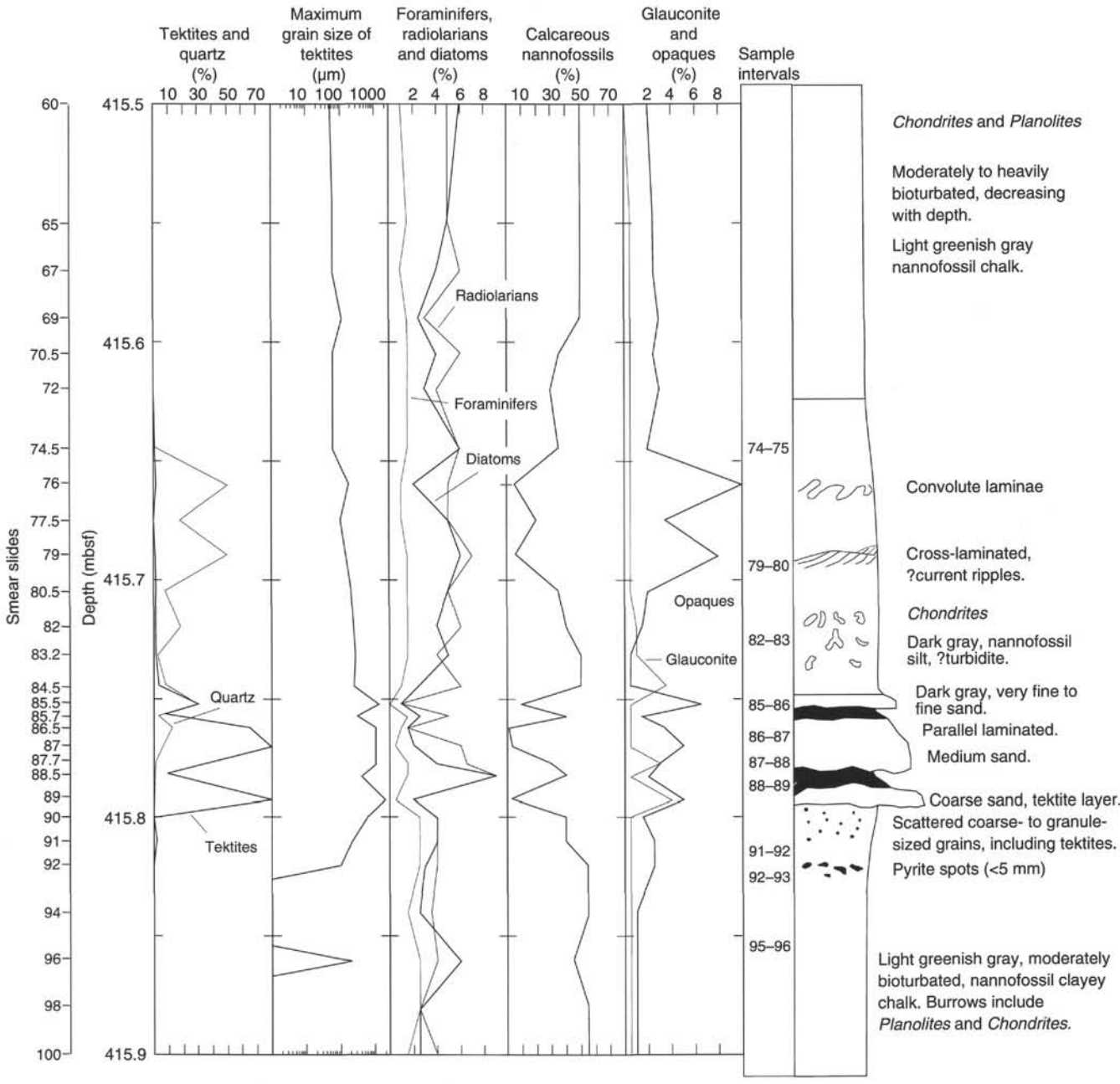

Figure 12. Detailed stratigraphy and smear-slide data for the tektite layer (Interval 150-904A-45X-2, 70–95 cm).

undeformed by compaction, and clayey laminae wrap around its outer margin, suggesting early diagenetic formation. The structure of this nodule is very similar to that of the carbonate nodule that occurs in Hole 903C at 1109.8 mbsf, below an interval of siliciclastic sand, which also bears microtektites.

Chalks with probable slump folds occur between 416.4 and 418.9 mbsf. The base of this slumped interval marks the base of Subunit VIIA. One meter higher in the section there occurs within slumped chalks an abrupt color change (5GY 6/1 to 5GY 7/1), coinciding with a boundary between calcareous nannofossil Zones NP19–20 and NP18 (see "Biostratigraphy" section, this chapter).

The nannofossil chalks contain abundant foraminifers and siliceous microfossils. The foraminifers at this site are better preserved than at Site 903. Test walls and pore structures are not altered or recrystallized, and less breakage and dissolution has occurred apparently. Foraminifer chambers maintain their initial primary structures but are commonly filled with opal-CT, which forms from the dissolution and reprecipitation of biogenic opal-A. The structures of siliceous microfossils (biogenic opal-A) are still recognizable, but, for the most part, siliceous tests have also been filled with opal-CT.

Former fluid-migration routes are more abundant downhole. These fluid pathways form broad zones delineated by dark-stained micrite and are filled in their central part by opal-CT. Foraminifer tests are rimmed by dark-stained micrite and are barely recognizable within these zones. Presumably, these fluid pathways indicate the occurrence of diagenetic dewatering that accompanies the transition of opal-A into opal-CT. This diagenetic reaction involves the expulsion of substantial amounts of water of crystallization. The abundance of fluid pathways downhole correlates with the occurrence of microfractures and with a change in the physical appearance of the sediment. Microfractures are

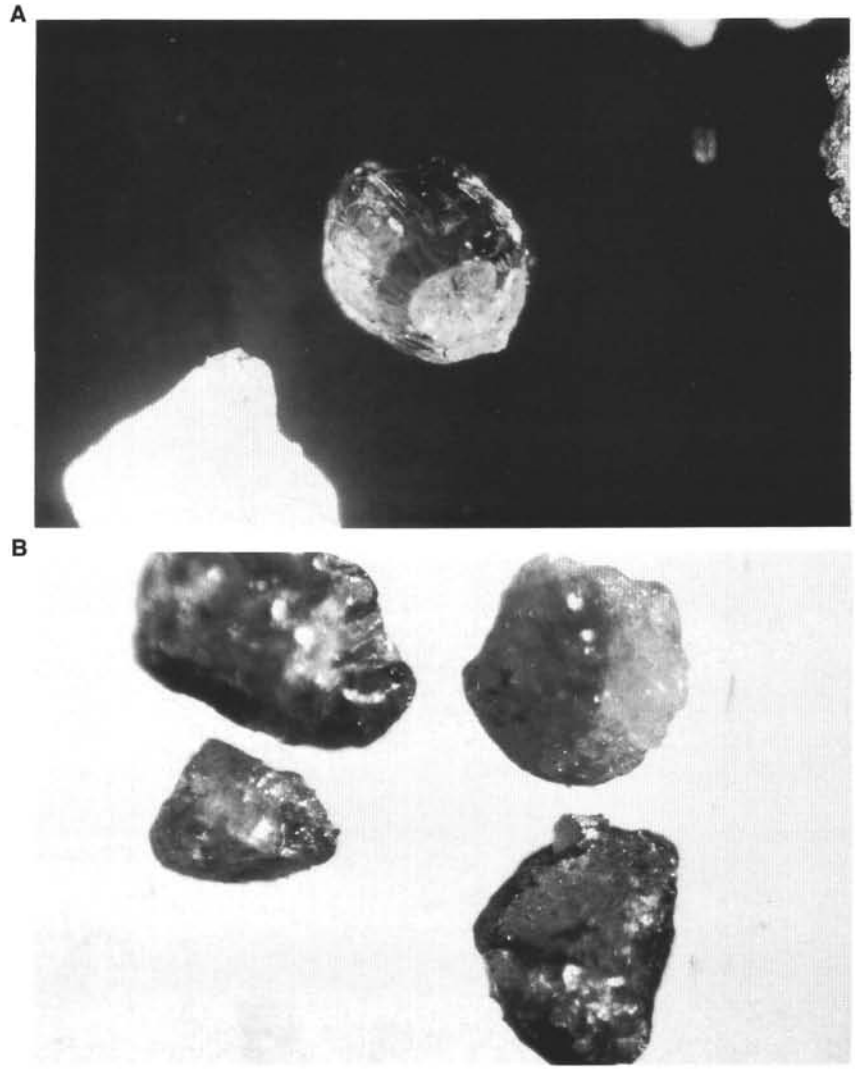

Figure 13. Microtektites from Sample 150-904A-45X-2, 87–88 cm. **A.** Microtektite with striated surface and spherical inclusions (axial dimensions are approximately 2.4 × 1.8 mm). Conchoidal fractures occur at both ends. Surface features and geometry were probably acquired through stresses during cooling. Crossed nichols; field of view 8 mm across. **B.** Irregularly shaped, possible microtektites with vitreous luster are common. Some of the glass fragments are up to 3 mm long. Euhedral pyrite crystals (e.g. on top left grain) common on surfaces. Plane-polarized transmitted light; field of view 8 mm across.

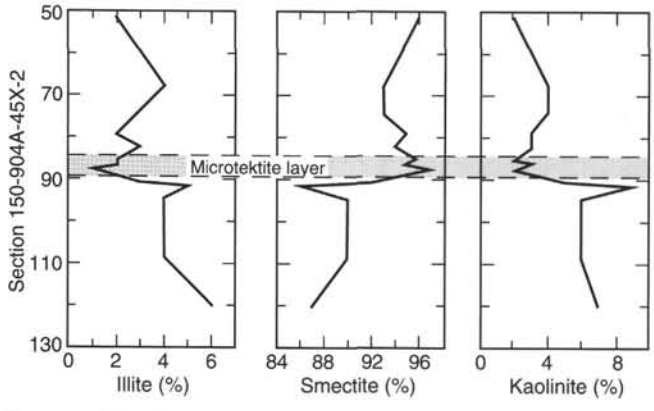

Figure 14. Clay mineralogy of sediments across the microtektite layer determined by XRD analysis.

delineated by darker stained micrite, are primarily oriented subparallel to depositional bedding planes, and are unmineralized. The occurrence of subvertical fractures filled with pyrite-cemented medium quartz sand at 390.8 mbsf (Interval 150-904A-42X-5, 30–60 cm; Fig. 15) is also indicative of fracture-controlled fluid flow. The relationship between the pyrite-bearing fractures and the microfractures associated with opal-A to opal-CT transformation is uncertain.

Lithologic changes associated with increased opal-CT abundance include greater induration and the occurrence of conchoidal fractures. These changes mark the onset of the diagenetic transition from chalks to porcellanitic chalks and porcellanites. Chalks most affected by this diagenetic change are of middle Eocene age and occur between approximately 525 and 560 mbsf in Hole 904A (Cores 150-904A-56X to -60X). This interval correlates with an increase in wet-bulk density (see "Physical Properties" section, this chapter). The XRD analyses indicate an increase in opal-CT below 520 mbsf (Fig. 5). This silica diagenetic alteration was also observed in Hole 903C and has been reported in Deep-Sea Drilling Program sites from the northwestern Atlantic Basin. The silica diagenetic front correlates with the seismic reflection A^c (see "Seismic Stratigraphy" section, this chapter).

BIOSTRATIGRAPHY

Introduction

At lower bathyal (1122.8 m) Site 904, Hole 904A penetrated a 576.7-m section of discontinuous Pleistocene to upper lower Eocene strata (Cores 150-904A-1H to -62X; Table 3). No Pliocene sediments were sampled. The lower upper Miocene to lower Miocene section extends from 106.2 to 308.40 mbsf (Samples 150-904A-12H-1, 85 cm, to -33X-CC). A thin upper Oligocene section was recovered between 318.31 and 337.47 mbsf (Samples 150-904A-34X-CC to -36X-CC). The upper to upper lower Eocene was recovered between 345.73 mbsf and the bottom of the hole (Samples 150-904A-37X-CC to -62X-CC). A microtektite layer was recovered near the base of the upper Eocene. This report is based on studies of core-catcher samples, so discrepancies may exist among interpretations from the different microfossil groups that will be addressed by shore-based analyses.

The upper Pleistocene/Holocene boundary probably falls within the upper part of Core 150-904A-1H, based on a lithologic change at 4.27 mbsf (Section 150-904A-1H-3, 127 cm) (see "Lithostratigraphy" section, this chapter). Pleistocene sediments were recovered between 8.62 mbsf and at least 104.85 mbsf (Sections 150-904A-1H-CC to -12H-1, 85 cm). The relatively continuous upper to middle Pleistocene section consists of dominantly greenish gray silty clay (lithologic Unit I, 0–106.2 mbsf; Core 150-904A-1H to Section 150-904A-12H-2, 65 cm) and probably spans oxygen isotope stage 5 at 5.4 mbsf, stage 8 at 37.0 mbsf (Sample 150-904A-4X-CC) (lowest occurrence [LO] of *Emiliania huxleyi*) and stage 12 at 104.12 mbsf (Sample 150-904A-12H-1, 12 cm) (highest occurrence [HO] of *Pseudoemiliania lacunosa*). The lower bounding Pleistocene surface is within Core 150-904A-12H. Middle to lower Pleistocene calcareous nannofossil Zone NN19 extends down to 104.85 mbsf (Section 150-904A-12H-1, 85 cm), but the remainder of Core 150-904A-12H and Section 150-904A-13H-CC are barren of calcareous nannofossils. Because this level is coincident with a lithologic change (see "Lithostratigraphy" section, this chapter) and because Sample 150-904A-12H-CC contains Miocene diatoms, placement of the Pleistocene/Miocene contact at 106.2 mbsf (Core 150-904A-12H-2, 65 cm), is reasonable.

A sand unit within Core 150-904A-12H separates the overlying Pleistocene (lithologic Unit I) from the underlying Miocene (lithologic Unit IV, 106.2–223.9 mbsf; Section 150-904A-12H-2, 65 cm, to -25X-2, 35 cm). This section is also greenish gray silty clay, but siderite nodules are present, and calcareous microfossils are scarce or absent. Sporadic middle Pliocene to Miocene calcareous nannofossil assemblages occur between 130.0 and 167.77 mbsf (Samples 150-904A-14H-CC to -18H-CC). Dinocysts provide most of the biostratigraphic framework for this Miocene interval. They indicate the lower upper Miocene Zone G from 111.23 to 130.30 mbsf (Samples 150-904A-12H-CC to -14H-CC; note that this zone may be, in part, middle Miocene; see "Biostratigraphy" section in Chapter 9, this volume) and the upper middle Miocene Zone F from 159.01 to 212.12 mbsf (Samples 150-904A-17H-CC, -19H-CC, and -21H-CC to -23H -CC). This is in partial agreement with diatom stratigraphy which indicates that the section from 111.23 to 148.61 mbsf (Sections 150-904A-12H-CC to -16H-CC) is lower upper Miocene and from 159.01 to 203.02 mbsf (Samples 150-904A-17H-CC to -22H-CC) is middle Miocene. Diagnostic late Miocene calcareous microfossils (planktonic foraminifer Zones N16–N17 and calcareous nannofossil Zones NN8–NN10) are found at 177.73 mbsf (Sample 150-904A-19H-CC). An unconformity between 177.73 and 185.21 mbsf (Samples 150-904A-19H-CC and -20H-CC) is suggested by planktonic foraminifer stratigraphy (Zone N16–N17 overlying Zone N10–N11).

Calcareous nannofossils indicate a middle Miocene age at 195.71 mbsf (Sample 150-904A-21H-CC), based on a tentative assignment to Zone NN6 to NN8, and diatoms indicate an early middle Miocene age for the section between 195.71 and 279.5 mbsf (Samples 150-904A-21H-CC to -30X-CC). Planktonic foraminifer zonal assignments (Zones

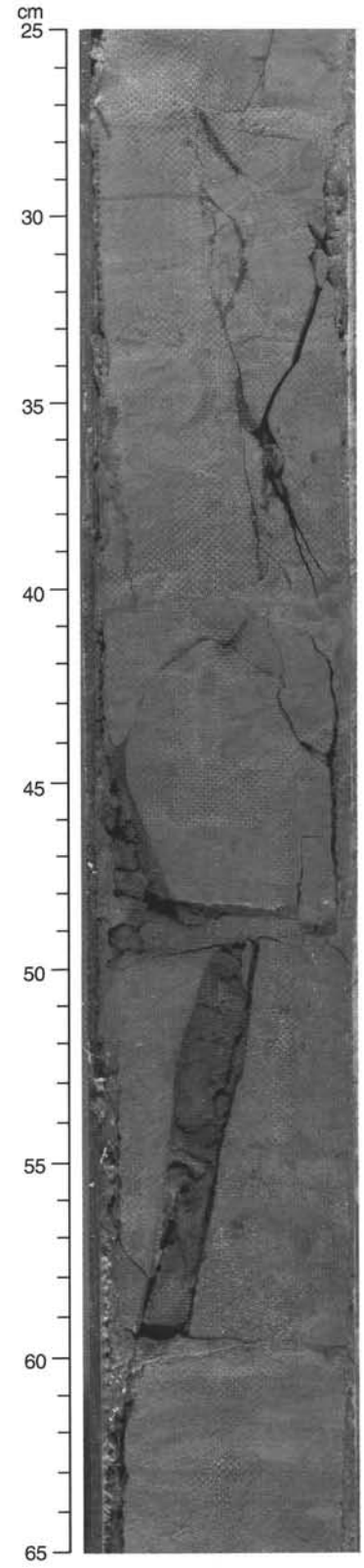

Figure 15. Subvertical fractures at 390.8 mbsf in the nannofossil chalks of Subunit VIIA (Interval 150-904A-42X-5, 25–65 cm) . The fractures are filled with pyrite-cemented, medium quartz sand.

Table 3. Biostratigraphic zonations and datum levels, Site 904.

Zone (base unless specified) and/or datum level	Code	Sample number	Depth (mbsf)
NN21	Cn	150-904A-5H-CC	47.14
HO *N. reinholdii*	Dm	150-904A-6H-CC	56.93
LO *G. truncatulinoides*	Pf	150-904A-11H-CC	104.46
NN20	Cn	150-904A-11H-CC	
Pleistocene	Df	150-904A-11H-CC	
NN19	Cn	150-904A-12H-1, 85 cm	104.85
HO *T. grunowii*	Dm	150-904A-12H-CC	111.23
Dinocyst Zone G	Df	150-904A-14H-CC	130.39
HO *D. punctata hustedtii*	Dm	150-904A-16H-CC	148.61
NN8 to NN10	Cn	150-904A-19H-CC	148.61
NN10	Cn	150-904A-19H-CC	177.73
N16–N17	Pf	150-904A-19H-CC	
HO *C. lewisianus*	Dm	150-904A-21H-CC	195.74
N11	Pf	150-904A-21H-CC	
NN6 to NN8	Cn	150-904A-21H-CC	
Dinocyst Zone F	Df	150-904A-23H-CC	212.12
NN5	Cn	150-904A-26X-CC	241.20
N8	Pf	150-904A-27X-CC	250.70
Lower Dinocyst Zone C	Df	150-904A-28X-CC	258.14
N7 or younger	Pf	150-904A-28X-CC	
NN3	Cn	150-904A-30X-CC	279.66
NN2	Cn	150-904A-30X-CC	
Dinocyst Zone A	Df	150-904A-31X-CC	289.30
NN2	Cn	150-904A-31X-CC	
NN1	Cn	150-904A-31X-CC	
N5–N6	Pf	150-904A-32X-CC	298.88
N4	Pf	150-904A-33X-CC	308.60
NN1	Cn	150-904A-34X-CC	318.31
NP25	Cn	150-904A-35X-CC	327.55
P20–mid P21	Pf	150-904A-36X-CC	337.47
NP24	Cn	150-904A-36X-CC	
NP25	Cn	150-904A-36X-CC	
P16–P17	Pf	150-904A-37X-CC	345.73
NP19 and/or NP20	Cn	150-904A-38X-CC	355.80
P13–P14	Pf	150-904A-42X-CC	394.21
NP19	Cn	150-904A-45X-4, 2 cm	417.92
NP18	Cn	150-904A-45X-4, 4 cm	417.94
P11–P12	Pf	150-904A-46X-CC	432.78
NP16	Cn	150-904A-47X-CC	442.35
NP15	Cn	150-904A-49X-CC	460.88
P9–P10	Pf	150-904A-56X-CC	527.73
NP15b	Cn	150-904A-60X-CC	548.47
P9–P11	Pf	150-904A-60X-CC	
NP14	Cn	150-904A-62X-CC	567.69

Notes: Dm = diatoms, Cn = calcareous nannofossils, Df = dinocysts, and Pf = planktonic foraminifers. HO = highest occurrence, LO = lowest occurrence.

N10–N12 at 185.21 mbsf, Sample 150-904A-20H-CC; and Zone N11 at 195.74 mbsf, Sample 150-904A-21H-CC) place this interval in the middle Miocene. Calcareous nannofossils are not diagnostic between 203.02 and 221.86 mbsf (Samples 150-904A-22H-CC to -24H-CC), although a broad assignment to Zones NN6–NN8 is consistent with stratigraphic determinations above and below. The planktonic foraminifer and calcareous nannofossil stratigraphy suggests a continuous section down to 269.88 mbsf (Sample 150-904A-29X-CC). An unconformity occurs below 279.66 mbsf (Sample 150-904A-30X-CC), based on calcareous nannofossil zonal assignments. Planktonic foraminifer zonal assignments at the base of this unit (Zone N5/N6 at 298.88 mbsf and Zone N4 at 308.60 mbsf; Samples 150-904A-32X-CC and -33X-CC) agree with the nannofossil, diatom (lower Miocene), and dinoflagellate cyst (Zone A) zonal assignments.

The upper Oligocene/lower Miocene boundary falls between 308.60 and 318.31 mbsf (Samples 150-904A-33X-CC and -34X-CC). It is unrelated to the lithologic change at 296.5 mbsf (Section 150-904A-32X-5, 140 cm) between lithologic Units V and VI. Diagnostic Zone NP25 calcareous nannofossils occur at 318.31 and 327.55 mbsf (Samples 150-904A-34X-CC and -35X-CC) and probable Zone NP24 at 337.47 mbsf (Sample 150-904A-36X-CC). Planktonic foraminifers indicate upper Oligocene at 318.31 mbsf (Sample 150-904A-34X-CC) and Zone P21 at 337.47 mbsf (Sample 150-904A-36X-CC) (Sections 150-904A-36X-CC and -37X-CC). The uppermost Eocene (Zone NP19–20; Zone P16–P17) is present below the unconformity of the contact between lithologic Units VI and VII.

The upper/middle Eocene contact is within Core 150-904A-45X, between 417.94 and 423.43 mbsf, Zone NP18 being unconformable with Zone NP16. The middle Eocene is unconformable with upper lower Eocene Subzone NP4a. The unconformity occurs between 548.47 and 565.28 mbsf (Samples 150-904A-60X-CC and -61X-CC). A tektite layer occurs within Core 150-904A-45X (see below and "Lithostratigraphy" section, this chapter) in the lower part of Zone NP19–20.

Planktonic Foraminifers

Hole 904A penetrated Pleistocene sediments downward from Samples 150-904A-1H-CC through, at least, -11H-CC at 104.0 mbsf. Based on the presence of *Globorotalia truncatulinoides,* which first appeared just before the Olduvai Subchron at 1.9 Ma (BKV85), Sample 150-904A-11H-CC is stratigraphically the lowest Pleistocene level that can be identified using planktonic foraminifers. As at Sites 902 and 903, the most common and persistent Pleistocene taxa are *Neogloboquadrina pachyderma* (cold-water indicator), *Globigerina bulloides* and *Globorotalia inflata* (cool-temperate water indicators), and *Globigerinoides ruber* and *Globorotalia truncatulinoides* (warm-water indicators). Variations in the relative abundance of these groupings can be used to infer glacial/interglacial patterns (Fig. 16 and Table 4). The assemblage in Sample 150-904A-1H-CC at 9.0 mbsf represents cool-temperate to cold conditions that may correspond to a glacial or immediate postglacial interval. Samples 150-904A-2H-CC through -4H-CC (18.5–37.5 mbsf) contain predominantly cool-temperate faunas with rare warm-water faunal elements. This interval, interpreted as interglacial, is immediately preceded by full interglacial conditions in

Table 4. Pleistocene biostratigraphy, Hole 904A.

Core, section	Depth (mbsf)	Planktonic foraminifer assemblage	Benthic foraminifer transport	Calcareous nannofossil assemblage	Interpreted glacial interval	Oxygen isotope stage
150-904A-						
1H-CC	8.62	Cool, temperate	Shallow		Glacial	5.4
2H-CC	18.31	Cool, temperate	Mixed		Interglacial	5.5
3H-CC	27.97	Cool, temperate	Deeper		Interglacial	5.5
4H-CC	37.08	Cool, temperate	Deeper	FO *E. huxleyi*	Interglacial	6.5
5H-CC	47.14	Warm, interglacial	Deeper		Interglacial	7.3
6H-CC	56.93		Mixed		Interglacial	8.3
7H-CC	66.43	Temperate	Mixed		Interglacial	9.1
8H-CC	75.81	Cool	Shallow		Glacial	10.2
9H-CC	85.42	Cool	Mixed		Glacial/interglacial	11.2
10H-CC	95.07	Cool	Shallow		Glacial	12.2
11H-CC	104.46	Warm, interglacial	Deeper		Interglacial	13.1
12H-1	105.50			LO *P. lacunosa*		13.1

Notes: Glacial/interglacial cycles are interpreted based on the planktonic foraminifer cool/warm assemblages and benthic foraminifer assemblages (shallow-water transported, deeper water transported, and mixed shallow water and in situ). Calcareous nannofossil datums allow correlation to the oxygen isotope stages. Correlation to GRAPE and MST data corroborates these interpretations. FO = first occurrence, LO = last occurrence.

Sample 150-904A-5H-CC at 47.0 mbsf where warm-water indicators are common and the relative abundance of cold-water indicators is reduced relative to overlying samples. The interval from Samples 150-904A-5H-CC through -7H-CC (47.0–66.0 mbsf) is interpreted as interglacial, whereas the preceding section, from Samples 150-904A-8H-CC through -10H-CC (75.5–94.5 mbsf) is dominated by cool to cold-water species, inferred to reflect a glacial interval. Sample 150-904A-11H-CC at 104.0 mbsf contains a fauna suggestive of an interglacial interval.

Samples 150-904A-12H-CC through -14H-CC (111.0–130.0 mbsf) contain sparse faunas with stratigraphically long-ranging species. The subjacent interval extending through Sample 150-904A-18H-CC at 168.0 mbsf is barren.

Samples 150-904A-19H-3, 90–92 cm, and -19H-CC (171.9 and 177.5 mbsf, respectively) yield species indicative of upper Miocene Zones N16–N17. Key taxa supporting assignment to this interval include *Neogloboquadrina acostaensis* with a first appearance datum (FAD) in Chron 11 (= C5n) at 10.2 Ma, *N. humerosa* with an FAD in Chron 8 (C4n) at 7.5 Ma, and *Globoquadrina dehiscens* with a last appearance datum (LAD) in Gilbert Chron (C2Ar–C3Ar) at 5.3 Ma (BKV85). Based on the presence of *N. humerosa,* planktonic foraminifer evidence would support assignment to Zone N17. However, because nannofossil evidence suggests assignment to Zones NN8–NN10, equivalent, in part, to planktonic foraminifer Zone N16, a more conservative interpretation encompassing Zones N16–N17 is adopted here. Assemblages in Samples 150-904A-19H-3, 90–92 cm, and -19H-CC also contain specimens from the middle Miocene; however, because they are sparse, somewhat abraded, and frequently iron-stained, they are interpreted to be reworked from older strata.

The assemblage in Sample 150-904A-20H-CC at 187.0 mbsf indicates the upper middle Miocene. The co-occurrence of *Globorotalia praemenardii, Globorotalia siakensis,* and *Globorotalia miozea* supports assignment to the N10–N12 zonal interval (Kennett and Srinivasan, 1983; Bolli and Saunders, 1985). Sample 150-904A-21H-CC at 196.5 mbsf contains *Globorotalia peripheroacuta* and *G. praefohsi,* the co-occurrence of which supports assignment to Zone N11 (Blow, 1979; Kennett and Srinivasan, 1983). The FAD of *Globorotalia peripheroacuta* is in Chron C5B at 14.9 Ma (BKV85); its LAD is near the top of Zone N11 (Kennett and Srinivasan, 1983), whereas the FAD of *G. praefohsi* is estimated at 13.0 Ma and the LAD of *G. fohsi* spp. is estimated at 12.1 Ma (Zhang et al., 1993; based on the recalibration of Site 563 by Wright and Miller, 1992). These data support assignment of Sample 150-904A-21H-CC to upper Zone N11. Samples 150-904A-22H-CC through -26X-CC (203.0–240.9 mbsf) are either barren or contain long-ranging species. In Sample 150-904A-27X-CC at 250.3 mbsf, the concurrent ranges of *Globorotalia praescitula* and *Globorotalia miozea* support assignment to Zone N8–lowermost Zone N9 (Bolli and Saunders, 1985). The FAD of *G. praescitula* is in Chron C5D at 17.7 Ma and that of *G. miozea* is in Chron C5C at 16.8 Ma (BKV85).

The next age-diagnostic sample (150-904A-29X-CC; 269.8 mbsf) is assignable to lower Miocene Zone N5 to mid Zone N6 based on the co-occurrence of *Globigerinoides altiaperturus* and *Globoquadrina praedehiscens.* Below a barren interval spanning Samples 150-904A-30X-CC and -31X-CC (279.5 and 289.1 mbsf), another assemblage assignable to Zone N5–mid Zone N6 was encountered in Sample 150-904A-32X-CC at 298.8 mbsf. In addition to *Globigerinoides altiaperturus* and *Globoquadrina praedehiscens,* this sample contains *Catapsydrax dissimilis* (LAD in Chron C5D at 17.6 Ma). Sample 150-904A-33X-CC at 308.4 mbsf is assigned to lower Miocene Zone N4, based on the occurrence of *Globorotalia kugleri* (FAD in Chron 23 [= C6C] at 23.7 Ma and LAD in Chron C6A at 21.8 Ma; BKV85).

Sample 150-904A-34X-CC at 317.8 mbsf is tentatively placed in the upper Oligocene. Rare specimens of *Globigerinoides* sp. may be contaminants. The remainder of the assemblage, although consistent with a late Oligocene age, does not permit assignment to a specific zone. Definitive Oligocene assemblages assignable to Zone P21 are encountered in Sample 150-904A-36X-CC at 336.5 mbsf. Key species are *Globigerina ciperoensis anguliofficinalis* (LAD in Zone P21) and *G. ciperoensis angulisuturalis* (FAD in Chron C11 at 31.6 Ma; BKF85).

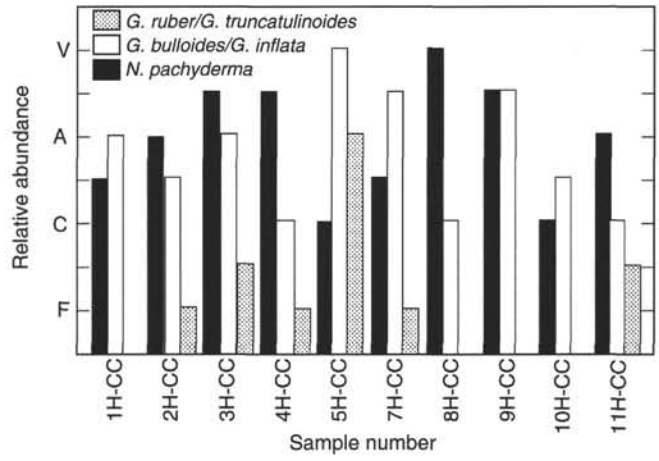

Figure 16. Relative abundances of selected groups of planktonic foraminifers indicating cold, cool temperate, and warm waters during the Pleistocene in Hole 904A. V = very abundant, A = abundant, C = common, and F = few.

Upper Eocene sediments were recovered at 345.8 mbsf in Sample 150-904A-37X-CC. The assemblage, which includes *Globorotalia cerroazulensis cerroazulensis* (LAD in Chron C13 at 36.6 Ma; BKF85), is assigned to Zones P16–P17. Sample 150-904A-39X-CC at 365.1 mbsf contains a mixed fauna with many fragmented specimens. Reworked middle Eocene specimens are mixed with upper Eocene indicators. *Hantkenina* spp. and *Globorotalia cerroazulensis cocoaensis,* occur in Sample 150-904A-40X-CC at 374.8 mbsf. This sample is assigned to Zones P16–P17.

Middle Eocene sediments, assignable to Zones P13–P14, were first encountered in Sample 150-904A-42X-CC at 394.1 mbsf. Diagnostic taxa include *Truncorotaloides rohri* and *Acarinina,* both with FADs in Chron 17 at 40.6 Ma (BKV85). A similar assemblage in Sample 150-904A-44X-CC at 413.4 mbsf also indicates Zones P13–P14. It is possible that this assemblage is reworked. Assemblages assignable to Zones P11–P12 were encountered in Sample 150-904A-46X-CC at 432.5 mbsf. In addition to species of *Acarinina* and *Morozovella,* the assemblage includes both *Globorotalia cerroazulensis pomeroli* with an FAD in Chron C19 at 44.7 Ma and *G. cerroazulensis frontosa* with an LAD in Chron C18 at 42.0 Ma (BKV85). Sample 150-904A-52X-CC at 490.2 mbsf contains a fauna that cannot be constrained more precisely than to the Zone P9–P12 interval. Samples 150-904A-56X-CC (528.4 mbsf) and -60X-CC (557.3 mbsf) are assignable to Zones P9–P10 based on an assemblage that includes *Morozovella* sp. cf. *M. quetra, Acarinina broedermanni,* and *Morozovella aragonensis.* The occurrence of *M. aragonensis,* with an LAD in Chron C20 at 46.0 Ma (BKF85), is particularly significant to this interpretation.

Benthic Foraminifers

Hole 904A was drilled in lower bathyal (1000–2000 m) water depths (1122.8 m) and penetrated 105.5 m of Pleistocene section in which transported assemblages dominated. Glacial-interglacial interpretations were made based on the distance of transport. Sediment transported from shallow water depths (predominantly shelf fauna) was interpreted as glacial and sediment from deeper water depths (dominantly outer shelf to upper bathyal taxa) as interglacial. Glacial/interglacial interpretations are corroborated by variations in the planktonic foraminifer assemblages (cool and warm intervals). Calcareous nannofossils stratigraphy, density data, and magnetic susceptibility data provide stratigraphic controls for oxygen isotope stage

interpretations (see "Sedimentation Rates" section, this chapter). Results are summarized in Table 4.

The shallow-water-transported assemblage is characterized by a dominance of *Elphidium* spp. in addition to other shallow-water forms (*Eggerella* spp., *Islandiella* spp., *Cassidulina* spp., *Fursenkoina* spp., *Buccella frigida,* miliolids, *Rosalina* spp., *Cibicides lobatulus, Cibicides* spp., *Elphidium* spp., and *Bulimina marginata*). High relative percentages of *Elphidium* spp. are associated with inner neritic (<30 m) depths (Gevirtz et al., 1971). *Elphidium* spp. are present on the slope of the western North Atlantic (Streeter and Lavery, 1982), although not in the high abundances noted on the shelf (see "Biostratigraphy" section in Chapter 6 [this volume] for further discussion). These low-diversity assemblages are interpreted as glacial and are found in association with subangular sand grains and high percentages of mica. Wood fragments, although present, are not as abundant as at the shallower water Sites 902 and 903.

The deeper water transported assemblage is characterized by outer shelf to upper bathyal taxa (e.g., *Melonis barleeanum* and *Bulimina aculeata*) similar to that found at Site 902 (water depth, 811 m). The deeper water transported material is characterized as interglacial based on the higher diversity assemblage. In addition to the shallow and deeper water transported assemblages, mixed faunas were found. These assemblages contain high percentages of *Elphidium* spp. and upper bathyal components such as *Bulimina marginata.* These mixed assemblages are interpreted as transitional intervals with faunas intermediate between glacial and interglacial periods.

Upper Miocene samples contained few to no planktonic foraminifers and impoverished benthic foraminifer assemblages (Cores 159-904A-13H through -18H). This interval is characterized by abundant *Uvigerina juncea* and foraminiferal tests with fair preservation. In addition, it yields *Bulimina* sp., *Cibicidoides* spp., *Chilostomella* sp., *Fissurina* spp., *Globobulimina* sp., *Lagena* spp., *Lenticulina* spp., *Melonis barleeanum, Nonionellina* sp., and *Stilostomella* spp. These *Uvigerina juncea*-dominated assemblages represent transported shelf faunas.

Miocene samples that contained no benthic foraminifers include Samples 150-904A-17H-CC and -24H-CC (159.01–221.86 mbsf). Sample 150-904A-30X-CC (279.66 mbsf) contained only rare *Stilostomella* spp.

Middle Miocene to upper Oligocene samples (Samples 150-904A-19H-CC through -36X-CC; 177.73–337.47 mbsf) contain typical bathyal faunas, such as *Bulimina alazanensis, Bulimina macilenta, Cibicidoides pachyderma, Hoeglundina elegans, Lenticulina* spp., *Plectofrondicularia* sp., *Pullenia bulloides, Pullenia quinqueloba, Sigmoilopsis schlumbergeri, Sphaeroidina bulloides, Stilostomella* spp., and *Uvigerina hispida.* An absence of specific depth-diagnostic taxa make it impossible to estimate accurately the paleodepth of this section. Sample 150-904A-20H-CC (185.21 mbsf) contains *Cibicidoides crebbsi,* indicating a lower paleodepth limit of 600 m. However, this sample also contains well preserved specimens of the shallow water taxon *Buliminella elongata,* indicating that components of this assemblage were likely transported.

Bathyal Eocene assemblages (Samples 150-904A-37X-CC to -62X-CC; 345.73 mbsf–567.69 mbsf) include *Anomalinoides* sp., *Bolivina* sp., *Cibicidoides praemundulus, Cibicidoides* spp., *Dentalina* spp., *Eggerella* sp., *Fissurina* spp., *Globobulimina* sp., *Globocassidulina subglobosa, Gyroidinoides* spp., *Karreriella bradyi, Karreriella chapapotensis, Karreriella* spp., *Lenticulina* spp., *Nonion* sp., *Nonionellina* sp., *Oridorsalis* sp., *Osangularia* sp., *Plectofrondicularia* spp., *Pleurostomella* spp., *Planulina renzi,* polymorphinids, *Pul- lenia bulloides, Pullenia eocenica, Pullenia quinqueloba, Sphaeroidina bulloides, Stilostomella* spp., *Tritaxia* spp., and *Vulvulina mexicana. Alabamina* sp. is common in samples examined from Cores 150- 904A-32X (298.88 mbsf) through -52X (490.20 mbsf), whereas *Bulimina* spp. (*Bulimina alazanensis, Bulimina macilenta,* and *Bulimina trinitatensis*) are common from Cores 150-904A-37X (345.73 mbsf) through -56X (527.73 mbsf). As *Alabamina* sp. and *Bulimina* spp. disappeared downcore, the agglutinated assemblage became more diverse in and below Sample 150-904A-52X-CC (490.20 mbsf) with *Dorothia* spp., *Gaudryna laevigata, Plectina elongata, Plectina nuttali, Spiroplectammina spectabilis, Spiroplectammina* spp., *Tritaxia* spp., and *Vulvulina* sp. Several species commonly found in Eocene sediments were identified in this section, including *Anomalinoides* sp. cf. *capitatus* (490.20 mbsf–537.84 mbsf; Samples 150-904A-52X-CC to -58X-CC), *Cibicidoides micrus* (413.60–567.69 mbsf; Samples 150-904A-44X-CC to -62X-CC), *Hanzawaia ammophila* (490.20 mbsf–537.84 mbsf; Samples 150-904A-52X-CC to -58X-CC), and *Nuttallides truempyi* (490.20 and 548.47 mbsf; Samples 150-904A-58X-CC and -60X-CC). Other species that are generally common in deep-water Eocene strata were scattered throughout the section at Hole 904A, including *Aragonia aragonensis, Cibicidoides eocaenus,* and *Planulina costata.* Several taxa indicate that the Eocene paleodepth of Site 904 was middle bathyal or deeper (>600 m). These include *Anom- alinoides* sp. cf. *capitatus, Bulimina trinitatensis, Nuttallides truempyi,* and *Uvigerina havanensis* (*Uvigerina havanensis* has a lower depth limit of about 2000 m) (van Morkhoven et al., 1986). *Hanza-waia ammophila* and *Osangularia* spp. were common in parts of the Eocene at Hole 904A; Tjalsma and Lohmann (1983) found these taxa to be most common at paleodepths shallower than 2000 m. In addition, there is a lack of species often found in abyssal Eocene sections, such as *Abyssamina poagi/quadrata* (Tjalsma and Lohmann, 1983; van Morkhoven et al., 1986) and *Quadrimorphina profunda* (Tjalsma and Lohmann, 1983).

Calcareous Nannofossils

The approximately 577 m of section penetrated extends from the Holocene at the ocean floor to upper lower Eocene in Sample 150-904A-62X-CC (567.69 mbsf). The Neogene hemipelagic muds contain rare to common nannofossils whereas these are the main constituent of the Paleogene clayey chalks. Several samples from Cores 150-904A-12H and -13H (111.23–120.94 mbsf) proved barren. Some nannofossils were recovered from the remaining samples that were examined.

A meager late Pleistocene assemblage, including *Emiliania huxleyi,* occurs in Samples 150-904A-1H-CC to -4H-CC (8.62–37.08 mbsf). Thus, the lowest occurrence of this species, which marks the base of nannofossil Zone NN21, is within Core 150-904A-5H (37.5–47.14 mbsf). The *Emiliania huxleyi* Acme Zone was not identified, but may be present above Sample 150-904A-1H-CC (0–8.62 mbsf). Samples 150-904A-5H-CC to -11H-CC (37.5–104.46 mbsf) yielded representative late Pleistocene assemblages but without *Emiliania huxleyi* or *Pseudoemiliania lacunosa,* which indicates middle Pleistocene Zone NN20. *Pseudoemiliania lacunosa* occurs with *Gephyrocapsa* spp. and other Pleistocene species in Samples 150-904A-12H-1, 12 and 85 cm (104.12 and 104.85 mbsf, respectively), identifying a thin interval of the mid- and lower Pleistocene Zone NN19 at the top of Core 150-904A-12H. The remainder of that core and the core catcher of the next lower core (Section 150-904A-13H-CC; 120.94 mbsf), are barren of nannofossils. Samples 150-904A-14H-CC to -18H-CC (130.39–167.77 mbsf) yielded sporadic nannofossils, including *Coccolithus pelagicus* and forms related to *Reticulofenestra pseudoumbilicus,* and long-ranging taxa that are compatible with a middle Pliocene to Miocene age.

A diverse upper Miocene assemblage was recovered from Sample 150-904A-19H-CC (177.73 mbsf); SG identified several elements with incompatible stratigraphic ranges in the assemblage (e.g., *Discoaster exilis, Catinaster coalitus,* and *Discoaster calcaris*) following a narrow species definition and ranges as given by Perch-Nielsen (1985). Assuming that redeposition of older material is responsible for the contamination, then the assemblage is assigned to the interval from Zones NN8 to NN10. Alternatively, an NN10 zonal assignment is proposed by MPA based on the occurrence of *Discoaster* sp. cf. *D. brouweri, D. bollii, D. challengeri, D. calcaris,* and *C. coalitus/C. mexicanus.* Sample 150-904A-20H-CC (185.21 mbsf) yielded only nondiagnostic species. Sample 150-904A-21H-CC (195.74 mbsf)

contains a variety of species, most of them not age-diagnostic, and including *Discoaster exilis, Discoaster challengeri, Discoaster subsurculus, Discoaster sanmiguelensis* (or possibly *Discoaster bollii*). This assemblage is tentatively assigned to Zones NN6–NN8. SG suggest that the grouping may contain redeposited contaminants. The next three samples, Samples 150-904A-22H-CC to -24H-CC (203.02–221.86 mbsf), yielded no diagnostic species except *Discoaster exilis,* which assigns these samples broadly to the interval of Zones NN5–NN8. In the absence of *S. heteromorphus,* assignment to Zones NN6–NN8 is preferred (MPA). Sample 150-904A-25X-CC (231.23 mbsf) yielded specimens most similar to *Discoaster kugleri,* which places this sample in Zone NN7. The next lower Sample 150-904A-26X-CC (241.2 mbsf) contains *Sphenolithus heteromorphus, Discoaster exilis,* and *Cyclicargolithus floridanus,* and this level is assigned to Zone NN5. *Helicosphaera ampliaperta* occurs together with *Sphenolithus heteromorphus* in Samples 150-904A-27X-CC to -29X-CC (250.3 and 269.8 mbsf), placing these in the lower Miocene Zone NN4. *Helicosphaera ampliaperta* occurs without *Sphenolithus heteromorphus* in Sample 150-904A-30X-CC (279.66 mbsf), which is assigned to Zone NN3 by SG. Because *Sphenolithus belemnos* was not observed in this sample and because the FAD of *H. ampliaperta* is within Biochron NN2, Sample 150-904A-30X-CC (279.66 mbsf) is assigned to Zone NN2 by MPA.

The assemblage in Sample 150-904A-31X-CC (289.30 mbsf) yielded no diagnostic sphenoliths or discoasters. The presence of *Cyclicargolithus abisectus* (or large *Cyclicargolithus floridanus*), suggest that the sample may be best assigned to basal Miocene Zone NN1 (SG), whereas an NN2 Zonal assignment is preferred by MPA. The next lower sample (150-904A-32X-CC; 298.88 mbsf), however, yields *Triquetrorhabdulus carinatus, Zygrhablithus bijugatus,* and *Ilselithina fusa,* along with several long-lived species, but not *Sphenolithus ciperoensis.* Sample 150-904A-33X-CC (308.60 mbsf) yielded *Sphenolithus capricornutus* and *Sphenolithus delphix* as well. Both belong to Zone NN1 and the two may straddle the Miocene/Oligocene boundary (SG). *Sphenolithus ciperoensis* is present in Samples 150-904A-34X-CC, -35X-CC, and -36X-CC (318.31, 327.55, and 336.5 mbsf, respectively). This interval is assigned to upper Oligocene Zone NP25 by MPA. Alternatively, SG places the upper two samples in Zone NP25, and the lower zone, which also contains *Chiasmolithus altus,* in Zone NP24.

A major stratigraphic gap occurs between Samples 150-904A-36X-CC and -37X-CC (336.5–345.8 mbsf). The rich assemblage from Sample 150-904A-37X-CC (345.8 mbsf) is upper Eocene. It contains *Discoaster barbadiensis, Discoaster saipanensis,* and *Isthmolithus recurvus.* This and the next lower Sample 150-904A-38X-CC (355.0 mbsf) lack *Cribrocentrum reticulatum* and, therefore, are assigned to the upper part of Zone NP19 and/or Zone NP20 (SG; see Perch-Nielsen, 1985, p. 431). *Cribrocentrum reticulatum* co-occurs with *Isthmolithus recurvus* through Sample 150-904A-45X-4, 2 cm (417.92 mbsf), where a sharp color change marks the boundary between Zone NP19 (SG) above and Zone NP18 below at Sample 150-904A-45X-4, 4 cm (418.30 mbsf). Zone NP18 is represented by only a thin interval. The lowermost sample in the core (Sample 150-904A-45X-CC; 423.30 mbsf) contains the middle Eocene indicators *Chiasmolithus grandis, Sphenolithus furcatolithoides,* and *Discoaster bifax.* This sample is assigned to Zone NP16.

Zone NP16 extends downward to Sample 150-904A-47X-CC (442.35 mbsf). Sample 150-904A-48X-CC (451.82 mbsf) also yielded a middle Eocene assemblage, which includes *Chiasmolithus eograndis* and *Sphenolithus spiniger* and, in Sample 150-904A-49X-CC (460.88 mbsf), *Lophodolithus acutus.* All are indicative of middle Eocene Zone NP15 (SG). *Chiasmolithus gigas* has its highest occurrence in Sample 150-904A-51X-CC (480.73 mbsf) and ranges through Sample 150-904A-60X-CC (548.47 mbsf). Its range characterizes Subzone NP15b. The last two samples, Samples 150-904A-61X-CC (565.28 mbsf) and -62X-CC (567.69 mbsf), contain *Discoaster sublodoensis,* with *Discoaster kuepperi* in the second sample and *D. lodoensis* (in both samples). This co-occurrence indicates the upper lower Eocene Subzone NP14a, in which the hole was terminated.

The several thin sandy layers that appear prominently in the clayey chalk of Section 2 in Core 150-904A-45X have been identified as tektite bearing and are thought to be correlative with the tektite layer described from Site 612 by Thein (1987) and Poag et al. (1992). A suite of nannofossil smear slides was prepared from samples across these sandy layers to determine the age of the event that caused these deposits (Fig. 17). Samples included in this suite are as follows: Samples 150-904A-45X-2, 76, 77, 80, 86, 88, 90, 93, and 103 cm (415.66, 415.67, 415.70, 415.86, 415.80, 415.83, and 415.93 mbsf, respectively). All but the last of these samples are from the sandy layers in the core, and all but the last of these samples have exotic fragments on the nannofossil slides, including angular quartz and feldspar, lithic fragments, glauconite, carbonate, pyrite, glass(?), benthic foraminifers, and an occasional teardrop-shaped spherule of unknown composition. Three additional samples from the clayey chalks are relevant to the dating of these sands, namely, Samples 150-904A-44X-CC (413.6 mbsf); -45X-4, 2 cm (417.92 mbsf); and -45-4, 4 cm (417.94 mbsf). The entire interval from Sample 150-904A-44X-CC (413.6 mbsf) to -45X-4, 2 cm (419.42 mbsf), is assigned to the lower part of Zone NP19 (SG) based on the co-occurrence of *Isthmolithus recurvus* and *Cribrocentrum reticulatum.* Unfortunately, the base of this interval seems to correspond to a subtle hiatus of unknown extent, marked only by a sharp but rather innocuous color change between Samples 150-904A-45X-4, 2 cm (419.42 mbsf), and -45X-4, 4 cm (419.44 mbsf) below which the assemblage is assignable to Zone NP18. The calcareous nannofossil succession in the vicinity of the sandy layer (tektite event) at Site 904 is similar to the succession near the corresponding but less clearly expressed horizon at Site 903. At both sites, no significant change in the nannofossil assemblage seems to be associated with the event.

Diatoms

Diatom concentrations ranged from rare to abundant; in the upper part of the hole, many of the samples were barren of diatoms. From the point of view of biostratigraphy, this hole has some importance in that we recovered diatoms in upper Eocene sediments, giving us the opportunity to devise a Oligocene–Eocene zonal scheme for this part of the North Atlantic. As at Sites 902 and 903, lower Miocene and Oligocene sediments were mostly barren of diatoms at Site 904.

Samples 150-904A-1H-CC to -11H-CC (0–104.46 mbsf) are mostly barren; however, a few contained rare diatoms. Sample 150-904A-6H-CC (56.93 mbsf), for example, contains *Coscinodiscus marginatus, Nitzschia reinholdii, Pseudoeunotia doliolus, Thalassionema nitzschioides,* and *Thalassiosira oestrupii.* The presence of *P. doliolus* places this sample in the upper Pleistocene *P. doliolus* Zone; however, the presence of *N. reinholdii* suggests that this sample may be placed in the lower Pleistocene. Although the *N. reinholdii* Zone is recognized in the equatorial Pacific, it has never been formally identified in the North Atlantic (Baldauf, 1984). Diatoms first occur in Core 150-904A-12H, where they underlie a prominent sand unit. Sample 150-904A-12H-5, 20–21 cm (110.20 mbsf), contains diatoms indicative of the lower upper Miocene *Coscinodiscus yabei* Zone. Other forms that are present in this sample include *Actinocyclus ellipticus, A. ingens, A. senarius, A. tenellus, Denticulopsis hustedtii, Mediara splendida, Paralia sulcata* var. *coronata, Rhizosolenia barboi,* and *Thalassionema nitzschioides.* We also observe the last appearance of *Delphineis novaecaesaraea* in this sample. Its presence is of interest because it is a zonal marker for the ECDZ of Andrews (1988), ranging through his Zones 5, 6, and 7 and part of his Zone 3–4.

Samples 150-904A-12H-CC to -15H-CC (111.23–139.17 mbsf) are also in the *Coscinodiscus yabei* Zone. Diatoms are generally few to common, and preservation ranges from moderate to good. Other species in this zone include *Actinocyclus ellipticus, A. ingens, A. senarius, A. tenellus, Coscinodiscus endoi, Delphineis novaecaesa-*

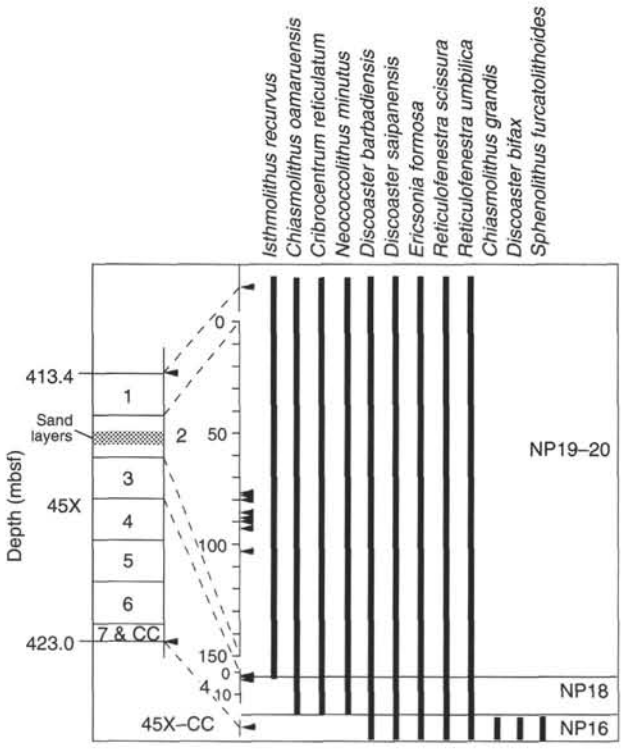

Figure 17. Calcareous nannofossil biostratigraphy of the upper Eocene tektite layer (Core 150-904A-45X).

raea, Denticulopsis hustedtii, Mediara splendida, Paralia sulcata var. *coronata, Rhizosolenia miocenica, R. barboi, Stephanogonia actinoptychus, S. grunowii, Thalassionema nitzschioides,* and *Thalassiosira grunowii.* The nominate taxon, *Coscinodiscus yabei,* is not always present in this zone; however, Baldauf (1984) has pointed out that *T. grunowii,* which is more common, approximates the range of *C. yabei.* As noted previously, we are unable to find the zonal markers for the *Denticulopsis praedimorpha* Zone, which underlies the *C. yabei* Zone, according to Baldauf (1984). Previously, we had suggested that the absence of this zone may represent an unconformity; because its absence is now confirmed in three sites, we suggest that the zonal markers never penetrated this far south and that no hiatus is indicated.

The *Rhizosolenia barboi* Zone occurs between Samples 150-904A-16H-CC and -20H-CC (148.61–185.21 mbsf). This zone, according to Baldauf (1984), is defined by the last occurrence of *Denticulopsis punctata* var. *hustedtii* at the top and by the first occurrence of *R. barboi* at the base. In contrast to other sites occupied by Leg 150, this zone is somewhat truncated in Hole 904A. Other species in this zone include *Actinocyclus ellipticus, A. ingens, A. tenellus, Actinoptychus senarius, Delphineis novaecaesaraea, Denticulopsis hustedtii, D. punctata* var. *hustedtii, Mediaria splendida, Melosira westii, Paralia complexa, P. sulcata, P. sulcata* var. *coronata, Stephanogonia actinoptychus, Thalassionema nitzschioides,* and *Thalassiosira grunowii.* The next zone below, the *Denticulopsis nicobarica* Zone, is considerably truncated (it is present in Sample 150-904A-20H-CC; 185.21 mbsf). In the other sites occupied by Leg 150, this zone was also very thin. It is not yet clear whether this is because of a regional hiatus or because of the absence of the requisite zonal markers from this area.

Samples 150-904A-21H-CC to approximately -30X-CC (195.74–279.66 mbsf) belong to the *Coscinodiscus lewisianus* Zone of Baldauf (1984). The base of this zone is only tentatively identified. Although diatoms are present into the upper Eocene in Hole 904A, increasing downcore dissolution has removed many of the zonal markers. Other species in this zone include *Actinocyclus ellipticus, A. ingens, A. tenellus, Actinoptychus senarius, Cavitas miocenica, Coscinodiscus marginatus, Delphineis novaecaesaraea, Denticulopsis hustedtii, D. punctata* var. *hustedtii, Mediaria splendida, Melosira complexa, M. westii, Paralia complexa, P. sulcata, P. sulcata* var. *coronata, Rossia paleacea, Stephanogonia actinoptychus, Thalassionema nitzschioides, Thalassiosira grunowii, Delphineis penelliptica, D. hustedtii,* and *D. novaecaesaraea. Delphineis penelliptica,* a species recognized by Andrews (1988) in his ECDZ, also occurs in this zone as does the first occurrence datum of *D. hustedtii.* The former species first occurs near the ECDZ 3–4/2 boundary and the latter species first occurs in the lower ECDZ 6 of Andrews (1988).

Although diatoms are present in Hole 904A down to near the base, increasing dissolution makes it difficult to tie this level into an existing zonal scheme although elements of those schemes do occur. Additional work will permit a zonal scheme to be developed.

Dinoflagellate Cysts

Hole 904A was spot sampled for dinocyst analyses between 104.46 and 289.3 mbsf. Within this interval, data are currently available for 12 core-catcher samples only. All samples were productive and preservation is moderate to good.

Sample 150-904A-11H-CC (104.46 mbsf) contains a low-diversity assemblage characterized by nondescript *Spiniferites* spp., *Bitectatodinium tepikiense, Protoperidinium avellana,* and undetermined round brown *Protoperidinioid* cysts. *Pinus* and *Picea* are common and rare specimens of freshwater *Pediastrum* sp. are present. Other than pollen and dinocysts, there are few organic clasts larger than 25 µm. The presence of *B. tepikiense* indicates only that this sample is from the upper Pliocene or higher. However, the absence of typical upper Pliocene taxa, and the overall similarity of the assemblage and kerogen to Pleistocene samples at Sites 902 and 903, suggests that Sample 150-904A-11H-CC is probably from the Pleistocene.

The next three cores, represented by Samples 150-904A-12H-CC, -13H-CC, and -14H-CC (111.23, 120.94, and 130.39 mbsf, respectively), belong to Zone G (Table 5). The zonal species, *Sumatradinium soucouyantiae,* is present in Sample 150-904A-12H-CC (111.23 mbsf) and *Operculodinium janducheneii,* which has a lowest occurrence within Zone G, is present in Sample 150-904A-14H-CC (130.39 mbsf). *Cannosphaeropsis* sp. cf. *C. utinensis,* the zonal species for the underlying zone, was not recorded in these samples.

The next interval for which data are available is between 159.01 and 212.12 mbsf and is represented by Samples 150-904A-17H-CC, -19H-CC, -21H-CC, -22H-CC, and -23H-CC (159.01, 177.73, 195.74, 203.02, and 212.12 mbsf, respectively). All of these samples contain *C.* sp. cf. *C. utinensis,* suggesting dinocyst Zone F. However, assignment of these samples to Zone F conflicts with various planktonic foraminifer and calcareous nannofossil data from this interval.

The ages of the Miocene dinocyst zones used in this volume are based on a selective synthesis of published dinoflagellate/dinocyst datum levels, plus a few planktonic foraminifer piercing points that hinge on the regional dinocyst correlations (L. de Verteuil and G. Norris, unpubl. data, 1993). Mainly on the basis of constraining data from adjacent Zones D and G, the age of Zone F was estimated to range from the middle middle Miocene to the latest middle Miocene (L. de Verteuil and G. Norris, unpubl. data, 1993; see Chapter 3, this volume). Therefore, they considered Zone F to correlate with all of calcareous nannofossil Zone NN7 and possibly to the lower part of Zone NN8 (Martini, 1971, and to planktonic foraminifer Zones N12, N13, N14, and possibly N15 (Blow, 1969). At Site 905, we established a direct tie in Core 150-905A-68X between Zone F (pars) and N14 and NN7, indicating that at least part of the dinocyst zone is late middle Miocene (see "Biostratigraphy" section in Chapter 9, this volume).

At Site 904, Sample 150-904A-17H-CC (159.01 mbsf) contains a moderately diverse dinocyst assemblage (about 25 species) with good preservation. The presence of *C.* sp. cf. *C. utinensis* suggests that this level belongs to Zone F. The rest of the assemblage constrains the sample to Zones E, F, or G. No evidence is present of reworking from

Table 5. Dinocyst data, Hole 904A.

Core, section	Depth (mbsf)	Zone
150-904A-		
11H-CC	104.46	Pleistocene
12H-CC	111.23	G
13H-CC	120.94	G
14H-CC	130.39	G
17H-CC	159.01	F
19H-CC	177.73	F
21H-CC	195.74	F
22H-CC	203.02	F
23H-CC	212.12	F
28X-CC	258.14	lower C
30X-CC	279.66	A
31X-CC	289.30	A

rocks older than Zone E. *Achomosphaera andalousiensis,* which generally has its lowest occurrence in Zone G, was not recorded from Sample 150-904A-17H-CC (159.01 mbsf). This level is barren of planktonic foraminifers and contains nondiagnostic calcareous nannofossils (Table 3).

Sample 150-904A-19H-CC (177.73 mbsf) has many species in common with Sample 150-904A-17H-CC, including the Zone F marker *C.* sp. cf. *C. utinensis.* However, the two assemblages differ in that the former is dominated by the subtropical neritic species *Polysphaeridium zoharyi,* which does not occur in the latter. Sample 150-904A-19H-CC (177.73 mbsf) contains upper Miocene planktonic foraminifers (Zones N16–N17). Furthermore, calcareous nannofossils from this level tentatively suggest it is lower upper Miocene (Zone NN8–NN10). These data suggest that Zone F strata, at 177.73 and 159.01 mbsf (Samples 150-904A-19H-CC and -17H-CC), have an age of middle late Miocene at most and are possibly younger. This is not consistent with dinocyst data from the North Atlantic constraining the ages of dinocyst Zones G and H to early to middle late Miocene (L. de Verteuil and G. Norris, unpubl. data, 1993).

An interval of coarse, poorly sorted sand occurs at the base of Core 150-904A-18H (166–168 mbsf; see "Lithostratigraphy" section, this chapter), providing some support for inferring reworking of *C.* sp. cf. *C. utinensis* at 159.01 mbsf (Sample 150-904A-17H-CC). Nevertheless, the presence of Zone G in overlying cores suggests that this level is older than middle late Miocene.

Sample 150-904A-21H-CC (195.74 mbsf) contains an assemblage typical of Zone F including *C.* sp. cf. *C. utinensis* (see "Biostratigraphy" section in Chapter 2, this volume). The most common species are *Operculodinium israelianum* s.l. and *P. zoharyi,* both indicators of warm temperate to subtropical surface temperatures and neritic water masses. Rare specimens of *Aptiodinium tectatum* and *Systematophora placacantha/ancyrea* complex are present. These taxa normally occur highest in Zone D, the latter being the zonal marker for that zone; they are interpreted to have been reworked at this level. Samples 150-904A-22H-CC and -23H-CC (203.02 and 212.12 mbsf) also belong to Zone F and contain assemblages typical of the zone. However, *P. zoharyi* was not recorded from these two samples, perhaps indicating more temperate conditions on the continental shelf at the time of deposition, with respect to the interval contained in Cores 150-904A-21H and -19H. Rare specimens of *A. tectatum* in Sample 150-904A-23H-CC (212.12 mbsf) indicate that some reworking has occurred at this level.

The next sample analyzed was 150-904A-28X-CC (258.14 mbsf). The presence of *Distatodinium paradoxum* indicates placement in Zone C or below. Well-developed *Labyrinthodinium truncatum* was not recorded. Rare specimens of *L.* sp. cf. *L. truncatum,* a smaller species with less well-defined appendages, are present. In some other sections in the region, the lowest occurrence of this species slightly predates that of *L. truncatum* s.s. and the two co-occur through Zone C and into Zone D (L. de Verteuil and G. Norris, unpubl. data, 1993). This suggests that this level is from the lower part of Zone C (latest early Miocene).

The lowest dinocyst data available for Site 904 are from Samples 150-904A-30X-CC and -31X-CC (279.66 and 289.3 mbsf). Both samples belong to Zone A based on the presence of *Cordosphaeridium cantharellum* and the absence of *Chiropteridium* spp. The assemblages are similar and contain *Cribroperidinium tenutabulatum, Lingulodinium* spp., *Aptiodinium spiridoides, Hystrichokolpoma rigaudiae, H. truncata, Systematophora ancyrea/placacantha* complex, *Cyclopsiella granulata,* and *P. zoharyi.* These assemblages are neritic in character and the last mentioned species indicates subtropical surface temperatures. The age of Zone A is middle early Miocene (L. de Verteuil and G. Norris, unpubl. data, 1993).

PALEOMAGNETISM

Paleomagnetic measurements were made for the purpose of constructing a magnetostratigraphy at Site 904, a single-hole drill site on the New Jersey margin (Hole 904A). Where recovery permitted, we measured and demagnetized whole sections of split core from Hole 904A over the intervals 0–140, 250–320, and 380–480 mbsf as well as a short interval near the bottom at 565 mbsf. Measurements and more thorough demagnetization of discrete samples taken from the upper 250 m augmented the pass-through data and provided coverage where APC and XCB coring disturbances had rendered pass-through measuring impractical.

The intensity of natural and demagnetized remanence is relatively strong in the upper 140 m at Site 904 (one to several tens of mA/m), but it becomes notably weak from this level to the bottom of the hole (~0.1 to 1 mA/m). Intensity variations at Hole 904A tend to mimic those seen in magnetic susceptibility to first and second order (Figs. 18–19). For example, relatively gradual fluctuations of magnetization intensity and susceptibility occur between 0 and 60 mbsf (Fig. 18); and, where sharp susceptibility "spikes" occur (generally at lithologic changes), there are correlative sharp increases in the magnetization intensity.

Following removal of a drilling-induced overprint, demagnetized remanence from pass-through data yields a uniform zone of normal polarity in the upper 105 m of Hole 904A (Fig. 18), which is confirmed by analysis of discrete samples. We interpret this zone as the Brunhes normal polarity interval (Chron C1n; Table 6). Between about 105 and 133 mbsf, magnetizations in half cores and discrete cubes are still relatively strong and switch to negative inclination (Fig. 18). Unfortunately, the extent of this reversed polarity zone can not be fully defined because at about 133 mbsf magnetization intensities begin to weaken to below practical cut-off limits (Fig. 18). Shipboard analyses of Hole 904A sediments suggest that reflectors p4 (purple) and m0.7 (blue) converge at about 105 mbsf, at which level a sharp change in magnetic susceptibility occurs. Based on the middle late Miocene age of the m0.7 reflector at Site 902 (see "Seismic Stratigraphy" section in Chapter 2, this volume) and the suggested occurrence of Zone NN10(?) and Zones N16–N17 below at about 178 mbsf (see "Biostratigraphy" section, this chapter), we tentatively correlate the sediments between 105 and 133 mbsf to Chron C4Ar or possibly Chron C4r (BKV85, CK92).

Between about 200 and 226 mbsf, magnetization intensities in discrete cubes strengthen to above the practical cut-off limit and suggest a reversed polarity zone over this 26-m interval (Fig. 18). Intensities weaken once again downhole to 370 mbsf, and so the polarity sense down to this level is largely unknown. However, in two short intervals where the magnetizations are sufficiently strong (259–270 and 309–320 mbsf), we suggest zones of normal polarity (Fig. 18). Preliminary correlations of these zones to the geomagnetic polarity time scale (GPTS) can be attempted based on the identification of nannofossil Zones NN7–NN8 in the interval 203–221.9 mbsf, planktonic foraminifer Zone N8 at about 250 mbsf, and nannofossil Zones NN4–NN5 between 241.2 and 258.14 mbsf, and Zones NN3 or NN2 at 279.66 mbsf (see "Biostratigraphy" section, this chapter). The relatively long reversed polarity interval from 200 to 226 mbsf

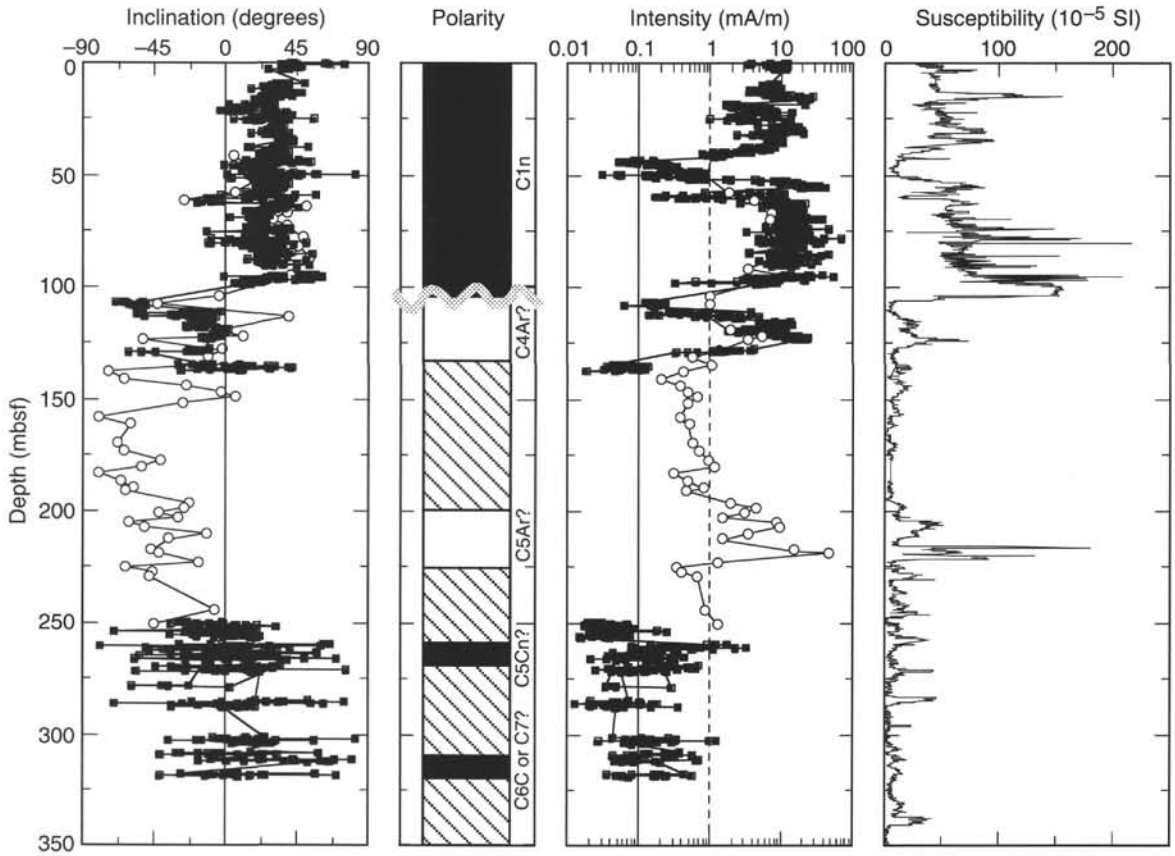

Figure 18. Inclination, magnetic polarity zones, magnetization intensity, and volume susceptibility for the interval from 0 to 350 mbsf in Hole 904A. Intensity cut-off value is 1 mA/m for discrete samples (open symbols), and 0.1 mA/m for pass-through measurements (closed symbols). In the polarity column, black = normal polarity, white = reversed polarity, and cross-hatched = uninterpretable.

Table 6. Reversal boundary depths, Site 904.

Depth (mbsf)	Polarity	Interpreted polarity zone
150-904A-		
0.0–105.0	N	C1n
105.0–133.0	R	C4Ar or C4r?
133.0–200.0	?	No zonation
200.0–226.0	R	C5Ar?
226.0–259.0	?	No zonation
259.0–270.0	N	C5Dn?
270.0–309.0	?	No zonation
309.0–320.0	N	C6C or C7?
320.0–370.0	?	No zonation
370.0–395.0	N	C15n?
395.0–400.0	R	C15r?
400.0–410.0	?	No zonation
410.0–435.0	N	No zonation
435.0–565.0	?	No zonation

Note: N = normal, R = reversed, and ? = uncertain.

may correlate to Chron C5Ar, and the short normal interval between 259 and 270 mbsf may represent Chrons C5Dn or C5Cn (Fig. 18 and Table 6). Identification of nannofossil Zone NP25 between 318 and 338 mbsf suggests a tentative correlation of the lower normal zone between 309 and 320 mbsf to one of the normal polarity subchrons within Chrons C6Cn or C7n (Fig. 18).

Magnetization intensities are fairly weak and inclinations somewhat scattered below 350 mbsf; thus, polarity is uninterpretable through much of the lower part of Hole 904A (Fig. 19). However, where magnetizations are relatively strong, there are indications of a normal polarity zone from about 370 to 395 mbsf, followed by a short reversed polarity zone to about 400 mbsf. We can also identify a zone of normal polarity between 410 and 435 mbsf (Fig. 19). The sediments at 375 mbsf belong to Zones NP19–20 and to Zones P16–P17 (see "Biostratigraphy" section, this chapter), which prompts us to assign the normal and reversed polarity zones between 370 and 400 mbsf to Chrons C15n and C15r, respectively. Several unconformities occur in the lower levels of Hole 904A and the normal polarity interval between 410 and 435 mbsf likely results from the concentration of several late and middle Eocene chrons. Thus, a correlation of the lower normal polarity interval to the GPTS is impossible at this time.

In summary, magnetization intensities are generally weak at Site 904, and we therefore judge our polarity zonations as working hypotheses for further work. More confident correlations to the GPTS await tests and confirmation in shore-based analyses.

SEDIMENTATION RATES

A Pleistocene to Eocene section was recovered at Site 904 (Fig. 20). It comprises a 106.20-m-thick upper to middle Pleistocene succession of silty clays, fine sands, and mass-flow deposits (see "Lithostratigraphy" section, this chapter). These rest on unconformably lower upper Miocene silty clays. The thickness of the upper Miocene is uncertain; dinocysts indicate ~33 m (based on dinocyst Zone G) of upper Miocene, whereas planktonic foraminifers indicate ~71 m (106.5–177.5 mbsf). The planktonic foraminifer biostratigraphy indicates that the upper Miocene unconformably overlies an approximately 70-m-thick middle Miocene section; calcareous nannofossil

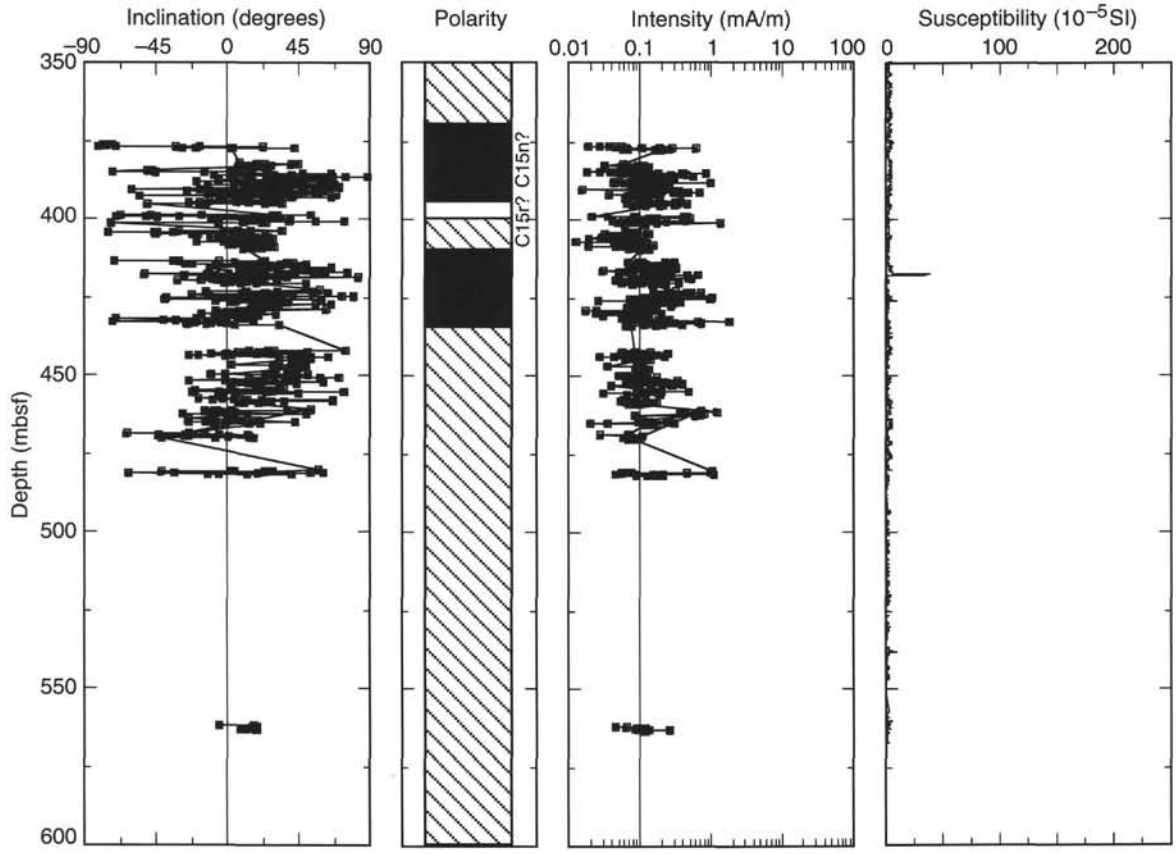

Figure 19. Inclination, magnetic polarity zones, magnetization intensity, and volume susceptibility for the interval from 350 to 600 mbsf in Hole 904A. Intensity cut-off value is 0.1 mA/m for pass-through measurements. In the polarity column, black = normal polarity, white = reversed polarity, and cross-hatched = uninterpretable.

data are consistent with this interpretation. Calcareous microfossils indicate that a ~65-m-thick lower Miocene interval of silty clays and sandy silts overlies a ~25 m section of upper Oligocene silty clay. Below, upper to upper lower Eocene nannofossil chalk constitutes a ~230-m-thick section that corresponds to lithologic Unit VII (see "Lithostratigraphy" section, this chapter); the uppermost lower Eocene (Subzone NP14a) was penetrated at total depth.

It is difficult to offer a comprehensive stratigraphic interpretation of the sedimentary section recovered at Hole 904A. The scarcity of diagnostic calcareous microfossil assemblages in most of the upper and middle Miocene section, the disagreements between relative age determinations based on various microfossil groups (see "Biostratigraphy" section, this chapter), and the weak magnetic signal in most of the section (see "Paleomagnetism" section, this chapter) result in uncertainties about specific chronostratigraphic details of the section and the position and ages of the unconformities. Shore-based analyses of larger volume discrete magnetostratigraphic samples, Sr-isotopic studies, and analyses of biostratigraphic samples from within cores should resolve many of these ambiguities.

The Pleistocene section at Site 904 is ~106.2 m thick (lithologic Unit I; Sections 150-904A-1H-3, 127 cm, to -12H-1, 85 cm). Sedimentation rates are high (mean = 22 cm/k.y.), similar to those determined at Site 902. This general estimate is based on two calcareous nannofossil datum levels: the lowest occurrence of *Emiliania huxleyi* at 37.5 mbsf (~285 ka) and the highest occurrence of *Pseudoemiliania lacunosa* at 104.12 mbsf (474 ka).

Site 902 sedimentation rates were successfully interpolated using a correlation of GRAPE data to the oxygen isotope stages (Fig. 21); however, at Sites 903 and 904, we successfully used magnetic susceptibility data to correlate to the SPECMAP oxygen isotopic time scale (Imbrie et al., 1984). Glacial-interglacial changes are often expressed in physical properties data (including susceptibility, density, and thermal conductivity) as a result of sedimentation changes. In this case, higher magnetic susceptibility values are associated with increased detrital content; these high values are interpreted as glacial in origin. The susceptibility record at Sites 902 to 904 mimics the GRAPE density data. For example, we compared the magnetic susceptibility to the widely spaced pycnometer density data at Site 904 and found generally good agreement (Fig. 21) with the susceptibility record.

Comparison with the SPECMAP scale is not as straightforward at Site 904 as it is at Sites 902 and 903. Although several clear susceptibility maxima (= inferred glacials) occur in the section, several possible correlations can be developed with the SPECMAP scale. There is some uncertainty in the age of the uppermost sediments because the *Emiliania huxleyi* abundance datum (less than about 84 ka) was not identified at Site 904, although it apparently lies above the first sample examined (8.62 mbsf; see "Biostratigraphy" section, this chapter). We pick the base of the Holocene drape by a distinct change from soupy, soft green muds to more lithified pink silty clays at 4.26 mbsf (Fig. 21; see "Core Photographs" and "Barrel Sheets" sections, this chapter).

The *P. lacunosa* datum establishes that the susceptibility maximum at 95–103 mbsf correlates with glacial stage 12 and the minimum at 82–95 mbsf with interglacial stage 11 (Fig. 21; note that the susceptibility scale has been inverted to mimic the SPECMAP scale). The lowest occurrence of *Emiliania huxleyi* at 37.5 mbsf occurs in a susceptibility minimum (= interglacial as verified by foraminiferal studies; see "Biostratigraphy" section, this chapter); its FAD has been correlated with oxygen isotope stage 8. At Site 903, it first appeared in early stage 7. Considering the 9.5-m sampling interval uncertainty

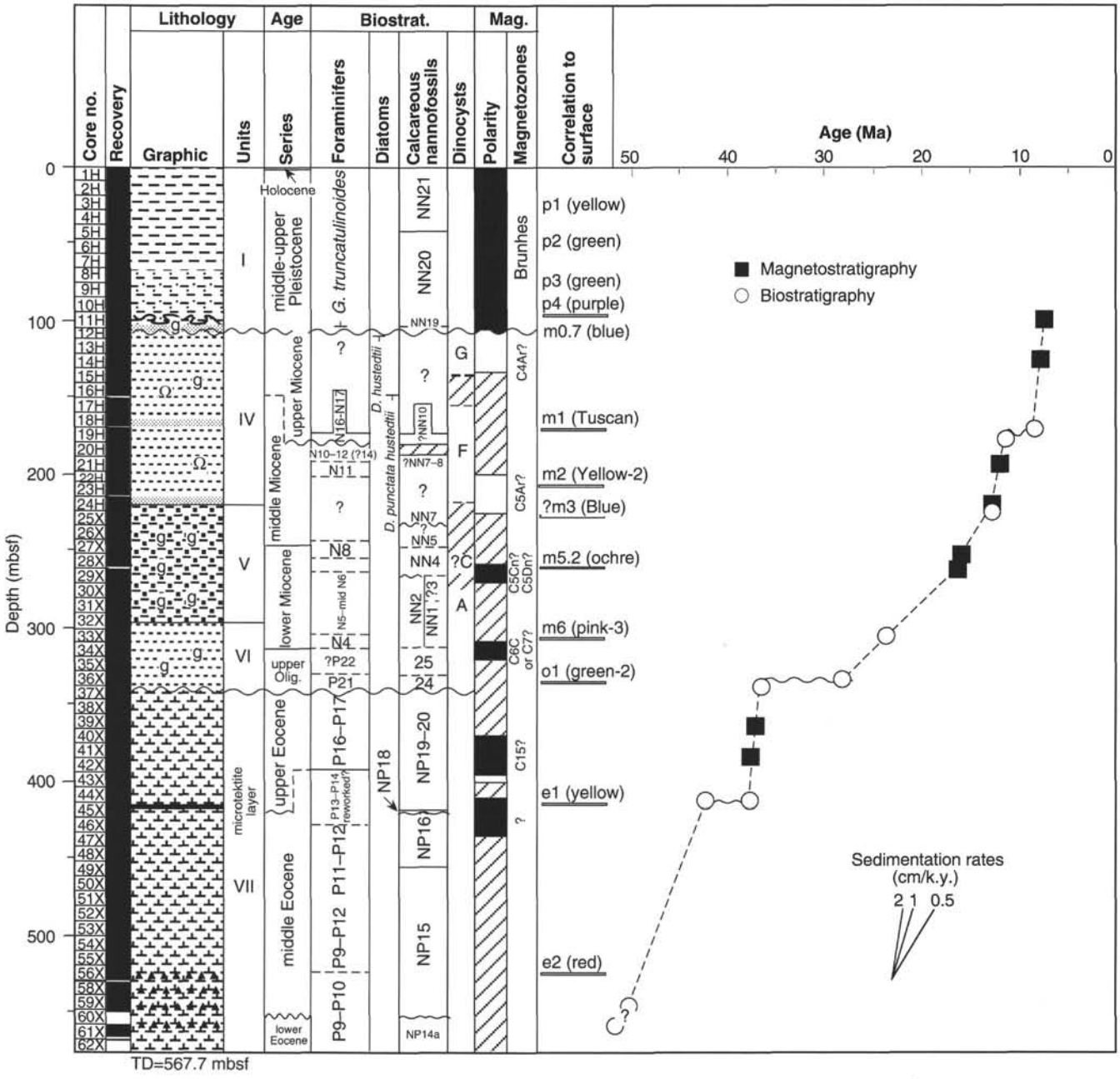

Figure 20. Age-depth diagram for Hole 904A showing lithostratigraphic units, series, biostratigraphy, magnetostratigraphy (black = normal polarities, white = reversed, cross-hatched = uncertain), and seismic reflectors. Wavy lines indicate hiatuses and/or unconformities noted in the borehole.

in the highest occurrence of *E. huxleyi* (Fig. 22), the susceptibility maximum at 55 mbsf can be correlated to glacial stage 8 and the minimum above with stage 7. The distinct susceptibility maximum at 15 m can then be correlated with stage 6.

Stage 10 is probably not well expressed because of a hiatus that correlates with a similar gap at Site 902. Several sharp susceptibility peaks between 80 and 70 mbsf and a pycnometer density peak at ~72 mbsf may be expressions of stage 10, although the distinct minimum associated with other glacial stages is not present.

The correlation to the SPECMAP time scale that is presented here (Figs. 21–22) is provisional and will be tested using other physical properties and biostratigraphic data. Based on the correlations presented here, Pleistocene sedimentation rates were 20–40 cm/k.y., except for stage 10, which is probably incomplete: stages 5.5–7.1 = 34 cm/k.y.; stages 7.0–8.2 = 39 cm/k.y.; stages 8.2–9.1 = 22 cm/k.y.; stages 9.1–10.0 = 21 cm/k.y.; stages 10.0–11.2 = 11 cm/k.y.; stages 11.2–12.2 = 29 cm/k.y.; and stages 12.2–12.4 = 22 cm/k.y. (Fig. 22).

As noted above, it is extremely difficult to provide even general estimates of Miocene–Oligocene sedimentation rates. Figure 20 shows a tentative curve based on several calcareous microfossil zonal boundaries; the sedimentation rates must be considered minimum estimates. Undetected stratigraphic gaps probably occur in the section, in addition to those clearly established across the upper lower/middle Eocene, middle/upper Eocene, Eocene/Oligocene, and middle/upper Miocene boundaries. Further refinements of the chronological control await shore-based magnetostratigraphic, biostratigraphic, and Sr-isotopic studies.

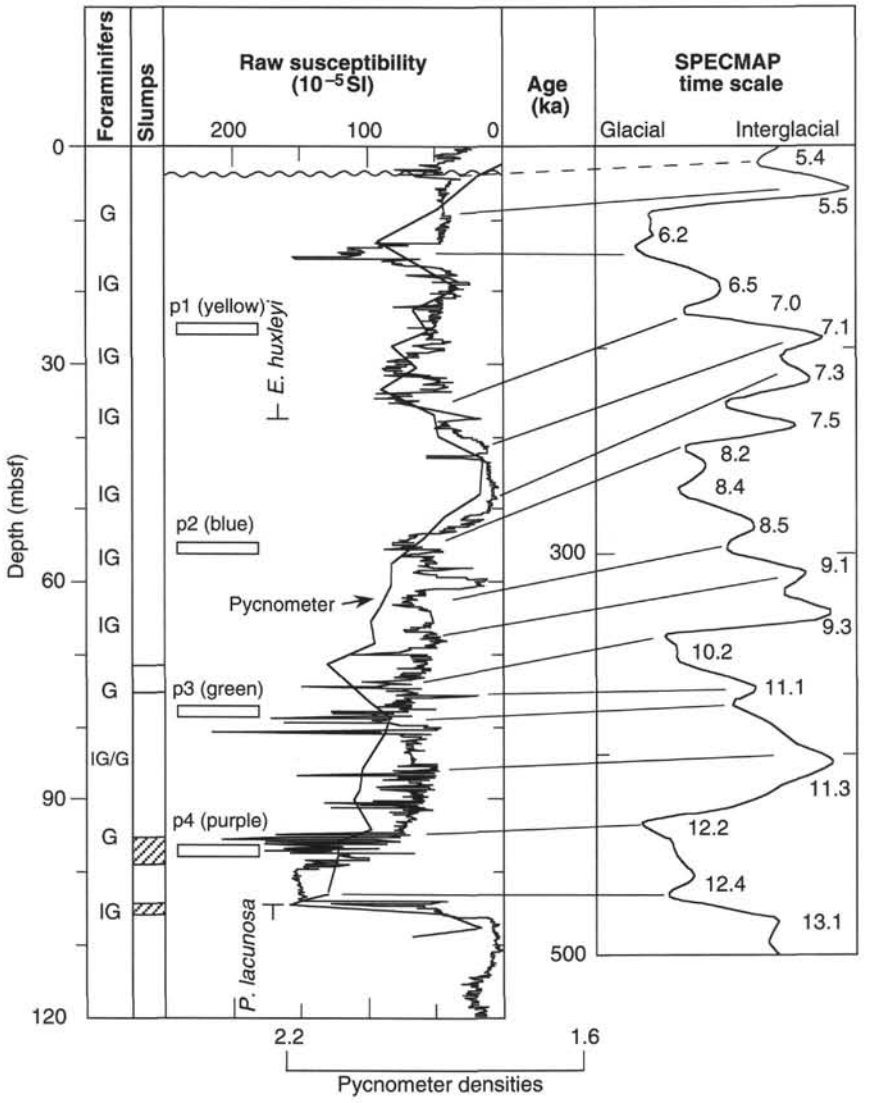

Figure 21. Correlations in Hole 904A between foraminiferal assemblages (G = glacial, IG = interglacial), slumped sediment, seismic reflectors, susceptibility data, and the SPECMAP time scale (from Imbrie et al., 1984). Oxygen isotopic substages are noted along the latter. The susceptibility scale has been inverted to match trends in the SPECMAP curve.

ORGANIC GEOCHEMISTRY

Shipboard organic geochemical analyses at Hole 904A included the measurement of hydrocarbon-gas concentrations contained within the sediment, together with bulk sediment studies, by using elemental and Rock-Eval analyses. The procedures are outlined in Chapter 3 (this volume).

Volatile Gases from Sediments

The initiation of methanogenesis in the sediment at Site 904 is at 32.5 mbsf, where trace levels (on the order of 10 ppm) of methane occur within the sulfate-reducing zone. Values increase exponentially with depth and reach a maximum at 446.5 mbsf with concentrations of 49,787 ppm. Values decrease downward from this maximum to the bottom of the site (Table 7 and Fig. 23). The vertical distribution of methane at Site 904 is consistent with the model of sulfate reduction vs. methanogenesis proposed by Claypool and Kaplan (1974), in which methane has an inverse relationship to sulfate in the depth profile (Fig. 24). The trace amounts of methane detected within the sulfate-reducing zone indicate that sulfate-reducing organisms and methanogens may coexist. However, methanogenesis is largely inhibited in the presence of sulfate because sulfate reducers overcome methanogenic bacteria in the competition for available hydrogen (Westbrook, Carson, Musgrave, Kennett, Baldauf, et al., 1994). Ethane was the only other hydrocarbon gas detected at Site 904, and its profile mimics that of methane (Fig. 23). Ethane is present at values of less than 15 ppm and is considered to be generated concurrently with methane by microorganisms.

Elemental Analysis

Inorganic-carbon content is less than 20 wt% $CaCO_3$ in the Pleistocene and Miocene sediments at Site 904; however, content increases abruptly to >50% in Oligocene and Eocene strata. At the Oligocene/Eocene boundary, high concentrations of glauconitic sands cause a minimum in the $CaCO_3$ profile; however, $CaCO_3$ abruptly increases to >60 wt% in the Eocene chalks.

Total organic carbon (TOC), nitrogen, and sulfur all covary and the highest values (up to 2.0, 0.2, and 2.8 wt%, respectively) occur in Mio-

Table 7. Headspace gas composition from sediments at Site 904.

Core, section, interval (cm)	Depth (mbsf)	C_1	C_2	C_3	C_1/C_2
150-904A-					
1H-4, 0–5	4.50	ND	ND	ND	
2H-4, 0–5	13.50	ND	ND	ND	
3H-4, 0–5	23.00	0	0	0	
4H-4, 0–5	32.50	12	0	0	
5H-4, 0–5	42.00	13	0	0	
6H-4, 0–5	51.50	14	0	0	
7H-4, 0–5	61.00	4	0	0	
8H-4, 0–5	70.50	101	0	0	
9H-4, 0–5	80.00	54	0	0	
10H-4, 0–5	89.50	14	0	0	
11H-4, 0–5	99.00	3	0	0	
12H-4, 0–5	108.50	12	0	0	
13H-4, 0–5	115.50	5	0	0	
14H-4, 0–5	125.00	15	0	0	
15H-5, 0–5	136.00	18	0	0	
16H-4, 0–5	144.00	9	0	0	
17H-4, 0–5	153.50	10	0	0	
18H-4, 0–5	163.00	11	0	0	
19H-4, 0–5	172.50	667	0	0	
20H-4, 0–5	182.00	1132	0	0	
21H-5, 0–5	193.00	2981	0	0	
22H-3, 0–5	199.50	17244	0	0	
23H-4, 0–5	207.50	9497	0	0	
24H-4, 0–5	217.00	6442	0	0	
25X-4, 0–5	226.50	10012	2	0	5006
26X-4, 0–5	235.80	18763	3	0	6254
27X-4, 0–5	245.40	12510	0	0	
28X-4, 0–5	254.80	9396	2	0	4698
29X-5, 0–5	266.10	6187	0	0	
30X-4, 0–5	274.30	8863	3	0	2954
31X-4, 0–5	284.00	6825	0	0	
32X-4, 0–5	293.60	9766	4	0	2442
33X-4, 0–5	303.30	9022	3	0	3007
34X-4, 0–5	312.90	933	0	0	
35X-4, 0–5	322.30	5075	0	0	
36X-4, 0–5	331.70	9060	5	0	1812
37X-4, 0–5	341.00	3277	0	0	
38X-4, 0–5	350.30	6166	0	0	
39X-4, 0–5	360.00	6942	0	0	
40X-3, 0–5	368.10	5080	0	0	
41X-4, 0–5	379.30	129	0	0	
42X-4, 0–5	388.90	14260	3	0	4753
43X-4, 0–5	398.60	9498	2	0	4749
44X-4, 0–5	408.30	21947	4	0	5487
45X-4, 0–5	417.90	10077	2	0	5039
46X-4, 0–5	427.50	20609	4	0	5152
47X-4, 0–5	437.00	23741	4	0	5935
48X-4, 0–5	446.50	39787	6	0	6631
49X-4, 0–5	456.00	9107	2	0	4554
50X-4, 0–5	465.70	21182	5	0	4236
51X-4, 0–5	475.40	33719	6	0	5620
52X-4, 0–5	485.00	36549	7	0	5221
53X-4, 0–5	494.70	23884	6	0	3981
54X-4, 0–5	504.30	18545	4	0	4636
55X-4, 0–5	514.00	21758	5	0	4352
56X-4, 0–5	523.30	24571	7	0	3510
58X-4, 0–5	533.90	11027	4	0	2757
59X-4, 0–5	542.50	24071	10	0	2407
61X-1, 135–140	558.65	11352	14	0	811
62X-1, 0–5	567.00	35	0	0	

Note: ND = no data.

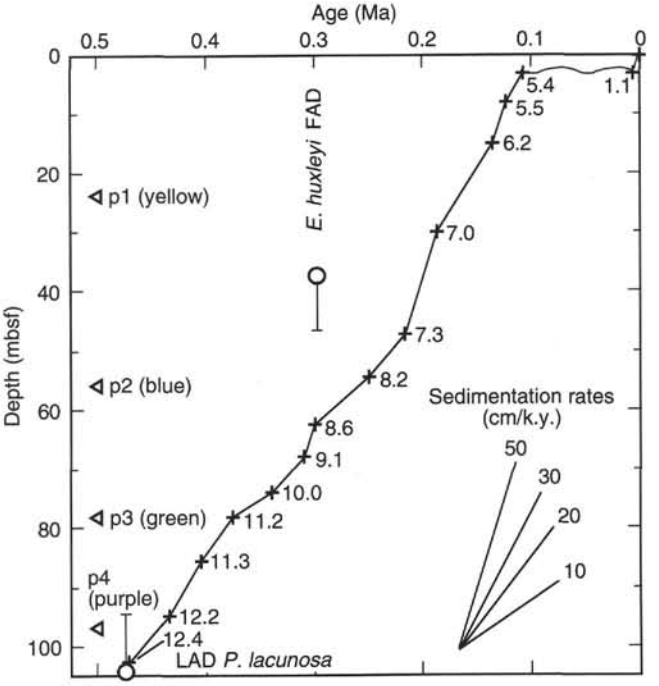

Figure 22. Age-depth diagram for the Pleistocene of Hole 904A based on the oxygen isotope correlations established using susceptibility data (Fig. 21). p1–p4 are correlations of seismic reflectors.

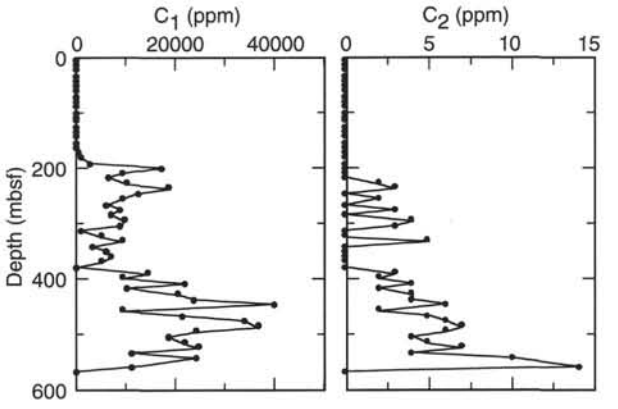

Figure 23. Headspace volatile hydrocarbon composition vs. depth for sediment samples from Hole 904A.

cene sediments between 106.8 and above 351.0 mbsf (Table 8 and Fig. 25). High variability in concentrations of these elements occurs throughout this interval; the reason for this variability is unclear. The minima do not appear to consistently correspond to sand-rich intervals, which would enhance oxic conditions, and no indication exists that the higher values are caused by an increased abundance of terrestrial organic matter, which was transported from the shelf.

Characterization of Organic Matter

The organic-matter content in marine environments is usually less than 0.5% (McIver, 1975). Based on Rock-Eval T_{max} values (Table 9), the organic matter appears to be immature throughout the section in Site 904. The T_{max} values higher than 435 are apparently not caused by increased maturity, but by an artifact of low TOC that causes pyrolyzed hydrocarbons to adhere to clays so that T_{max} is overestimated.

All of the samples plot between the type II and type III kerogen evolutionary pathways at points far from the origin on the van Krevelen-type diagram; this indicates that the organic matter is of mixed marine and terrigenous origin and is thermally immature (Fig. 26). A group of samples, mainly from Eocene chalks, has very high oxygen indexes (>300) and low hydrogen indexes (<100), suggesting that their organic matter has been highly oxidized, either during transportation or by diagenesis. These samples contain low TOC (<0.5%), which suggests that the environment was not ideal for the high preservation of organic matter.

The organic C/N ratios of the organic matter are typically ≤10 (Table 8); these ratios indicate that marine organisms were the principal contributors to these sediments and that the contribution of organic matter from continental runoff is minor. The very low C/N ratios (<5) in the Eocene sediments (below 341 mbsf) are less than the original C/N ratios of any living organisms (plankton, 5–8; higher plants, 20–100) and, therefore, cannot be used as indicators of organic-matter

Table 8. Inorganic carbon, organic carbon, and elemental analysis data from sediments at Site 904.

Core, section, interval (cm)	Depth (mbsf)	Total carbon (wt%)	Inorganic carbon (wt%)	Total organic carbon (wt%)	$CaCO_3$ (wt%)	Nitrogen (wt%)	Sulfur (wt%)	C/N	C/S
150-904A-									
1H-4, 85–87	5.35	0.70	0.33	0.37	2.70	0.04	0.17	9	2
2H-4, 67–69	14.17	1.51	1.16	0.35	9.70	0.04	0.24	9	1
3H-4, 80–82	23.80	0.76	0.38	0.38	3.20	0.04	0.19	10	2
4H-3, 66–67	31.66	1.99	1.59	0.40	13.20	0.06	0.08	7	5
5H-3, 60–61	41.10	2.25	1.71	0.54	14.20	0.06	0.14	9	4
6H-5, 55–56	53.55	1.56	1.18	0.38	9.80	0.06	0.90	6	0
7H-4, 77–78	61.77	1.89	1.46	0.43	12.20	0.06	0.18	7	2
8H-4, 79–81	71.29	2.06	1.75	0.31	14.60	0.06	0.13	5	2
9H-3, 67–68	79.17	1.66	1.36	0.30	11.30	0.05	0.13	6	2
10H-2, 79–81	87.29	0.74	0.42	0.32	3.50	0.04	0.09	8	4
11H-2, 133–135	97.33	0.86	0.51	0.35	4.20	0.04	0.07	9	5
12H-2, 134–135	106.84	1.69	0.06	1.63	0.50	0.14	1.87	12	1
13H-4, 45–47	115.95	1.61	0.36	1.25	3.00	0.12	0.39	10	3
14H-4, 68–70	125.68	1.30	0.52	0.78	4.30	0.10	0.43	8	2
15H-4, 67–69	135.17	1.32	0.21	1.11	1.70	0.12	0.81	9	1
16H-3, 80–82	143.30	1.77	0.11	1.66	0.90	0.15	2.02	11	1
17H-3, 71–73	152.71	1.65	0.10	1.55	0.80	0.13	1.61	12	1
18H-3, 78–79	162.28	2.26	1.03	1.23	8.60	0.17	2.76	7	0
19H-3, 53–54	171.53	1.04	0.46	0.58	3.84	0.105	1.81	6	0
20H-3, 77–78	181.27	1.97	0.69	1.28	5.70	0.18	2.32	7	1
21H-3, 80–81	190.80	2.60	1.83	0.77	15.20	0.20	2.26	4	0
22H-3, 63–65	200.13	1.49	0.79	0.70	6.60	0.14	1.86	5	0
23H-3, 84–86	206.84	1.92	0.77	1.15	6.40	0.13	0.20	9	6
24H-3, 86–87	216.36	1.07	0.63	0.44	5.20	0.06	0.13	7	3
24H-4, 7–10	217.07	0.53	0.21	0.32	1.70	0.04	0.23	8	1
25X-3, 98–100	225.98	1.73	0.53	1.20	4.40	0.15	2.34	8	1
26X-3, 79–80	235.09	3.23	1.16	2.07	9.70	0.20	2.38	10	1
27X-4, 38–40	245.78	2.99	1.42	1.57	11.80	0.15	2.32	10	1
28X-4, 80–82	255.60	2.87	1.44	1.43	12.00	0.13	1.26	11	1
29X-3, 85–87	263.95	4.18	2.22	1.96	18.50	0.16	1.40	12	1
30X-4, 60–61	274.90	2.16	0.75	1.41	6.20	0.12	1.22	12	1
31X-4, 80–82	284.80	1.47	0.63	0.84	5.20	0.12	2.13	7	0
32X-6, 78–79	297.38	6.69	5.10	1.59	42.50	0.13	0.89	12	2
33X-3, 48–49	302.28	6.61	5.42	1.19	45.10	0.18	0.65	7	2
34X-1, 71–72	309.11	7.35	6.07	1.28	50.60	0.12	1.25	11	1
35X-3, 68–70	321.48	4.30	3.11	1.19	25.90	0.12	1.02	10	1
36X-6, 28–30	334.98	2.72	1.54	1.18	12.80	0.12	2.31	10	1
37X-1, 48–49	336.98	3.12	1.76	1.36	14.70	0.13	1.51	10	1
38X-4, 67–68	350.97	5.19	5.00	0.19	41.70	0.07	0.17	3	1
39X-4, 83–84	360.83	6.34	6.08	0.26	50.60	0.12	0.13	2	2
40X-3, 58–59	368.68	4.69	4.38	0.31	36.50	0.08	0.28	4	1
41X-3, 58–59	378.38	5.59	5.31	0.28	44.20	0.08	0.44	4	1
42X-3, 78–79	388.18	5.27	5.02	0.25	41.80	0.07	0.48	4	1
43X-3, 80–81	397.90	6.00	5.85	0.15	48.70	0.13	0.29	1	1
44X-3, 67–69	407.47	4.34	4.00	0.34	33.30	0.08	0.33	4	1
45X-3, 78–80	417.18	5.25	4.83	0.42	40.20	0.07	0.29	6	1
46X-4, 84–85	428.34	4.95	4.80	0.15	40.00	0.05	0.14	3	1
47X-3, 65–66	436.15	5.72	5.41	0.31	45.10	0.05	0.09	6	3
48X-3, 80–81	445.80	6.19	6.03	0.16	50.20	0.04	0.00	4	—
49X-5, 70–71	458.20	6.66	6.50	0.16	54.10	0.05	0.00	3	—
50X-5, 70–72	467.90	5.48	5.30	0.18	44.10	0.05	0.03	4	6
51X-4, 82–83	476.22	6.59	6.31	0.28	52.60	0.05	0.00	6	—
52X-6, 24–25	488.24	5.85	5.77	0.08	48.10	0.05	0.04	1	2
53X-4, 86–88	495.56	6.93	6.73	0.20	56.10	0.04	0.05	5	4
54X-3, 61–62	503.41	6.23	6.06	0.17	50.50	0.05	0.00	3	—
55X-4, 62–63	514.62	6.65	6.57	0.08	54.70	0.05	0.05	1	1
56X-3, 80–81	522.60	6.22	6.11	0.11	50.90	0.04	0.05	3	2
58X-1, 68–69	530.08	6.25	6.03	0.22	50.20	0.04	0.11	0	1
59X-5, 98–99	544.98	7.25	7.08	0.17	59.00	0.03	0.03	6	6
61X-3, 76–77	561.06	5.67	5.36	0.31	44.60	0.06	0.09	5	3

origin. These low ratios are considered to be artifacts of the very low TOC content of the Eocene chalks, which causes the organic C/N ratio to be interfered by ammoniacal nitrogen residing on clay surfaces and within the clay mineral lattice.

INORGANIC GEOCHEMISTRY

Interstitial water trends at Site 904 are similar to those observed at the nearby slope Sites 902 and 903. Twenty-one interstitial water samples were collected from Site 904 and sampled depths range from 4.5 to 559 mbsf. Analytical results (Table 10 and Fig. 27) were determined on samples from approximately every third core.

Bacterial degradation of organic matter at this site by means of sulfate reduction results in the depletion of sulfate ion and an increase in alkalinity, ammonium, and phosphate (Fig. 27). The sulfate-ion concentration decreases to 1.0 mM by 108 mbsf, then increases across the Pleistocene/Miocene contact to 2.4 mM at 135 mbsf, and finally decreases to near-zero values at greater depths (Fig. 27). The offset in the sulfate profile may reflect rapid deposition of overlying Pleistocene slump deposits (see "Lithostratigraphy" section, this chapter). The decrease in sulfate results from the degradation of organic matter by sulfate-reducing bacteria in these sediments. Alkalinity increases to 19 mM by 51 mbsf, decreases to 12 mM at 80 mbsf, and then increases to a maximum of 34 mM by 217 mbsf (Fig. 27). Below 217 mbsf, alkalinity decreases gradually to 21 mM by 559 mbsf. The first alkalinity maximum occurs in the current sulfate-reduction zone, whereas the second alkalinity maximum is associated with the rapid increase in average organic-matter content from 0.4 wt% in the overlying Pleistocene sediment to 1.3 wt% in the upper Miocene (see "Organic Geochemistry" section, this chapter). The high alkalinity is a byproduct of bacterial degradation of organic matter. The maximum alkalinity corresponds to the rapid increase in headspace methane, indicating that methanogenesis is very active at 217 mbsf. Ammonium shows a gradual increase with depth to 4 mM by 193 mbsf,

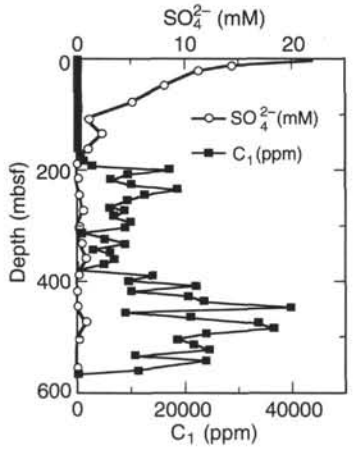

Figure 24. Diagenetic relationship between sulfate and methane at Site 904.

followed by a more rapid increase to a maximum concentration of 9 mM by 446 mbsf (Fig. 27). Phosphate ranges from 16 to 35 µM to a depth of 193 mbsf and is low (<5 µM) below 193 mbsf. The ammonium maximum occurs below the alkalinity and phosphate maxima, reflecting the preferential metabolism of phosphorus to nitrogen-rich organic matter (Gieskes, 1981).

In addition to organic-matter degradation, the other important trends shown in the pore-water profiles at Site 904 is the sharp salinity and chloride gradients below the Pleistocene/Miocene boundary. These gradients increase with depth to a similar asymptotic concentration throughout the New Jersey slope (including DSDP Site 612; Poag, Watts, et al., 1987) and are apparently released to dissolution of salt diapirs at depth (Grow et al., 1988). Salinity initially decreases downward from 35.5‰ to 34.0‰ at 4.5 mbsf and then remains at ~35‰ to 51 mbsf (Fig. 27). The lowered salinity reflects the loss of sulfate, calcium, and magnesium corresponding to dolomite precipitation in the sulfate-reduction zone. Salinity then increases to a maximum of 55.5‰ by 559 mbsf. The largely parallel increase in chloride indicates that the increase in salinity is caused mainly by diffusion of sodium and chloride ions from below (Fig. 27).

The chloride profile represents the net result of two competing processes: diffusion of Cl ion from a Cl-rich brine below vs. the accumulation of sediment above with a Cl concentration of seawater (559 mM). The Cl brine appears to have an asymptotic Cl concentration of ~980 to 990 mM on the basis of the Cl gradients of nearby slope sites. At Site 904, chloride is close to the seawater value of 559 mM to 23 mbsf, increases gradually to 583 mM at 80 mbsf, and then increases rapidly below the Pleistocene/Miocene boundary. A steep increase was also observed across the top of the Miocene at all other sites on the slope, reflecting the rapid increase in sedimentation rates during the Pleistocene. The steep gradient occurs at a depth that defines the disconformable Pleistocene/Miocene boundary between lithologic Units I and IV and the proposed m0.7 (blue) seismic reflec-

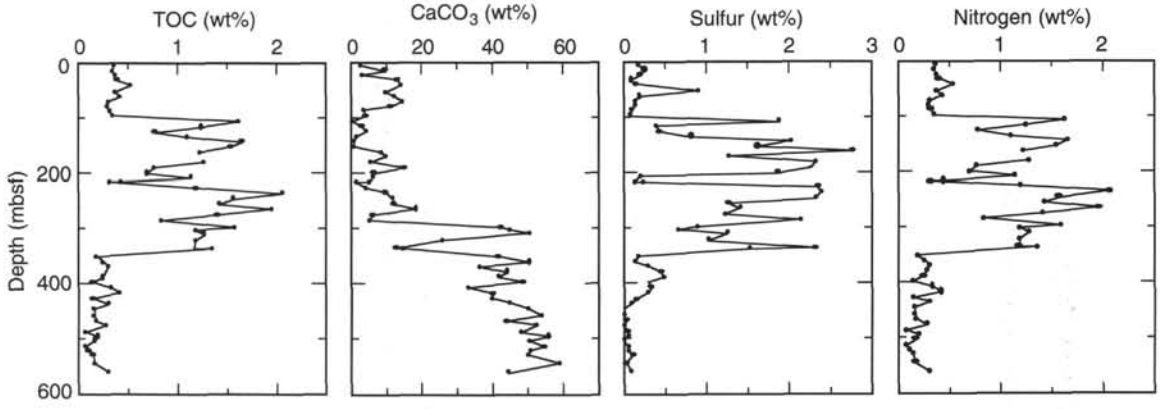

Figure 25. Total organic carbon (TOC), carbonate concentration (calculated as $CaCO_3$), sulfur, and nitrogen vs. depth for sediment samples from Site 904.

Table 9. Results of Rock-Eval pyrolysis, Site 904.

Core, section, interval (cm)	Depth (mbsf)	T_{max} (°C)	S_1 (mg/g)	S_2 (mg/g)	S_3 (mg/g)	TOC (wt%)	HI	OI	PI	S_2/S_3
150-904A-										
1H-4, 85–87	5.35	594	0.11	0.54	0.78	0.41	131	190	0.17	0.69
4H-3, 66–67	31.66	409	0.10	0.28	1.27	0.32	87	396	0.26	0.22
7H-4, 77–78	61.77	397	0.10	0.33	0.98	0.41	80	239	0.24	0.33
10H-2, 79–81	87.29	463	0.06	0.25	1.21	0.3	83	403	0.20	0.20
13H-4, 45–47	115.95	423	0.37	3.35	1.97	1.39	241	141	0.10	1.70
16H-3, 80–82	143.30	419	0.51	3.73	1.06	1.74	214	60	0.12	3.51
19H-3, 53–54	171.53	584	0.19	1.51	1.07	0.53	284	201	0.11	1.41
22H-3, 63–65	200.13	421	0.34	2.55	2.15	1.09	233	197	0.12	1.18
24H-4, 38–40	217.07	587	0.05	1.14	1.04	0.36	316	288	0.04	1.09
27X-3, 38–40	245.78	413	0.30	2.39	2.14	1.52	157	140	0.11	1.11
30X-3, 60–61	274.90	414	0.45	2.11	1.46	1.21	174	120	0.18	1.44
41X-3, 58–59	378.38	417	0.08	0.41	1.38	0.36	113	383	0.17	0.29
42X-3, 78–79	388.18	415	0.07	0.36	1.42	0.33	109	430	0.17	0.25
45X-3, 78–80	417.18	413	0.08	0.40	1.44	0.39	102	369	0.17	0.27
48X-3, 80–81	445.80	431	0.07	0.22	1.15	0.14	157	821	0.25	0.19
51X-4, 82–83	476.22	409	0.05	0.26	1.04	0.14	185	742	0.17	0.25
54X-3, 61–62	503.41	396	0.04	0.25	1.06	0.16	156	662	0.14	0.23
59X-5, 98–99	544.98	413	0.05	0.22	1.16	0.24	91	483	0.19	0.18

Note: TOC = total organic carbon, HI = hydrogen index, OI = oxygen index, and PI = production index.

tor. Cl reaches a value of 759 mM by 217 mbsf and corresponds to an interval of thin sandy turbidites (see "Lithostratigraphy" section, this chapter). Chloride increases slowly between 217 and 274 mbsf to a value of 776 mM, and then increases more rapidly to 861 mM by 389 mbsf. Chloride remains constant at 862 mM from 389 to 446 mbsf and then increases to a maximum of 951 mM by 559 mbsf. The asymptotic Cl concentration was apparently not reached at Site 904. The increased gradient below 446 mbsf does not appear to correspond to any obvious lithologic change, age boundary, or seismic reflector.

The increase in salinity at the slope sites is associated with a drop in pH that may explain, in part, the paucity of calcareous fossils within parts of the Miocene section. The pH profiles of the slope sites are generally similar, showing a near-surface Pleistocene maximum, followed by a gradual decrease to slightly acidic values at depths below the chloride gradient. At Site 904, the pH shows a maximum value of 7.7 at 23 mbsf before decreasing to a minimum of 6.5 by 504 mbsf (Fig. 27). The relatively high pH values centered around 23 mbsf correspond to low values of Ca, Mg, and Sr that indicate carbonate precipitation is occurring at these depths. This is supported by the occurrence of dolomite in the uppermost 100 mbsf (see "Lithostratigraphy" section, this chapter). An unusual feature of the pH profile at this site is a large positive offset in pH of 0.8 to a range of 7.5 to 7.4 in the interval from 389 to 475 mbsf. The cause of this offset in pH is uncertain, but it corresponds to an increase in the Ca, Mg, and Sr profiles and the interval having a nearly constant Cl concentration (Fig. 27).

The increase in alkalinity associated with the degradation of organic matter promotes the precipitation of diagenetic carbonates by increasing the degree of supersaturation of the pore waters (Compton, 1988). Precipitation of diagenetic carbonate at depths centered around 80 mbsf is indicated by the Ca, Sr, and Mg ion minima in the uppermost 100 mbsf. Calcium decreases to 5.4 mM by 51 mbsf and remains fairly constant at around 5.5 to 6.0 mM to 80 mbsf (Fig. 27). Ca increases rapidly to 12.3 mM by 241 mbsf and then increases more gradually to a maximum of 17.7 mM by 559 mbsf. The Ca trend is similar to the Cl profile below 108 mbsf and may reflect an additional diffusional source of Ca associated with the Cl brine from the dissolution of anhydrite in addition to halite. Strontium is similar to Ca, decreasing to a minimum of 67 µM by 51 mbsf and then increasing with depth to a maximum of 454 µM by 559 mbsf (Fig. 27). The relatively high Sr concentrations at Site 904 probably reflect the recrystallization of abundant biogenic carbonate at this site (40–60 wt% below 300 mbsf; see "Organic Geochemistry" section, this chapter). Magnesium ion decreases to a minimum concentration of 39 mM by 80 mbsf (Fig. 27). This decrease combined with the relatively high Mg/Ca ratios are consistent with dolomite precipitation. Mg increases to a value of 45 mM by 217 mbsf and remains somewhat below or close to 45 mM to 559 mbsf. The fairly constant concentration of Mg below 217 mbsf contrasts with the increase in Ca and Sr, and suggests that dolomitization is not currently occurring below 217 mbsf and that diffusion of Cl is not associated with an increase in Mg.

Concentrations of potassium and iron pore-water ions are important because of the abundance of glauconite (K- and Fe-rich illite), pyrite (FeS_2), and siderite ($FeCO_3$) in these sediments. Most of the pyrite and siderite is formed in place; however, the glauconite is probably a mixture of authigenic and reworked shelfal glauconite. Site 904 is similar to Site 903 in that the pore-water K maximum corresponds to the interval of greatest glauconite abundance (see "Lithostratigraphy" section, this chapter). Potassium at Site 904 decreases to 8.8 mM by 80 mbsf, increases to a maximum of 12.7 mM at 245 mbsf, and then decreases to a minimum of 9.6 mM by 418 mbsf before returning to near-seawater values below 446 mbsf (Fig. 27). The maximum pore-water K value corresponds to a particularly rich glauconite interval from 240 to 250 mbsf. The pore-water profiles suggest that the glauconite-rich interval is a source of K and that there are K sinks above and below. The nature of these K sinks above and below the glauconite interval is unknown, but may include authigenic

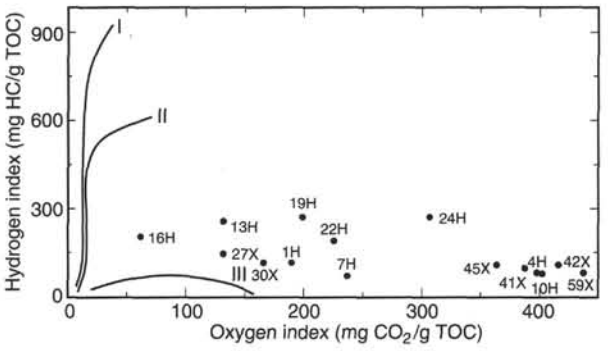

Figure 26. Van Krevelen-type diagram of sediment samples from Hole 904A. The numbers and letters adjacent to the data points (solid dots) refer to core numbers.

K-feldspar. The increase in K may also be explained by the temperature-of-squeezing effect, an artifact of the sampling procedure that has been observed to cause an increase in K concentration (Waterman, 1973). However, it seems unlikely that this effect would only occur in the glauconite-rich intervals.

The Fe-rich terrigenous material is abundant in these largely reducing slope sequences and provides an ample source of Fe for the formation of diagenetic minerals such as Fe-sulfides, Fe-carbonates, and glauconite. There is an iron maximum of 26 µM at 4.5 mbsf that decreases rapidly to 6 µM by 23 mbsf (Fig. 27). Fe remains low (6–16 µM) from 13 to 245 mbsf and then increases to maximum values of 19 to 85 µM below 245 mbsf. Variations in the Fe concentrations may be related to pyrite, siderite, and glauconite abundance. The first occurrence of pyrite between 10 and 20 mbsf corresponds to the rapid decrease following the first Fe maximum (see "Lithostratigraphy" section, this chapter). The interval of high Fe content generally corresponds to the pyrite and glauconite intervals, but the exact relationship among them is unclear. Dolomite dominates the diagenetic carbonate above 108 mbsf and siderite tends to dominate below 108 mbsf (see "Lithostratigraphy" section, this chapter). Siderite formation is favored below the sulfate reduction zone because the sulfide sink of Fe is no longer available. Replacement of glauconite by pyrite may explain the high Fe and K values associated with the glauconite intervals. In addition to sulfate that diffuses into the sediment from the overlying seawater, sulfate may diffuse in with the brine from below.

High silica concentrations primarily reflect the abundance of highly soluble opaline (opal-A) silica, which is largely present as diatoms. A decrease in the silica concentration can indicate the opal-A to opal-CT transformation at greater depth in the sediment. Silica tends to increase sporadically with depth to a maximum of 1515 µM at 504 mbsf (Fig. 27). The decrease in silica to 902 µM at 559 mbsf may indicate that the transformation of opal-A to opal-CT is beginning to occur at or below this depth.

PHYSICAL PROPERTIES

Sampling Procedures

On average, three wet-bulk-density measurements with the wet mass-volume (MV) method were made per core, to a total depth of 567.16 mbsf.

We were able to make more velocity measurements at Site 904 than at previous Sites 902 and 903, probably because of the much lower concentration of gas in the sediment. An average of three compressional-wave velocity measurements per core were conducted using either the digital sound velocimeter (DSV) tool or the Hamilton Frame velocimeter. The *P*-wave logger was run on those sections that showed good core-to-liner contact. *P*-wave logger results were obtained to about 250 mbsf.

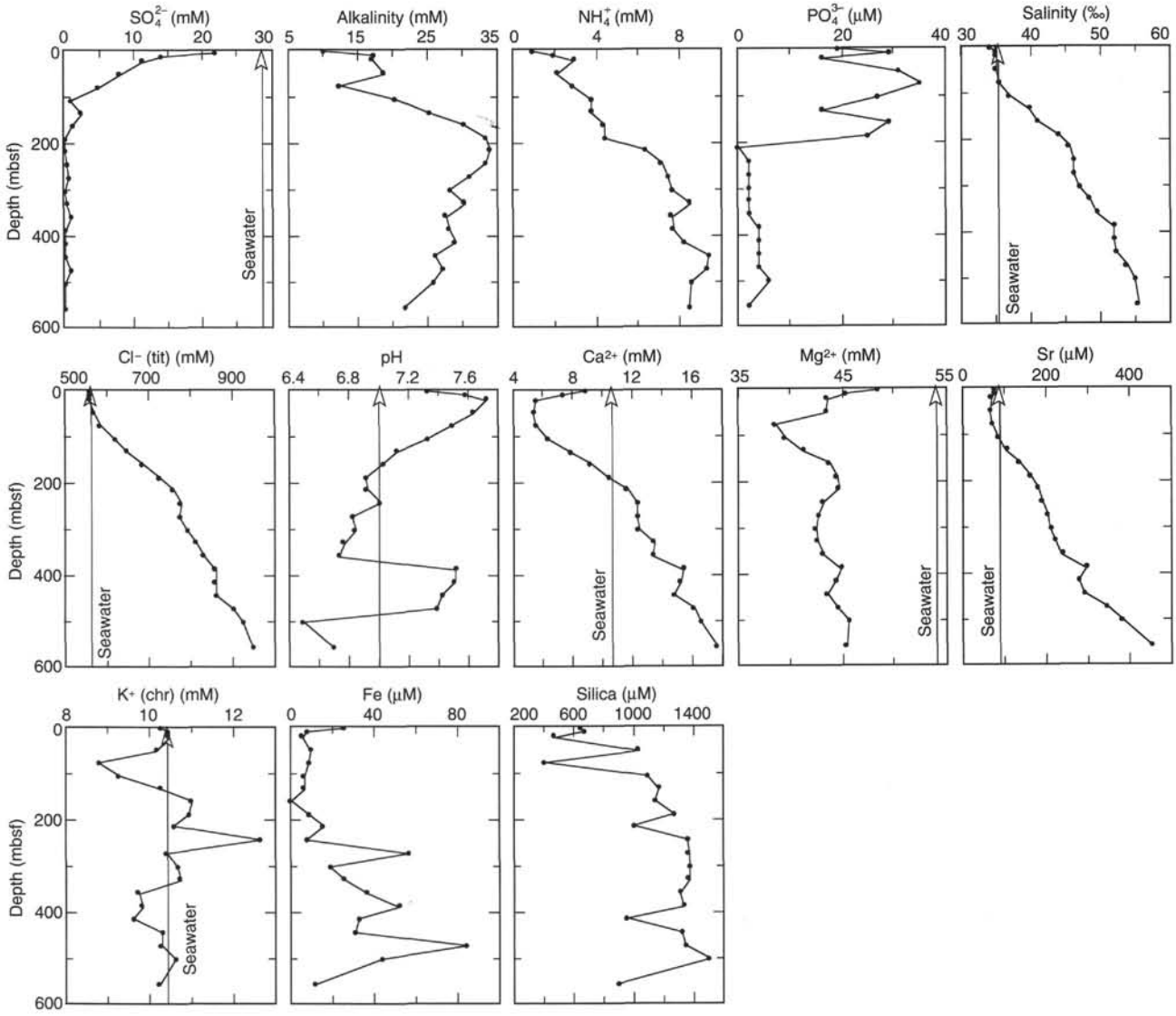

Figure 27. Interstitial-water geochemical data vs. depth, Site 904. tit = titration, chr = chromatography.

On average, one thermal conductivity measurement was made every 3 m. Near the bottom of Hole 904A, at about 520 mbsf, the sediment became too indurated to insert the thermal probes.

The first complete log of MST natural gamma-ray (MST NGR) emission from cores on Leg 150 was obtained at Hole 904A (Fig. 28 and also Fig. 29). Correlation with the downhole gamma-ray measurements proved to be excellent. From seafloor to 88.2 mbsf we used a scan time of 45 s, measuring MST NGR counts 20 cm below the top of each section. We increased the number of sampling positions to one every 20 cm in each section and correspondingly decreased the scan time to 30 s from 88.2 to 105.7 mbsf. A 30-s exposure rate proved appropriate for the rest of the hole, although, to improve core flow, we decreased the sampling interval to once every 40 cm in each section from 105.7 mbsf to total depth. Final data were normalized to a 30-s scan window. We refer the reader to the "Downhole Logging" section (this chapter) for a comparison of this data set with that from the equivalent downhole logging tool (see also Chapter 5, this volume).

GRAPE and Index Properties

GRAPE and MV bulk-density measurements are the most densely sampled and complete physical properties data sets at Site 904, and these values are used to distinguish five major units (Fig. 28). Six additional subunits are recognized as well. Reference to the boundaries of bulk-density units is made with respect to the location of the nearest physical properties point of measurement.

Bulk-density Units

Unit I

Interval: Sample 150-904A-12H-2, 7–9 cm
Depth: 0–105.60 mbsf

Unit I represents a high-density Pleistocene "cap" (see "Biostratigraphy" section, this chapter), with a maximum density of 2.19 g/cm^3 at its base in an interval of mass flow deposits (see "Lithostratigraphy" section, this chapter). Subunits IA and IB are separated by a local density minimum of 1.68 g/cm^3 at 44.24 mbsf (Sample 150-904A-5H-5, 74–76 cm), approximately correlative with seismic reflector p2 (blue). The base of Unit I correlates well with the base of lithologic Unit I and seismic reflector m0.7 (blue).

Unit II

Interval: Sample 150-904A-18H-3, 74–76 cm
Depth: 105.70–189.24 mbsf

Table 10. Interstitial-water data, Site 904.

Core, section, interval (cm)	Depth (mbsf)	IW (mL)	pH	Alkalinity (mM)	Salinity (‰)	Cl^- (tit) (mM)	Cl^- (chr) (mM)	SO_4^{2-} (mM)	NH_4^+ (mM)	PO_4^{3-} (μM)	SiO_2 (μM)	Sr (μM)	Mn (μM)	Fe (μM)	Na^+ (calc) (mM)	Na^+ (chr) (mM)	K^+ (chr) (mM)	Mg^{2+} (chr) (mM)	Ca^{2+} (chr) (mM)
150-904A-																			
1H-3, 145–150	4.48	44	7.33	9.99	34.0	558	565	21.99	0.9	19	636	79	12.2	25.9	486	487	10.27	48.45	8.86
2H-3, 145-150	13.48	30	7.58	17.19	35.0	559	557	14.09	1.9	29	667	76	6.8	8.0	486	480	10.48	45.31	7.38
3H-3, 145-150	22.98	38	7.72	17.04	35.0	559	565	11.19	2.9	16	466	69	1.4	5.5	487	488	10.47	43.49	5.45
6H-3, 145-150	51.48	38	7.63	18.66	35.0	570	577	7.80	2.1	31	1035	67	2.7	9.8	495	488	10.17	43.42	5.35
9H-3, 145-150	79.98	38	7.49	12.41	35.5	583	588	4.91	2.8	35	399	71	1.5	8.9	505	525	8.77	38.55	5.51
12H-3, 145-150	108.48	45	7.32	20.32	37.0	617	624	0.79	3.77	27	1091	84	2.4	6.6	534	527	9.26	39.46	6.29
15H-3, 145-150	135.08	41	7.12	25.15	39.8	648	662	2.39	3.74	16	1172	105	3	6.6	566	551	10.28	41.20	7.85
18H-2, 145-150	161.78	34	7.03	30.05	41.0	686	695	1.06	4.35	29	1149	134	3.5	NM	597	566	11.02	43.69	9.20
21H-4, 145-150	192.98	62	6.91	33.28	44.0	726	730	0.00	4.38	25	1275	161	2.2	9	634	609	10.95	44.46	10.37
24H-3, 145-150	216.98	40	6.92	33.85	45.5	759	770	0.00	6.34	0	1000	181	2.2	16	663	625	10.59	44.59	11.61
27X-3, 145-150	245.38	37	7.01	33.28	46.2	778	804	0.31	7.09	2	1368	189	1.4	8	680	661	12.70	43.11	12.34
30X-3, 145-150	274.28	52	6.82	30.87	46.2	776	800	0.64	7.43	2	1371	203	NM	57	679	665	10.43	42.70	12.33
33X-3, 145-150	303.28	33	6.84	28.21	47.0	794	817	0.00	7.6	2	1382	210	1.2	19	694	679	10.67	42.36	12.42
36X-3, 145-150	331.68	32	6.76	30.22	48.5	813	853	0.27	8.5	2	1371	221	1.1	26	712	689	10.74	42.55	13.41
39X-3, 145-150	359.98	28	6.73	27.52	49.5	833	845	0.93	7.58	2	1315	238	1.1	37	731	705	9.73	43.10	13.35
42X-3, 140-150	389.25	22	7.52	28.01	52.0	861	920	0.00	7.66	4	1338	299	1.3	52	751	756	9.82	44.83	15.45
45X-3, 140-150	417.85	16	7.51	28.90	52.0	861	896	0.00	8.18	4	958	279	1.5	33	753	729	9.61	44.29	15.25
48X-3, 140-150	446.45	22	7.43	25.92	52.2	862	910	0.00	9.39	4	1324	293	1.5	31	751	744	10.30	43.53	14.81
51X-3, 140-150	475.35	42	7.39	27.14	53.8	905	943	0.92	9.25	4	1354	347	1.4	85	792	771	10.28	44.54	16.16
54X-3, 140-150	504.25	37	6.49	25.68	55.0	927	994	0.00	8.53	6	1515	383	1.4	44	808	776	10.64	45.57	16.56
61X-1, 140-150	558.75	18	6.69	21.47	55.5	951	979	0.04	8.47	2	902	454	1.7	12.2	827	772	10.23	45.38	17.66

Notes: IW = interstitial water, NM = not measured, tit = titration, and chr = chromatography.

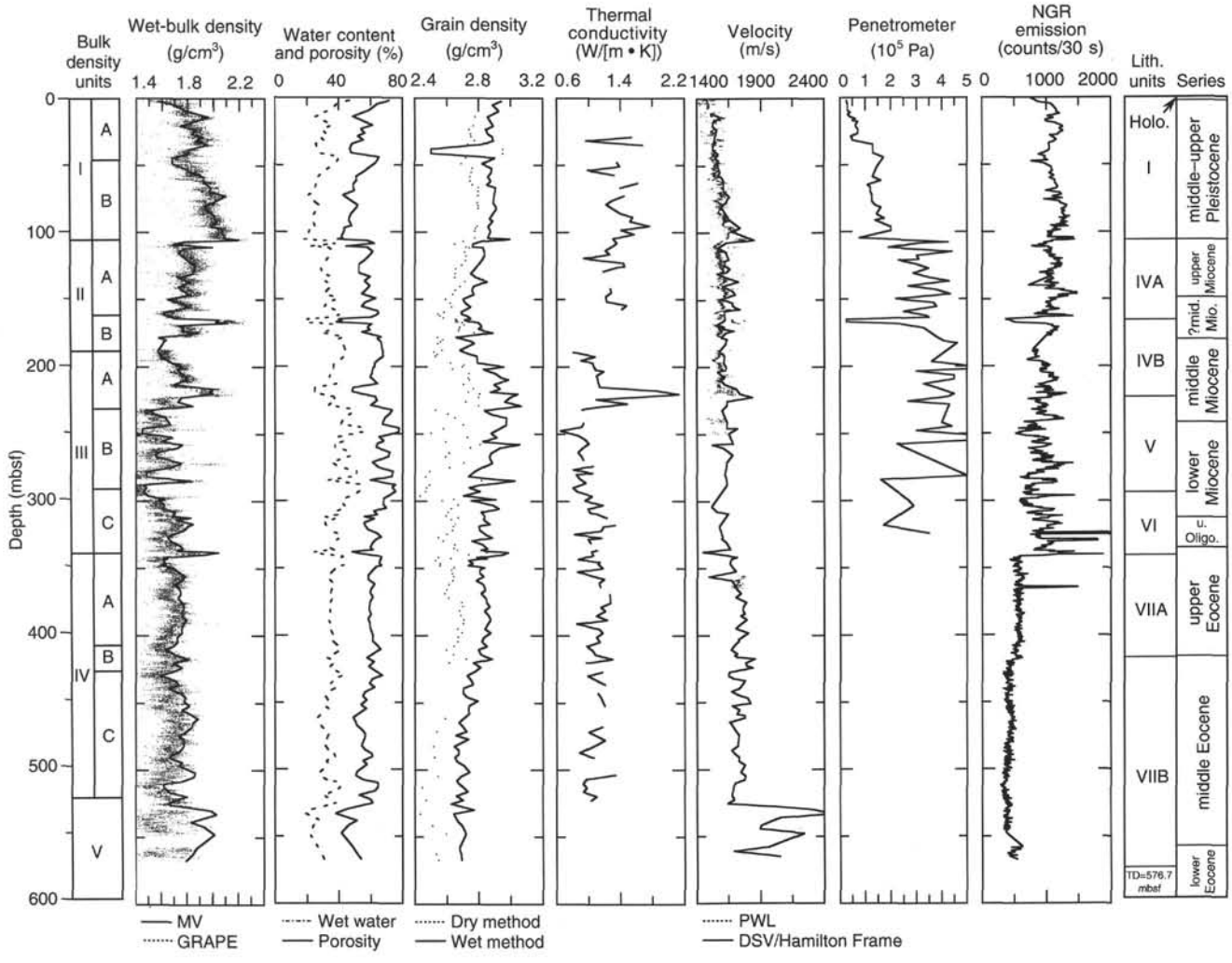

Figure 28. Physical properties results (wet-bulk density, water content and porosity, grain density, thermal conductivity, compressional velocity, penetrometer readings, and multisensor track natural gamma-ray log), Hole 904A. Penetrometer readings exceeding the instrument scale of 4.5×10^5 Pa are plotted at 5×10^5 Pa. MV = mass-volume method.

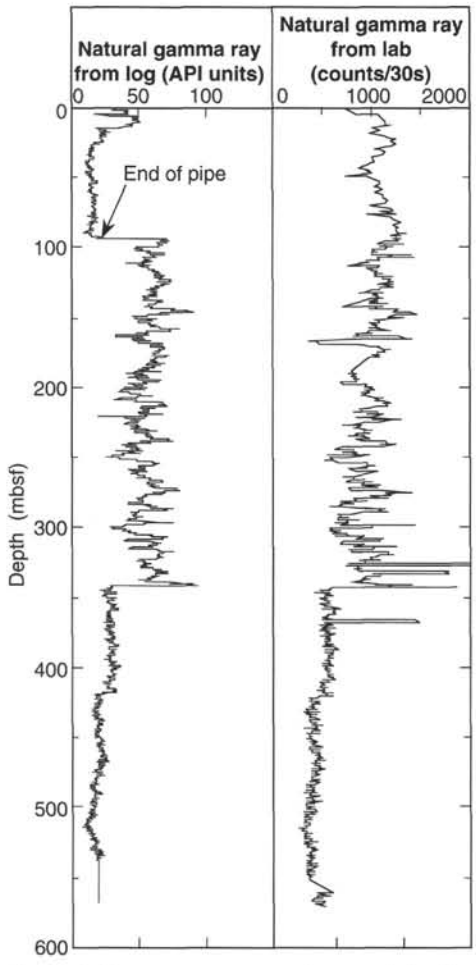

Figure 29. Correlation between gamma-ray values recorded with wireline logs and laboratory measurements on cores.

Unit II is marked by an overall downhole decreasing trend in density from 1.78 g/cm^3 at its top to 1.57 g/cm^3 at its base. The base of Subunit IIA is at 162.4 mbsf (Sample 150-904A-18H-3, 74–76 cm) and roughly correlates with the base of lithologic Subunit IVA. Subunit IIB contains a local maximum value of 2.11 g/cm^3 (sands at 167.35 mbsf; Sample 150-904A-18H-7, 35–37 cm; also see "Lithostratigraphy" section, this chapter). Unit II is upper Miocene; its base approximately correlates with seismic reflector m1 (Tuscan).

Unit III

Sample 150-904A-37X-4, 74–76 cm
Depth: 189.24–341.74 mbsf

Unit III corresponds to upper Oligocene to middle Miocene siliciclastic sediment. It is marked by bulk-density cycles of high variability and is distinguished as a zone of locally high density values attributable to a sand-rich interval (Sample 150-904A-24H-3, 74–76 cm, 2.0 g/cm^3, 216.24 mbsf; also see "Lithostratigraphy" section, this chapter). The base of Subunit IIIA lies at 232.33 mbsf (Sample 150-904A-26X-1, 103–105 cm), and it correlates with seismic reflector m3 (Blue), close to the base of lithologic Unit IV. Subunit IIIB (232.33–292.84 mbsf; Sample 150-904A-32X-3, 74–76 cm) is the central low density interval of Unit III and has an average density of about 1.55 g/cm^3. The base of Subunit IIIB correlates well with the base of lithologic Unit V. Subunit IIIC (292.84–341.74 mbsf) displays a general downhole trend of increasing density, culminating at its base in a glauconitic sandy interval (1.61 g/cm^3) that corresponds to the base of lithologic Unit VI and reflector o1 (green-2).

Unit IV

Interval: Sample 150-904A-56X-5, 74–76 cm
Depth: 341.74–525.54 mbsf

Unit IV displays bulk-density values that average about 1.7 g/cm^3. It is divided into three subunits based on local minima between units. Subunit IVA extends from 341.74 to 410.57 mbsf (Sample 150-904A-44X-5, 77–79 cm; 1.63 g/cm^3); Subunit IVB spans from 410.57 to 429.7 mbsf (Sample 150-904A-46X-5, 70–72 cm; 1.59 g/cm^3), roughly correlating with seismic reflector e1 (yellow); and Subunit IVC lies between 429.7 and 525.54 mbsf (Sample 150-904A-56X-5, 74–76 cm; 1.65 g/cm^3). Unit IV correlates with Eocene chalk and corresponds to lithologic Subunit VIIA and upper Subunit VIIB. Seismic reflector o1 (green-2) lies at the top of Unit IV.

Unit V

Interval: Sample 150-904A-62X-1, 16–18 cm
Depth: 525.54–567.16 mbsf (TD = 576.7 mbsf)

This basal unit corresponds to a porcellanitic chalk (see "Lithostratigraphy" section, this chapter). Bulk-density values are significantly higher (~0.4 g/cm^3 than in the overlying Subunit IVC, and this abrupt increase at the top of Unit V correlates with seismic reflector e2 (red-3) (see "Seismic Stratigraphy" section, this chapter).

Porosity and wet water content (Fig. 28) vary inversely with the trend of bulk density throughout Site 904, suggesting a causal relationship between the two properties not attributable to other factors such as grain composition variations (Fig. 28). Over the entire hole, calculated wet water contents average about 50%. Porosity values are about 70%.

Grain density (Fig. 28) shows an overall decrease toward the bottom of the hole. Average grain densities in Unit I are about 2.9 g/cm^3, whereas in Unit V, they are 2.7 g/cm^3. In Units II and III, grain density does not express this tendency but varies concomitantly with the bulk-density values.

Compressional-wave Velocity

In general, velocity values increase monotonically from about 1517 to near 1700 m/s above Unit V. The largest velocity change is observed at the top of Unit V. Velocity measurements increase from 1641 m/s near the base of Subunit IVC (525.51 mbsf) to 2288 m/s near the top of Unit V (529.96 mbsf). This notable increase in velocity corresponds to a diagenetic change from opal-A to opal-CT (see "Lithostratigraphy" section, this chapter) and to reflector e2 (see "Seismic Stratigraphy" section, this chapter). Local velocity maxima appear near the base of Subunit IB at 99.21 mbsf (1677.70 m/s) and coincide with the highest bulk-density values of Subunit IIIA (1595.40 m/s at 232.33 mbsf).

Thermal Conductivity

Thermal conductivity measurements follow the trends of the bulk-density measurements (Fig. 28). Values range from 0.64670 W/(m · K) to 2.1298 W/(m · K). The maximum value is obtained within Subunit IIIA.

Penetrometer

Penetrometer readings correlate well with the bulk-density unit classification scheme (Fig. 28). Penetrometer readings increase from 2×10^5 Pa near the base of Subunit IB to over 4×10^5 Pa near the top of Subunit IIA. Notable is the correlation near the top of Subunit IIB, where penetrometer readings drop to 2.5×10^6 Pa at 104.70 mbsf.

Natural Gamma-ray Emission

Natural gamma-ray (NGR) emission trends confirm the definition of bulk-density units and subunits (see also Chapter 5, this volume),

and in what follows we describe the natural gamma-ray emission counts using the same divisions. Marked double peaks (a local maximum immediately followed by a local minimum) in the NGR counts coincide with boundaries between Subunits IB and IIA and between Subunits IIA and IIB. A major decrease in the NGR emission counts coincides with the Unit III/IV transition and corresponds to a major change from terrigenous sediments (Unit III) to hemipelagic chalk (Unit IV) (see "Lithostratigraphy" section, this chapter). Unit III shows several small-order cycles of varying NGR counts. Within Subunit IVB, another slight drop in the natural gamma-ray counts takes place at about 420 mbsf. No noticeable shift takes place in the NGR emission counts upon entering Unit V, probably because no change occurs in the radioactive content of the sediment, only in its siliceous content. A large spike at about 325 mbsf is a result of contamination by steel fragments during core-handling procedures.

DOWNHOLE LOGGING

Introduction

Logging was conducted with three logging tool strings at Hole 904A: sonic-induction, porosity, and Formation MicroScanner (see Chapter 3 [this volume] for a description of the tools). Below we describe the acquisition and preliminary interpretations of log data completed at sea. Additional processing and display were conducted onshore by the Borehole Research Group, and their results are presented at the end of this chapter and on the CD-ROM disk in the back pocket of this volume. FMS data are found only on the CD-ROM disk.

The first run was made after the hole was drilled to 587 mbsf. A wiper trip was made to the bottom, and the hole was prepared for logging. Experience from the two previous sites showed that the side-entry sub (SES) was useful in these sediments; consequently, the SES was used from the beginning. As usual, the sonic-induction tool string was used in the first run. The drill pipe and the tool string reached a total depth of 578 m.

During the first run, logging was continued up across the mudline, as can be seen on the gamma-ray curve in Figure 30. This way, the logging depth was correlated with depth recorded during drilling operations.

The second run was made directly after the first. Material had accumulated in the bottom of the borehole either during the first run or when the pipe was lowered in the hole, preventing the logging tools from reaching the same depth as in the first run. Run 2 was made with the porosity tool string beginning at a total depth of 569 mbsf. Logging continued up to 97 mbsf. Before the tool string entered the drill pipe, a repeated run was made upward from 216 mbsf.

The FMS tool was used for the final run in Hole 904A. The FMS was run through almost the entire borehole, even though readings in the upper part were affected by hole enlargement. Because of fill accumulation in the bottom of the hole, run 3 was made from 564 mbsf up to 112 mbsf. Only one pass of the FMS was made because of a time short- age. A repeated run was performed in the lower part of the hole. Table 11 summarizes logging tools and logging parameters in Hole 904A.

Log Quality

The logging heave compensator was not used during the first run; however, during runs 2 and 3, it was used as a precaution even though sea conditions were calm. After each logging run, a short interval at the bottom of the borehole was lost as a result of fill accumulation.

Hole conditions were very good compared with Holes 902D and 903C. The lower part of Hole 904A was especially good, as can be seen on the caliper curve in Figure 30. One of the reasons for good hole conditions in Hole 904A might be the use of the SES from the beginning of logging. The SES enabled the tool string to go down to the bottom directly without flushing and unnecessary movements of the logging string in attempts to pass tight spots.

Table 11. Total drilling depth, SES, tool configuration, logging interval, and logging speed at Hole 904A.

Total depth (mbsf)	SES	Tools (string and combination)	Logging interval (mbsf)	Logging speed (m/hr)
587	Yes	Sonic-induction tool string NGT/SDT/MCD/DIT/LDEO temperature	–23 to 578	275
587	Yes	Porosity tool string NGT/CNT/HLDT/LDEO temperature	97 to 569	275
587	Yes	Formation MicroScanner tool string NGT/MEST/LDEO temperature	112 to 564	275

Note: SES = side-entry sub.

Because of hole conditions, logging data from Hole 904A are generally of very good quality. Only in the upper part of the hole is the quality of log data degraded because of eroded intervals, as can be seen on the caliper curve.

Depth Shifting

The various logs correlate well, and several distinct peaks could have been used for depth shifting. Gamma-ray emissions were recorded on every run, and this log was primarily used for depth shifting. All log curves are displayed in adjusted depth (Fig. 30).

Logging Results

Tight spots were present only in the upper 100 m of the logged interval. This section also contained many intervals in which the caliper measured the maximum diameter of 19 in., indicating hole caving. It is difficult to detect distinct "log units" within this part of the borehole, even though there are intervals with good correlation between logs.

Borehole conditions below 220 mbsf were extremely good, resulting in good correlation between log measurements. Several log units have been defined based on major changes in log character.

By using data from all logs presented in Figure 30 and the FMS tool string, five distinct log units have been identified. Smaller variations occur within the log units. FMS readings in the chalk yield especially detailed information on changes in stratification (data contained on CD-ROM, this volume). The deviation of Hole 904A increases from <1.5° at 117 mbsf to ~8° at 562 mbsf.

Log Unit 1 (base of pipe to 220 mbsf)

The lower boundary of log Unit 1 is located in a section of the borehole where several enlarged intervals make it difficult to determine an unequivocal position for the boundary. Unit 1 is based primarily on the velocity, resistivity, and, to some extent, density curves. The unit is characterized by low density values and is affected by enlarged hole diameter. Resistivity values decrease from ~1 Ωm to 0.7 Ωm in the lower part of the unit, where they become more constant. Velocity values are not reliable because of poor hole conditions. The lower boundary of Unit 1 corresponds with the contact between lithologic Units IV and V (see "Lithostratigraphy" section, this chapter).

Log Unit 2 (220–342 mbsf)

The lower boundary of Unit 2 can be seen on all logs except neutron porosity. The boundary is also the contact between lithologic Units VI and VII and corresponds to seismic reflector o1 (green-2). Velocity in Unit 2 increases with depth, from 1650 m/s at the top to 1800–1900 m/s. Resistivity varies around 0.8 Ωm, with some peaks in the middle of the unit. These peaks, which can also be seen in the other curves, correlate with intervals of enlarged hole diameter. Den-

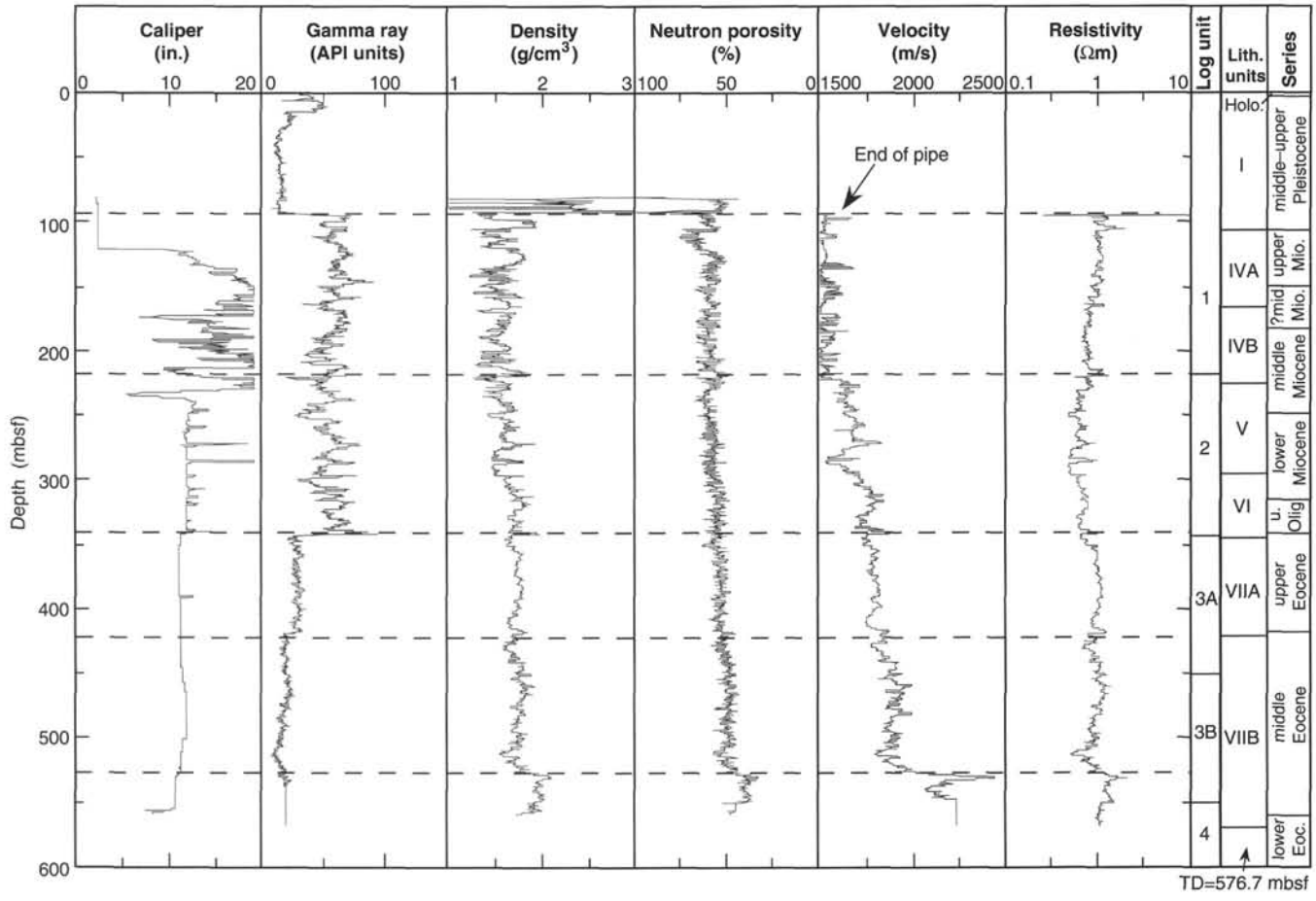

Figure 30. Log units based on observations of density, caliper, gamma-ray, lithodensity, neutron porosity, sonic velocity, and deep resistivity logs run in Hole 904A.

sity increases from about 1.6 to 1.8 g/cm^3 below 295 mbsf. Other logs also exhibit this trend, notably velocity. Unit 2 is also characterized by a borehole size closer to bit size than was found in Unit 1.

Log Unit 3 (342–528 mbsf)

In general, Unit 3 is characterized by constant log curves with only minor variations. Unit 3 shows much lower gamma-ray values (~30 API units) than overlying log units, and resistivity values that are higher and approximately constant at 1 Ωm. The upper part of the chalk (upper to middle Eocene) can be divided into Subunits 3A and 3B. The subunit boundary can be seen on all log curves at 419 mbsf and corresponds to seismic reflector e1 (yellow). Velocity in Subunit 3A is constant at 1800 m/s. Subunits 3A and 3B correspond to lithologic Subunits VIIA and VIIIB (Eocene chalk).

Velocity values are higher in Subunit 3B than in Subunit 3A, varying between 1800 and 2000 m/s. Gamma-ray values (15–20 API units) are lower than in Subunit 3A. Porosity is lower, but only by a few percent. Density values are similar to those of Subunit 3A, except that more variations are present. FMS images show that the chalk in Subunit 3B is more stratified than in Subunit 3A.

Log Unit 4 (528 mbsf to TD)

The upper boundary of Unit 4 is characterized by marked changes in all log curves. All log values increase except porosity, which decreases from 50% to 40%. This decrease corresponds with a density increase of 0.20 g/cm^3 to a mean value of 1.95 g/cm^3. Velocity increases to about 2200 m/s, with a peak of 2450 m/s in the upper part of Unit 4. Unit 4 corresponds to porcellanitic nannofossil chalk within lithologic Subunit VIIB. The increases in both density and velocity at the top of Unit 4 correspond to seismic reflector e2.

Log-core Correlation

Natural gamma-ray measurements were used to study the correlation of laboratory measurements with in situ measurements (see Chapter 5, this volume). At Site 904, the first complete laboratory log of natural gamma-ray emission was obtained. Laboratory natural gamma-ray count times varied in the upper 88 mbsf, but the curve presented in Figure 29 is normalized to an exposure time of 30 s (see also "Physical Properties" section, this chapter for full discussion of laboratory procedures). Figure 29 shows excellent correlation between the log and laboratory natural gamma-ray measurements. Even though the units for gamma-ray measurement differ, the shapes of the curves are similar. Log gamma-ray readings in the upper part of the hole are affected by the pipe and therefore show little variation. Correlation is not possible without detailed knowledge of the borehole shape in this interval.

Downhole Temperature Measurements

The Lamont-Doherty temperature tool was used in all three logging runs. The profiles shown in Figure 31 do not accurately reflect the thermal regime at this site as they are all disturbed by operations preceding logging and by fluid circulation. Nevertheless, there is a tendency to return to thermal equilibrium and a higher thermal gradient between the first (sonic-induction) and the last (FMS) runs.

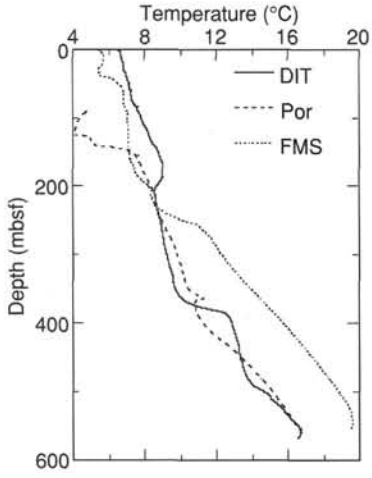

Figure 31. Temperature profiles for Site 904 based on Lamont-Doherty temperature tool. DIT = sonic-induction run, Por = porosity run, and FMS = Formation MicroScanner run.

The differing "anomalies" in the profiles result from fluid circulation and exits/entries of the temperature tool at the bit. They cannot, therefore, be linked to changes in the properties of the surrounding formation. These data must be processed to obtain more realistic temperature profiles, but the trend of the recorded data provides a minimum estimate of the thermal gradient of 25°C/km.

Synthetic Seismogram

The excellent quality of the logs measured in Hole 904A made it possible to produce a satisfactory synthetic seismogram from the density and sonic logs. The convolution of a suitable theoretical wavelet with the reflection coefficients series computed from the logs resulted in the seismogram shown in Figure 32.

Most of the reflectors can be correlated with lithologic features observed in the cores (see "Lithostratigraphy" section, this chapter). Among the most significant signatures, m3 (Blue), at 275 ms or 224 mbsf, corresponds to the transition between lithologic Units IV and V; m6 (pink-3), at 375 ms or 297 mbsf, is at the boundary between lithologic Units V and VI; and o1 (green-2), at 410 ms or 340 mbsf, corresponds to the boundary between lithologic Units VI and VII. Another prominent reflector is e1 (yellow), at 500 ms or 418 mbsf, coincides with the microtektite layer at the transition between lithologic Subunits VIIA and VIIB.

SEISMIC STRATIGRAPHY

Introduction

Seismic profiles crossing Site 904 (Cruise Ew9009 MCS Line 1027; Fig. 2) show that the middle Miocene to Oligocene section thins downdip between Sites 902 and 904. Because of this and downlap and erosional truncation between reflectors m1 (Tuscan) and o1 (green-2), many of the correlations presented below are tentative. Nevertheless, several Oligocene–Miocene reflectors traced from the shelf to Sites 903 (on Cruise Ew9009 MCS Line 1005) and 902 (on Cruise Ew9009 MCS Line 1027) can be traced downdip to Site 904 as well (Table 12). These include m0.7 (blue), m1 (Tuscan), m2 (Yellow-2), ?m3 (Blue), m5 (Green), m6 (pink-3), and o1 (green-2). Although several Pleistocene reflectors are observed at Site 904, reflectors p1–p4 cannot be traced without interruption from Sites 902 and 903 because of intervening canyons. The reflector terminology we use is a combination of the local alphanumeric scheme developed at Sites 902 and 903, the shelf reflectors of Greenlee et al. (1992; indicated as capitalized color names), and the informal shelf seismic scheme of

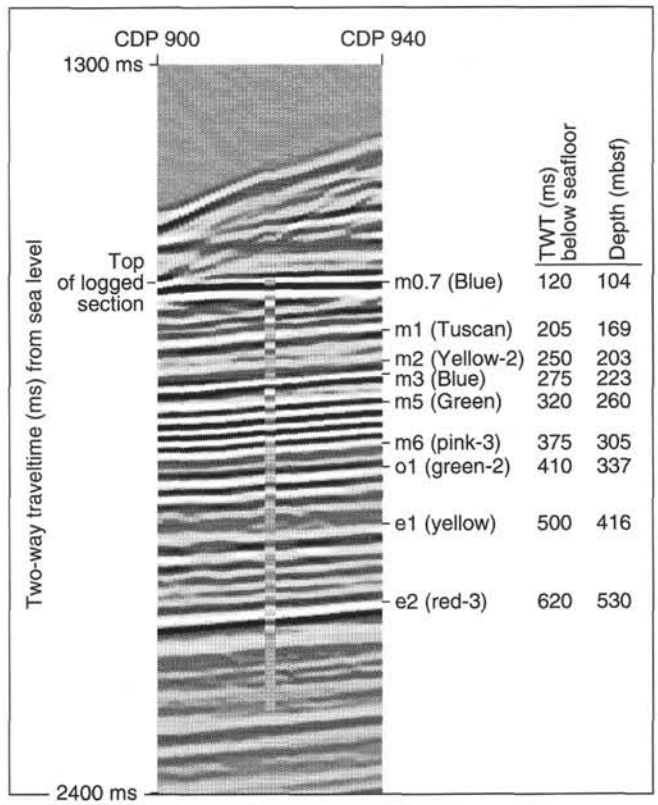

Figure 32. Synthetic seismogram from logging data for Site 904 inserted between CDP 900 and 940 on Ew9009 MCS Line 1027.

G.S. Mountain, K.G. Miller, and N. Christie-Blick (unpubl. data, 1990; indicated by lowercase color names). Correlations for Eocene reflectors e1 (yellow) and e2 (red/A^c) are clear because of the thick, seismically well-resolved, middle-upper Eocene section. Time-depth relationships for correlation of seismic profiles to the boreholes were initially derived from sediment sound velocities that resulted from seismic-borehole correlations made at Site 902 (see "Seismic Stratigraphy" sections in Chapters 6 and 7, this volume). These predicted sub-bottom depths proved to be less accurate (typically correct within 5%) than were similar predictions at Site 903.

Pleistocene Sequences

Pleistocene correlations at Site 904 are limited by the inability to trace key reflectors from Site 902 across the upper Carteret Canyon on Cruise Ew9009 MCS Line 1027. We tentatively identified Pleistocene seismic reflections p1 (yellow), p2 (blue), p3 (green), and p4 (purple) at Site 904, that may correspond to reflectors p1–p4 noted at Sites 902 and 903 (see Table 16 in Chapter 6, this volume).

Reflectors p1 (yellow), p2 (blue), p3 (green), and p4 (purple) lie at about 30, 65, 90, and 110 ms at Site 904 with predicted depths of 23, 53, 72, and 87 mbsf, respectively. We correlate these changes to the borehole by matching them with the nearest density reflectors (e.g., Fig. 21) while maintaining reasonable interval velocities (Table 12). Based on the preliminary correlations of magnetic susceptibility measurements, these reflectors may correlate with the oxygen isotope stage 6/7 transition, stage 9/8 transition, a possible hiatus within stage 10, and stage 12 (see Fig. 18 in Chapter 7, this volume) at 25, 56, 78, and 97 mbsf, respectively. These correlations yield reasonable interval velocities (Table 12), although they are tentative because of uncertainties in measuring exact placement caused by steeply sloping reflections and the relatively thin sedimentary section. Despite these uncertainties, the correlations appear reasonable within biostratigraphic constraints:

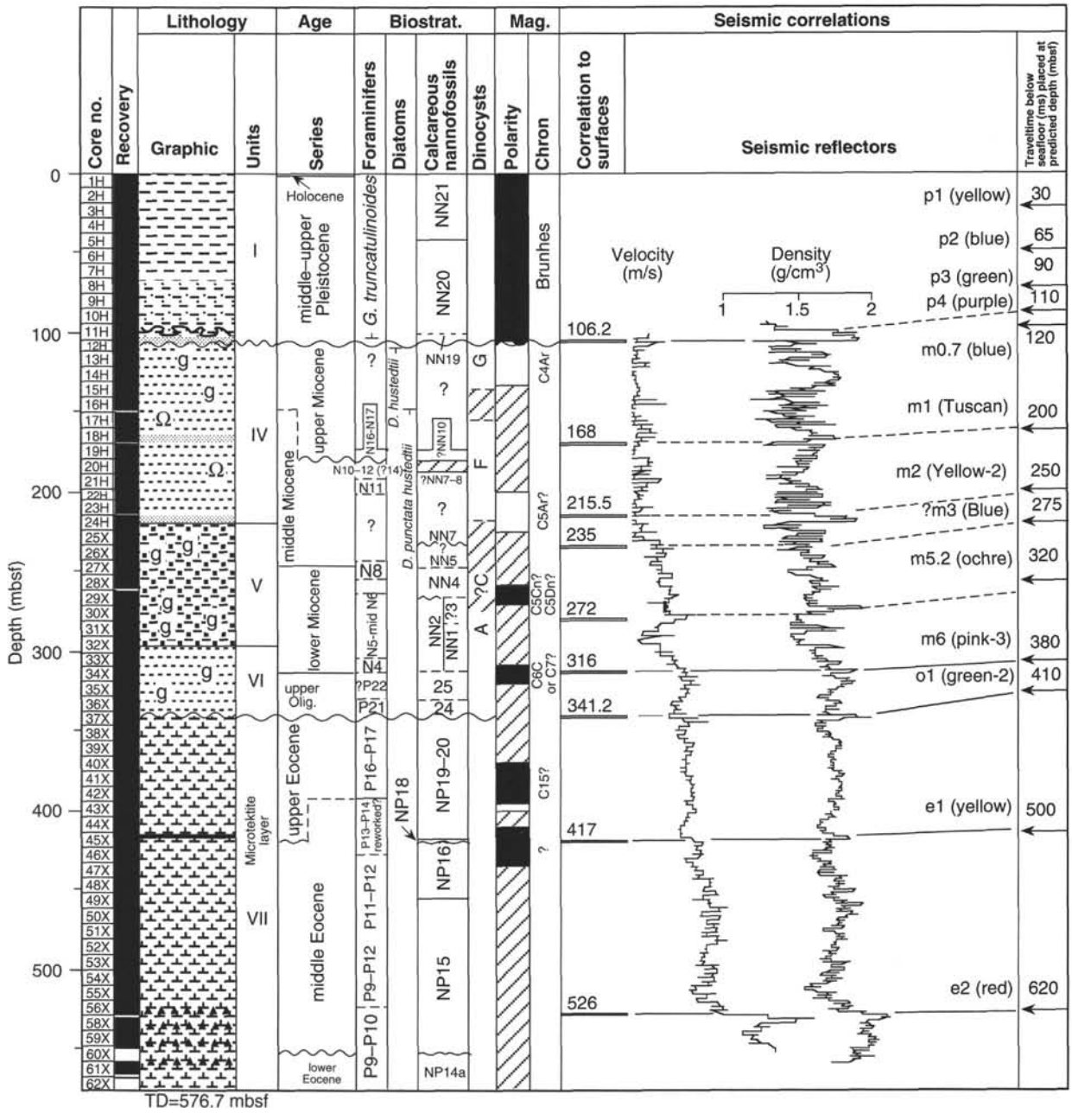

Figure 33. Seismic-core correlations for Hole 904A showing lithology, age, biostratigraphic zones, magnetozones (white = reversed polarity; black = normal polarity; cross-hatched = uncertain), and seismic reflections discussed in text.

for example, reflector p4 (purple) occurs just above the LO of *Pseudoemiliania lacunosa* in stage 12 at both Sites 903 and 904. Thus, preliminary correlations are consistent with an association of reflectors with transitions into glacial stages 6, 8, 10, and 12 (i.e., with glacioeustatic lowerings).

Miocene and Older Sequences

A major disconformity at 106.2 mbsf separates the middle Pleistocene from the upper Miocene section at Site 904, corresponding to the contact between lithologic Units I and IV (see "Lithostratigraphy" section, this chapter). The first Miocene reflector observed, m0.7 (blue), lies at approximately 123 ms with a predicted depth of 95 mbsf; correlation of this reflector to the sharp lithologic change yields a reasonable average velocity of 1727 m/s from 0 to 106.2 mbsf (Table 12). A sharp decrease in density and a minor increase in velocity is noted at 106 mbsf on the logs; however, log quality is not good down to 235 mbsf because of washouts, and the density log shows considerable variability to this level. We conclude that 106.2 mbsf is the best correlation for reflector m0.7. At Site 902, this reflector is underlain by a reversed magnetozone tentatively correlated to Chron C4Ar. At Site 904, this reflector is also underlain by an upper Miocene reversed magnetozone tentatively correlated with Chron C4Ar (~8.5 Ma).

The age and placement of reflector m1 (Tuscan of Greenlee et al., 1992) at Site 904 is uncertain. Reflector m1 lies at 200–210 ms with a predicted depth (based on velocities developed at Site 902) of 161 mbsf (Table 12 and Fig. 33); another cycle at 190 ms is interpreted as a supra-m1 sand. We correlate a distinct sand layer at 168 mbsf with this reflector, although this indicates especially low interval velocities between m0.7 and m1 (1605 m/s). Alternatively, reflector m1 could

Table 12. Seismic reflectors identified at Site 904.

Name	Color	Two-way traveltime (ms)	Depth (mbsf)	Calculated velocities (m/s)		Correlation to borehole
				Interval	Average	
p1	yellow	30	25	1667	1667	Stage 6.
p2	blue	65	56	1771	1723	Stage 8/7 transition.
p3	green	90	78	1760	1733	Condensed Stage 10.
p4	purple	–113	97	1652	1717	12.4/12.3 transition; purple truncates to near blue.
m0.7	blue	–123	106.2	1840	1727	Below blue is Chronozone C4Ar as at Site 902.
m1	Tuscan*	200	168	1605	1680	Posiibly correlates with glauconite sands at 180.29 mbsf.
m2	Yellow-2*	250	215.5	1900	1724	Top sands, 215.5 mbsf; base sands, 220.7 mbsf.
?m3	Blue*	275	235	1560	1709	Possible break between Zones NN7 and NN5.
?m5.2	ochre**	320	272	1644	1700	Above Zone N6 sample, 269.9 mbsf; within Chronozone C5Cn/C5Dn.
m6	pink-3**	–377	316	1544	1676	Zone N4, 308.4 mbsf; Oligocene, 317.8 mbsf; density and velocity kicks, 312/316 mbsf.
o1	green-2**	410	341.2	1527	1664	Top of chalk.
e1	yellow	500	417	1684	1668	Near top of middle Eocene.
e2	red-3**	620	526	1817	1697	Top of porcellanites "porcellanitic limestone?".

Note: Single asterisk (*) = possibly equivalent to the shelf reflectors of this color (Greenlee et al., 1992); double asterisk (**) = possibly equivalent to the shelf reflectors of this color (G.S. Mountain, K.G. Miller, and N. Christie Blick, unpubl. data, 1990).

lie at 180.29 mbsf at the base of a glauconite sand layer where planktonic foraminifers indicate a hiatus between upper Miocene Zones N16–N17 and middle Miocene strata (Zones N10–N12 or possibly Zone N14, given uncertainties in the LAD of *Globorotalia praemenardii;* see discussion in "Sedimentation Rates" section, Chapter 7, this volume). Nannofossil data are consistent with this hiatus. This correlation imposes a m0.7–m1 interval velocity of 1925 m/s. Unfortunately, to complicate things further, both diatoms and dinocysts place the section below about 148 mbsf in the middle Miocene. These discrepancies have not been resolved, and, given the dinocyst and diatom data, it is possible to correlate reflector m1 further upsection at 168 mbsf. However, considering the foraminiferal data, it is not possible to correlate reflector m1 above 177 mbsf because it would make reflector m1 upper Miocene, although we have shown at Site 903 that it is clearly upper middle Miocene (see also Greenlee et al., 1992).

Tracing reflector m2 (= Yellow-2 of Greenlee et al., 1992) to Site 904 is uncertain because of downlapping relationships between closely spaced reflectors. We tentatively place reflector m2 at 250 ms and correlate it with the top of a sand layer at 215.5 mbsf and with the lower part of a reversed magnetozone within Zone NN7 (Fig. 33). Placement at the base of the sand layer yields apparently unrealistic interval velocities, although this is probably a result of minor uncertainties in the traveltime to this reflector. Correlation to 215.5 mbsf is consistent with the correlation of reflector m2 at Site 903 with Chron C5Ar (less than about 12.46 Ma) and is the tentative correlation shown in Figure 33 (see "Seismic Stratigraphy" section in Chapter 6, this volume).

Reflector m3 (= Blue of Greenlee et al., 1992) is not readily traceable to Site 904 because it downlaps onto an underlying reflection (unnamed) between Sites 902 and 904. However, if the cycle at 275 ms is identified as reflector m3 (Blue), then it can be correlated to ~235 mbsf, a possible disconformity separating Zones NN5 and NN7, and a minor velocity peak (Fig. 33). This is consistent with its correlation with ?Zone NN6 at Site 903 and with the estimate of Greenlee et al. (1992) of 13.5 ± 0.7 Ma.

Reflector m4 (= Pink-2 of Greenlee et al., 1992) downlaps onto reflector m5 (Green of Greenlee et al., 1992) between Sites 902 and 904 and crosses Site 904 at 320 ms (256 mbsf predicted depth; Table 12). Based on interval velocities and a density log peak, this two-way traveltime best correlates with about 272 mbsf, within Zone NN2 (Fig. 33). This is slightly older than the correlation of m5 to the borehole at Sites 902 and 903. The several high-amplitude, closely spaced reflectors between 300 and 360 ms at Site 904 may be complicated by internal multiples, and we conclude at this preliminary stage of interpretation that the reflector at 320 ms more reasonably correlates with m5.2 (ochre).

Reflector m6 (pink-3) and o1 (green-2) lie at about 380 and 410 ms, bracketing the Oligocene section at Site 904 as they do at Sites 902 and 903 (Fig. 33). These reflectors are associated with velocity and density peaks at ~316 and 341 mbsf (Fig. 33). At all three sites, reflector o1 correlates with the contact between upper Eocene chalks and Oligocene siliciclastics, which is the contact between lithologic Units VI and VII and a disconformity separating the Oligocene from the uppermost Eocene (Zone NP19–20).

Reflector e1 (yellow) lies at 500 ms, correlating well with velocity and density peaks at 417 mbsf. This density peak immediately underlies the microtektite horizon at 415 mbsf, and immediately overlies the disconformable upper/middle Eocene boundary (418.9 mbsf).

Reflector e2 (red = A^c) lies at 620 ms and correlates with sharp log density and velocity increases associated with the diagenetic transition between chalks and porcellanitic chalks at 526 mbsf. This transition separates biosiliceous (opal-A) sediments above from biosiliceous-poor porcellanites (opal-CT) and porcellanitic cherts below (Tucholke and Vogt, 1979). This diagenetic "Horizon A^c" occurs throughout the western North Atlantic Basin and is time transgressive, spanning the late early to early middle Eocene (Zones P9–P11; ~NP13–lower NP15; Tucholke and Vogt, 1979). At nearby Site 612, this horizon correlates with the lower middle Eocene (Zone CP13b [= middle NP15] and Zone P10; Poag, Watts, et al., 1987) as it does at Site 904 (Fig. 33).

Summary

Oligocene–Pleistocene seismic correlations at Site 904 are the least certain of the Leg 150 slope sites because of the thin sedimentary section at this location. The Oligocene–Pleistocene correlations presented above are consistent with those at Sites 902 and 903, but they are not definitive. In contrast, the upper and middle Eocene section is well developed at Site 904, and reflectors e1 and e2 (A^c) clearly correlate with the disconformable upper/middle Eocene boundary and the top of a diagenetic horizon.

SUMMARY AND CONCLUSIONS

A lower slope (1123 m water depth) section was recovered at Site 904 that complements DSDP Site 612 (1400 m water depth; Poag, Watts, et al., 1987). A thick middle and upper Eocene section like that at Site 612 was recovered, but in addition we recovered an upper Oligocene to middle Miocene section. The latter is of similar lithology, but thinner than the Oligocene–Miocene sections recovered at Sites 902 and 903. Although calcareous-fossil preservation is marginal, Site 904 contains sufficient marker taxa and carbonate for

Sr-isotopic studies; thus, shore-based studies should provide a good early Miocene chronology.

Eocene pelagic carbonate deposition at Site 904 was characterized by moderate biosiliceous input; however, most of the biogenic silica in the lower middle Eocene has been mobilized and reprecipitated as opal-CT. A probable hiatus occurs near the early/middle Eocene boundary at Site 904, and correlates with a similar hiatus at Site 612. Another hiatus occurs in association with the middle/late Eocene boundary at both Sites 904 and 612. An early late Eocene extraterrestrial impact event produced a microtektite layer, which was recovered at both sites. As observed at Sites 902 and 903, an early Oligocene hiatus marks a change to siliciclastic deposition.

As observed at Sites 902 and 903, early to early middle Miocene sedimentation at Site 904 was dominated by organic-rich (>1%), diatomaceous glauconitic silty clays with occasional sand interbeds, suggesting high surface-water productivity beginning in the early Miocene. Late early to early middle Miocene deposition was characterized by interbeds of glauconite silty sands and silty clays. Late middle to late Miocene deposition was characterized by silty clays; much of the carbonate was dissolved and reprecipitated as nodules. Probable hiatuses in the early Miocene (Zones NN2 or NN3/NN4), middle Miocene (Zones NN5/NN7), and across the middle/late Miocene boundary may correlate with inferred glacioeustatic lowerings, although shipboard magnetobiostratigraphy is not sufficient to allow determination of the ages of these hiatuses.

A late Miocene to Pleistocene hiatus at this site was followed by deposition of middle Pleistocene to Holocene hemipelagic silty clays to clayey silts, punctuated by mass-transport deposits. Integration of magnetic susceptibility, density, and biostratigraphic data provide preliminary correlations of the Pleistocene section to the SPECMAP time scale.

The principal result from Site 904 was the recovery of a good lower Miocene section with calcareous microfossils needed for biostratigraphic, Sr-isotopic, and magnetostratigraphic studies. In addition, Site 904 yielded the thickest upper Eocene section yet recovered in this region. Definitive age estimates of seismic reflectors require further study; the interpretations completed thus far are consistent with the ages of reflectors traced from sequences identified beneath the modern continental shelf and dated at Sites 902 and 903. For example,

1. Reflector m1 (Tuscan) may correlate with a possible disconformity spanning the middle/upper Miocene boundary;
2. Reflector m2 (Yellow-2) correlates with a sand layer associated with ?Chron C5Ar (~12.5 Ma; a similar correlation was observed at Site 903); and
3. Reflector e2 (= A^e) correlates with the top of a porcellanitic chalk, which has an age approximately the same as at nearby Site 612 (middle–lower part of Zone NP15).

Ms 150IR-108

NOTE: For all sites drilled, core-description forms ("barrel sheets") and core photographs can be found in Section 4, beginning on page 369. Forms containing smear-slide data can be found in Section 5, beginning on page 833. Thin-section data are given in Section 6, beginning on page 875.

SHORE-BASED LOG PROCESSING

Hole 904A

Bottom felt: 1134 mbrf (used for depth shift to seafloor)
Total penetration: 576.7 mbsf
Total core recovered: 557.55 m (96.7%)

Logging Runs

Logging string 1: DIT/DSI/NGT
Logging string 2: HLDT/CNTG/NGT
Logging string 3: FMS/GPIT/NGT

Drill Pipe

The following drill-pipe depths are as they appear on the logs after differential depth shift (see **Depth shift** section) and depth shift to the seafloor. As such, there might be a discrepancy with the original depths given by the drillers on board. Possible reasons for depth discrepancies are ship heave and drill-string and/or wireline stretch.

DIT/DSI/NGT: Bottom of drill pipe at ~94 mbsf
HLDT/CNTG/NGT: Bottom of drill pipe at ~94 mbsf
FMS/GPIT/NGT: Bottom of drill pipe at ~94 mbsf

Processing

Depth Shift: All logs have been interactively depth shifted with reference to NGT from DIT/DSI/NGT run, and to the seafloor (– 1134 m).
Gamma-ray processing: NGT data have been processed to correct for borehole size and type of drilling fluid.
Acoustic data processing: The DSI (Dipole Sonic Imager) data were processed on the ship's MAXIS unit.

Quality Control

Hole diameter was recorded by the hydraulic caliper on the HLDT tool (CALI), and by the caliper on the FMS string (C1 and C2).
Invalid gamma-ray readings were detected at 61, 72–73, and 80–86 mbsf (DIT/DSI/NGT run).

Hole 904A: Resistivity-Velocity-Natural Gamma Ray Log Summary

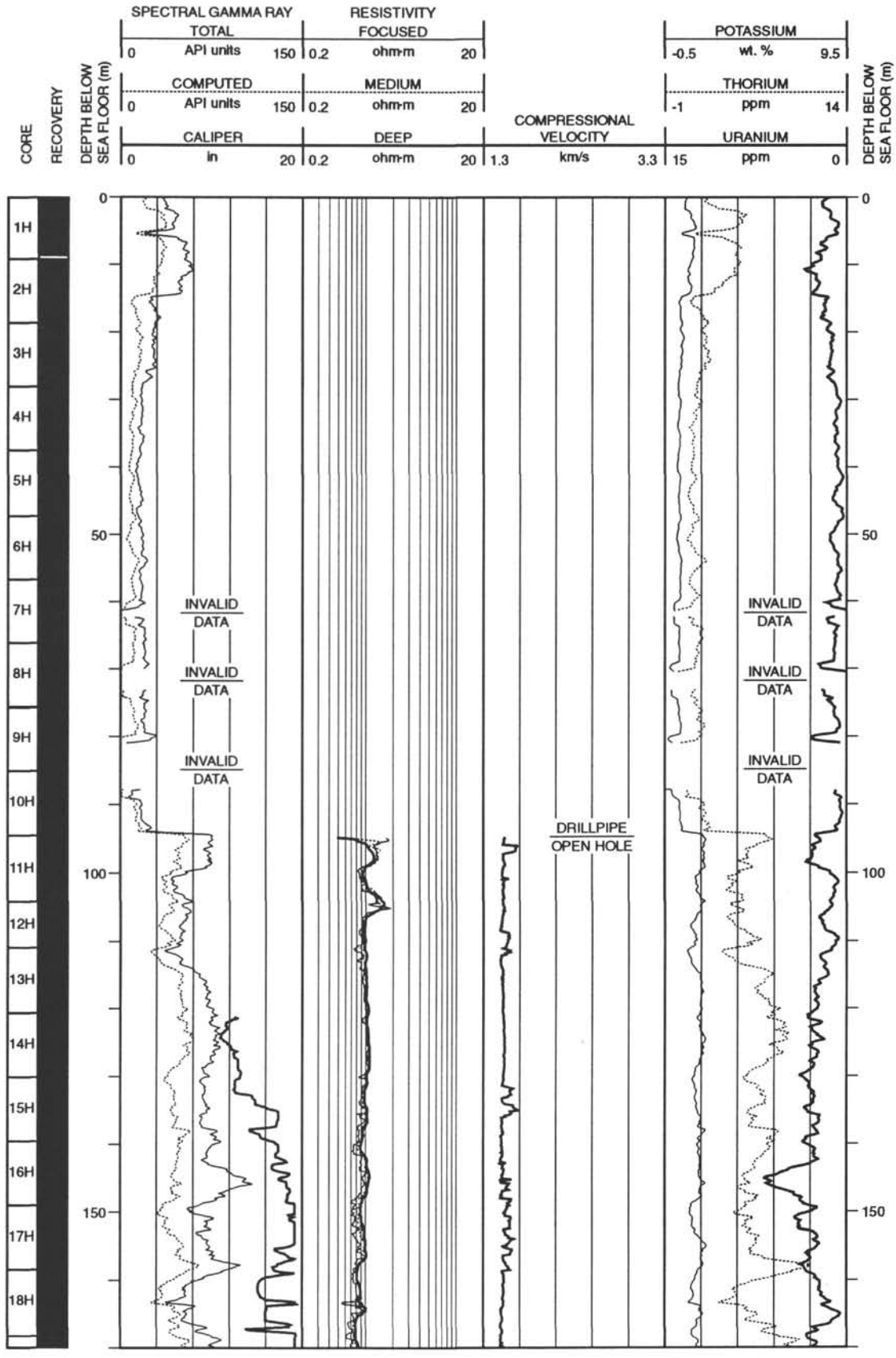

Hole 904A: Resistivity-Velocity-Natural Gamma Ray Log Summary (continued)

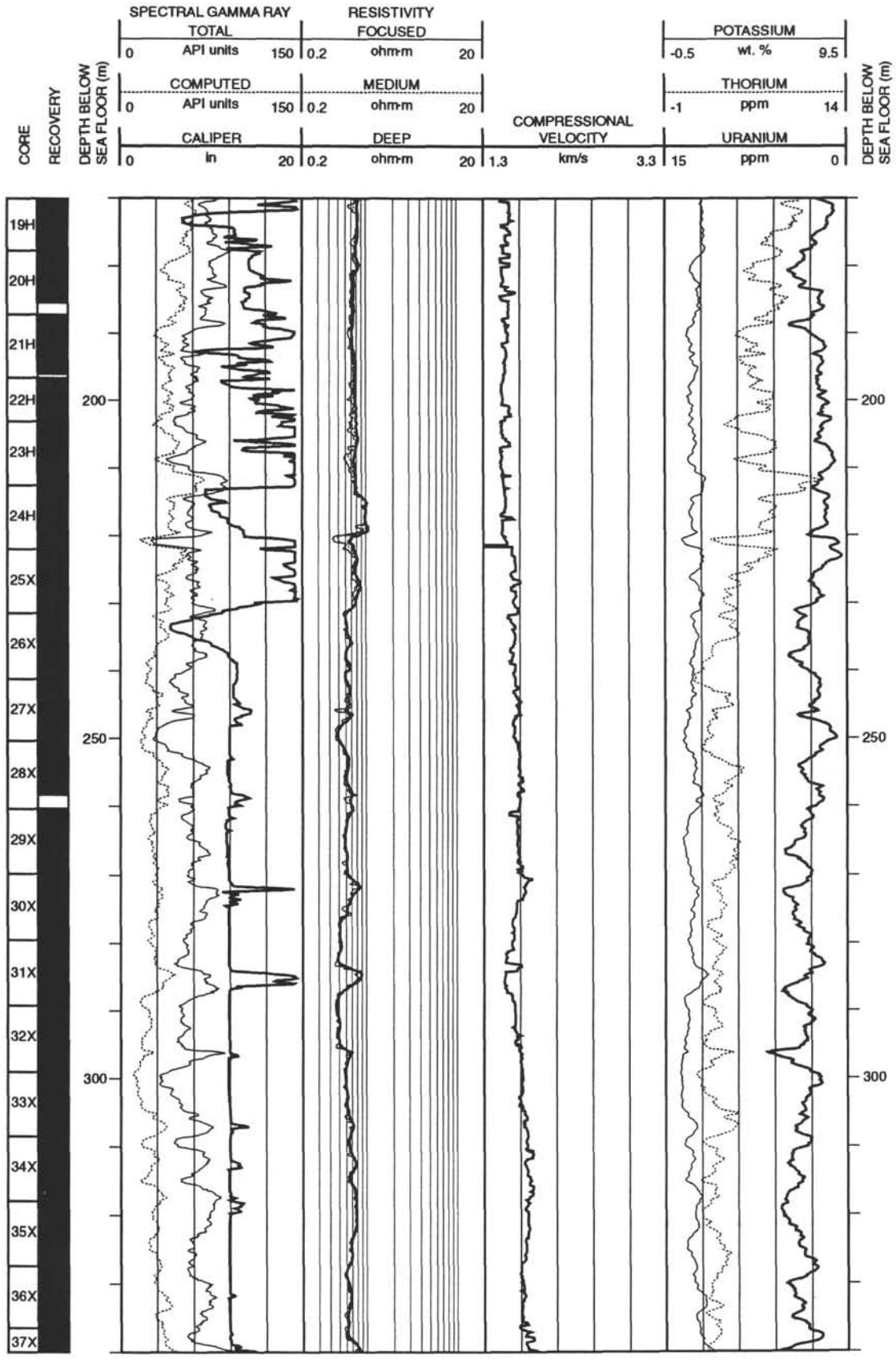

Hole 904A: Resistivity-Velocity-Natural Gamma Ray Log Summary (continued)

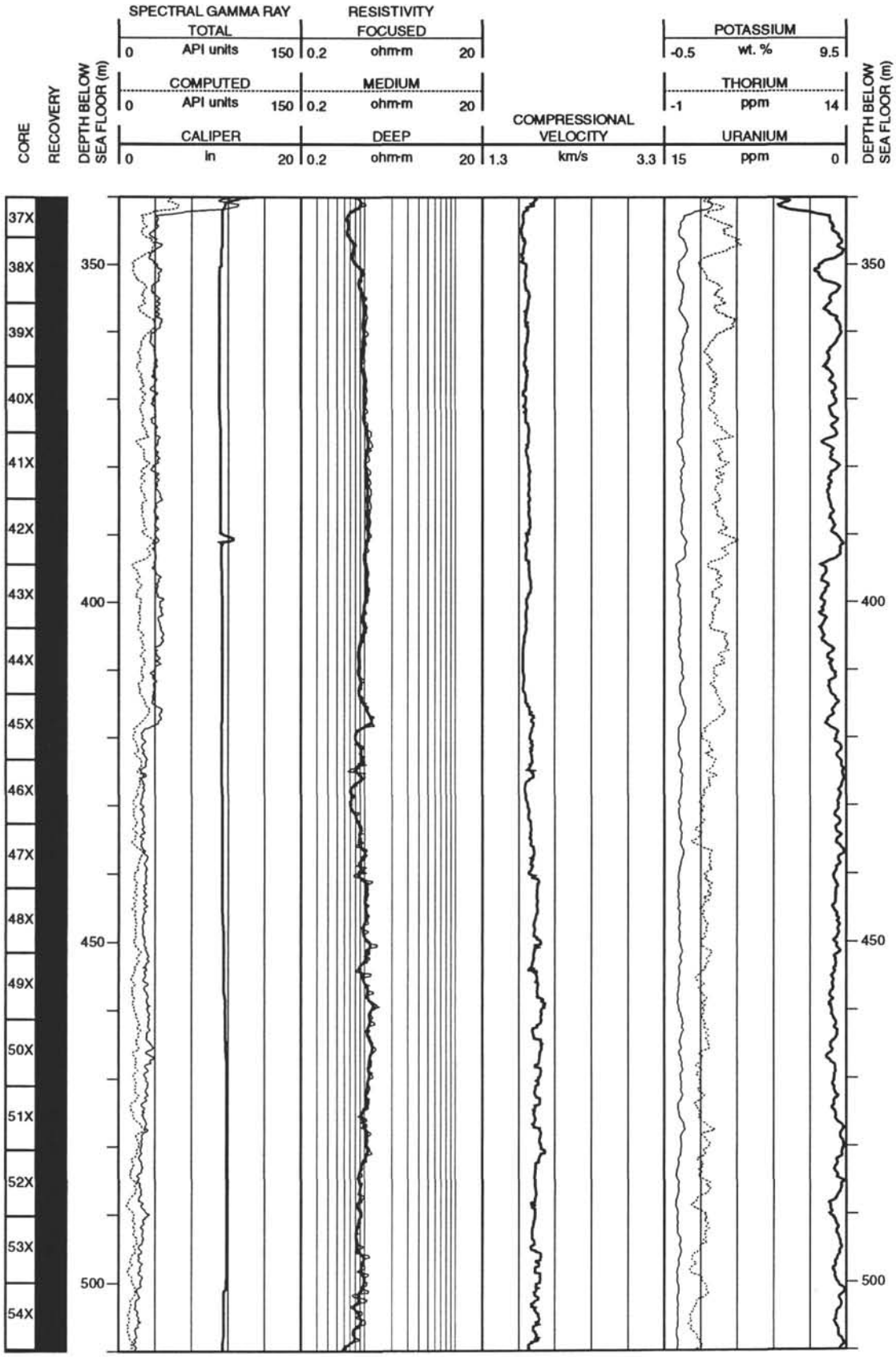

Hole 904A: Resistivity-Velocity-Natural Gamma Ray Log Summary (continued)

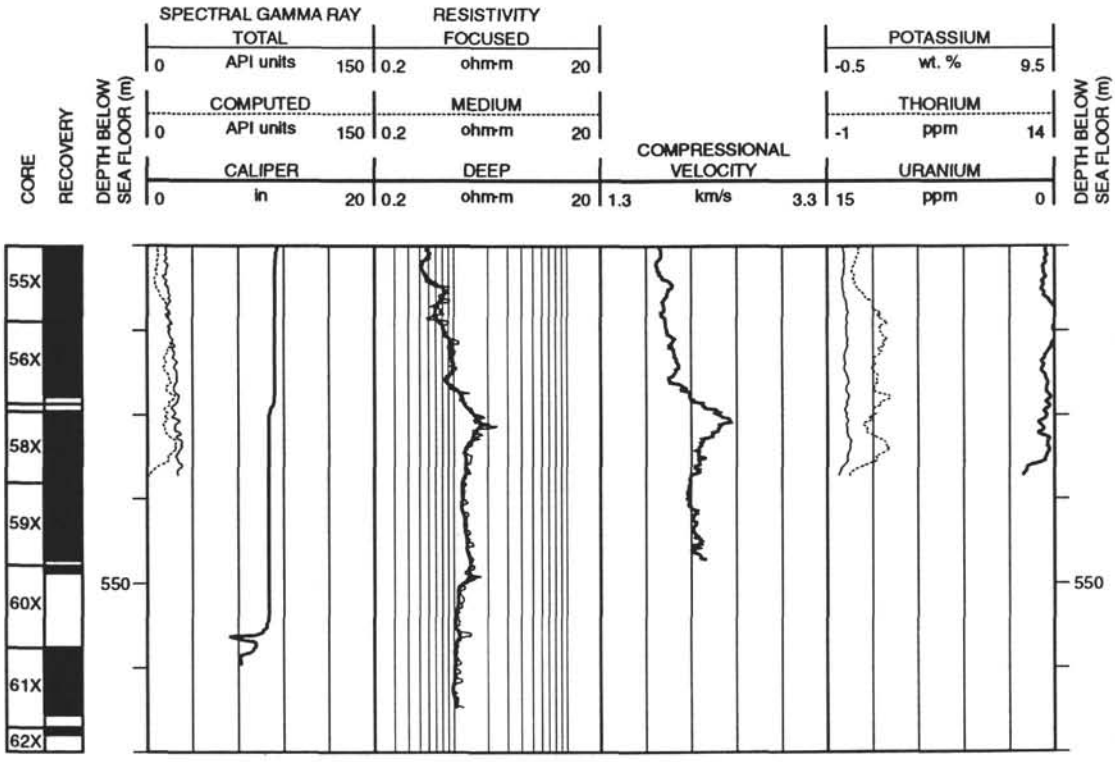

Hole 904A: Density-Porosity-Natural Gamma Ray Log Summary

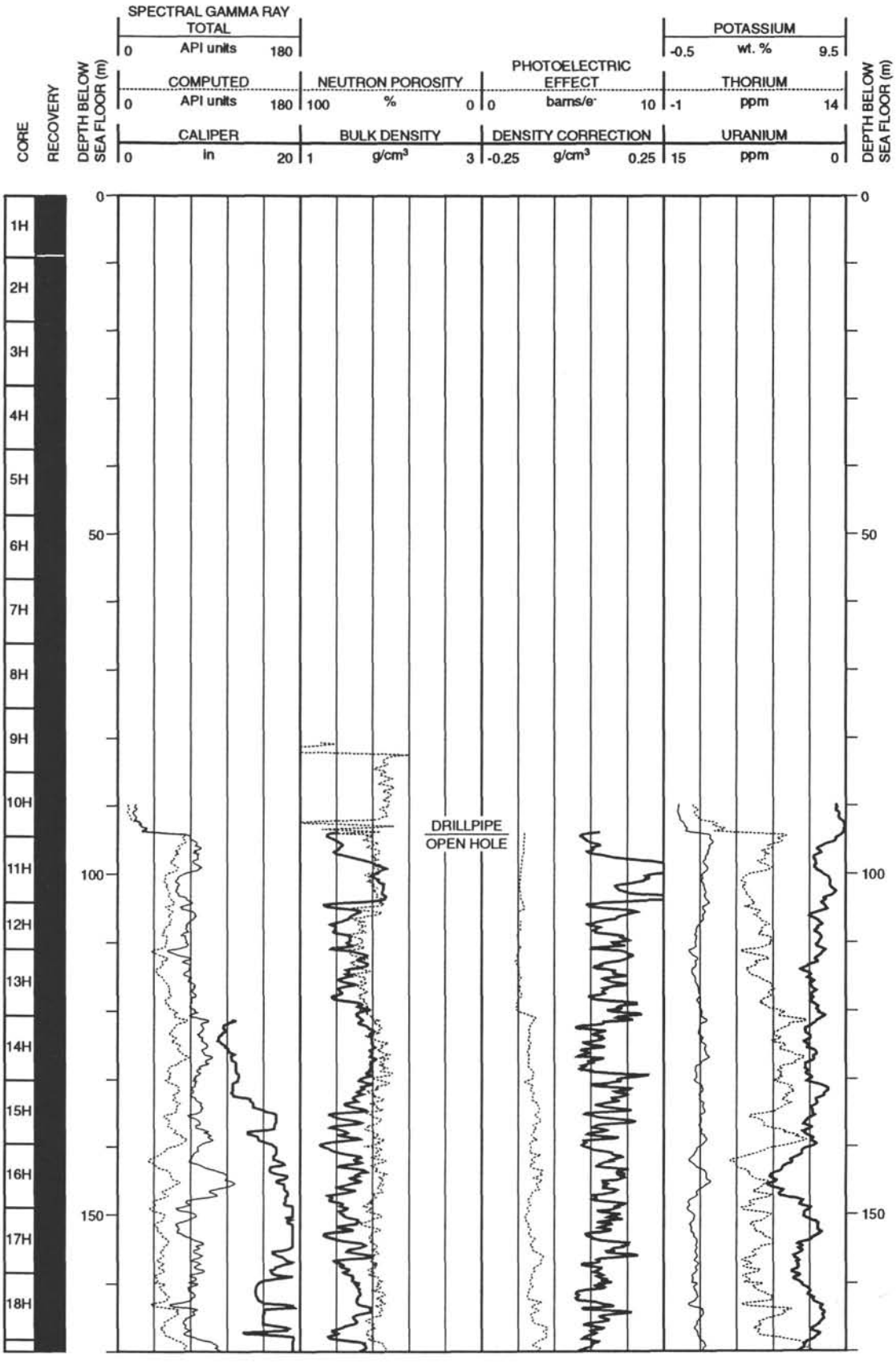

Hole 904A: Density-Porosity-Natural Gamma Ray Log Summary (continued)

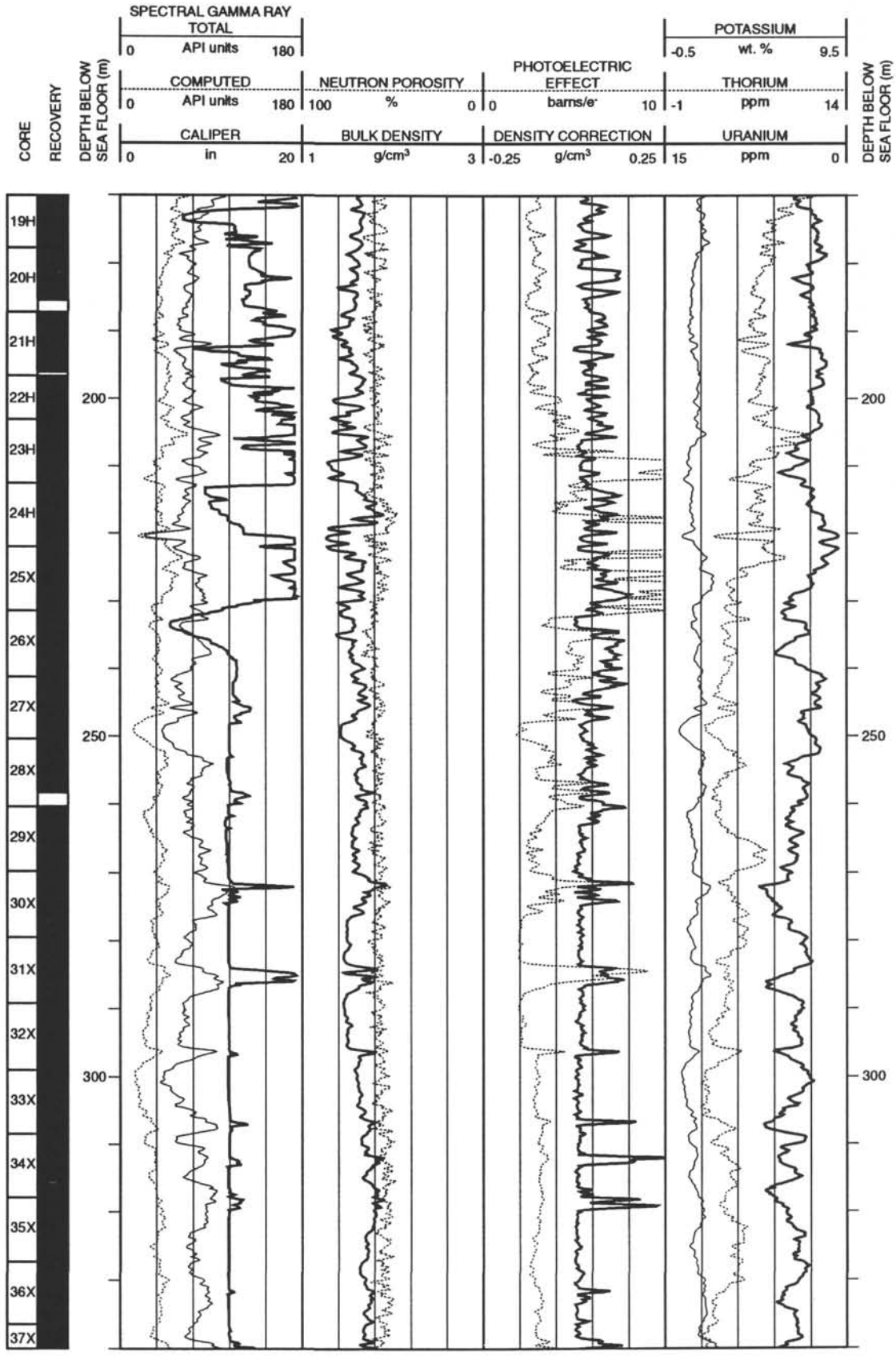

Hole 904A: Density-Porosity-Natural Gamma Ray Log Summary (continued)

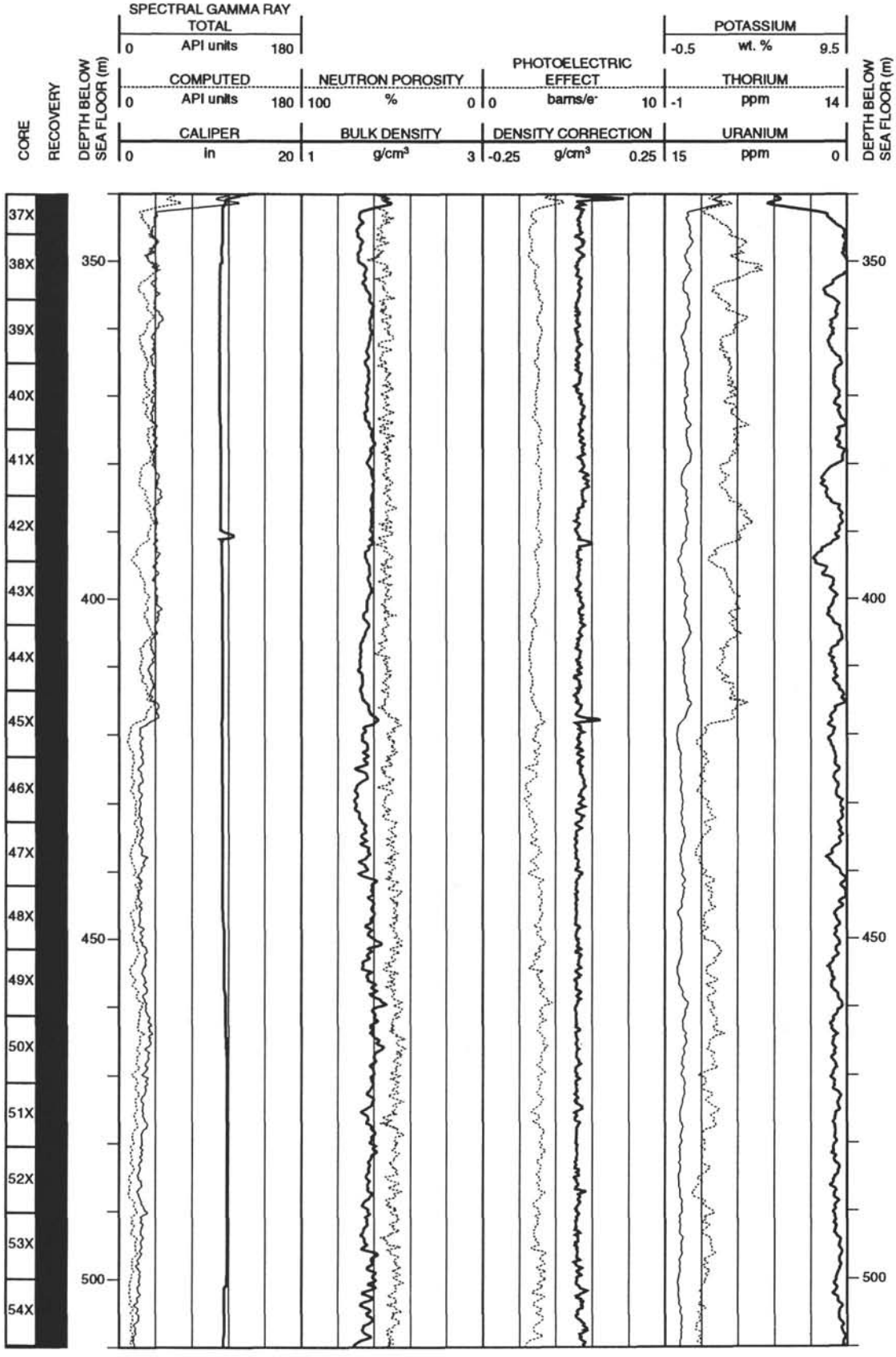

Hole 904A: Density-Porosity-Natural Gamma Ray Log Summary (continued)